9 Circulatory System (Cardiovascular and Lymphatic Systems)

Abdelhamid H. Elgazzar, Saud A. Alenezi, and Mohamed A. Elfawal

9.1 Introduction

This chapter will review anatomic, physiologic, and pathophysiologic principles of major nuclear medicine relevant heart diseases. It will also discuss the role of radionuclide imaging in the diagnosis and management of these conditions including coronary artery disease, acute ischemic syndromes, and heart failure. The chapter includes the pertinent radiotracers and imaging techniques and the clinical circumstances under which these tools are applied to clinical decision making. The chapter will also review the lymphoscintigraphy and its basis and applications.

9.2 Anatomical Considerations

The heart consists of muscle, valves, specialized tissue, coronary arteries, and pericardium. In the embryo, during the first month of gestation, a primitive straight cardiac tube is formed. The tube comprises the sinoatrium, the bulbus cordis, and the truncus arteriosus. In the second month of gestation, this tube doubles over on itself to form two parallel pumping systems, each with two chambers and a great artery. The two atria develop from the sinoatrium; the right and left ventricles develop from the bulbus cordis. Differential growth of myocardial cells causes the straight cardiac tube to bear to the right, and the ventricular portion of the tube doubles over on itself, bringing the ventricles side by side (Fig. 9.1) [1].

The coronary arteries originate from the left and right coronary sinuses of the aorta (Fig. 9.2). The left main coronary artery, which comes off the left coronary sinus, continues for a variable distance before it divides into two major arteries, the left anterior descending and circumflex arteries [2]. The left anterior descending artery (LAD) descends in the anterior interventricular groove and, most of the time, continues to the apex, supplying the apical and inferior apical portion. The LAD gives off septal branches that course deep into the interventricular septum. The septal branches vary in size and number. The anterior two thirds of the septum derive their supply from the septal LAD branches, while the rest of the septum is supplied by the perforator branches from the posterior descending branch of the right coronary artery. The LAD provides also diagonal branches, which run on the epicardial surface diagonally to supply the lateral wall of the left ventricle. Usually, the first one or two diagonal branches are large enough for angioplasty or bypass consideration.

A. H. Elgazzar (✉) · S. A. Alenezi
Department of Nuclear Medicine, Faculty of Medicine, Kuwait University, Kuwait City, Kuwait

M. A. Elfawal
Department of Pathology, Faculty of Medicine, Kuwait University, Kuwait City, Kuwait

© The Author(s), under exclusive license to Springer Nature Switzerland AG 2022

A. H. Elgazzar (ed.), *The Pathophysiologic Basis of Nuclear Medicine*,
https://doi.org/10.1007/978-3-030-96252-4_9

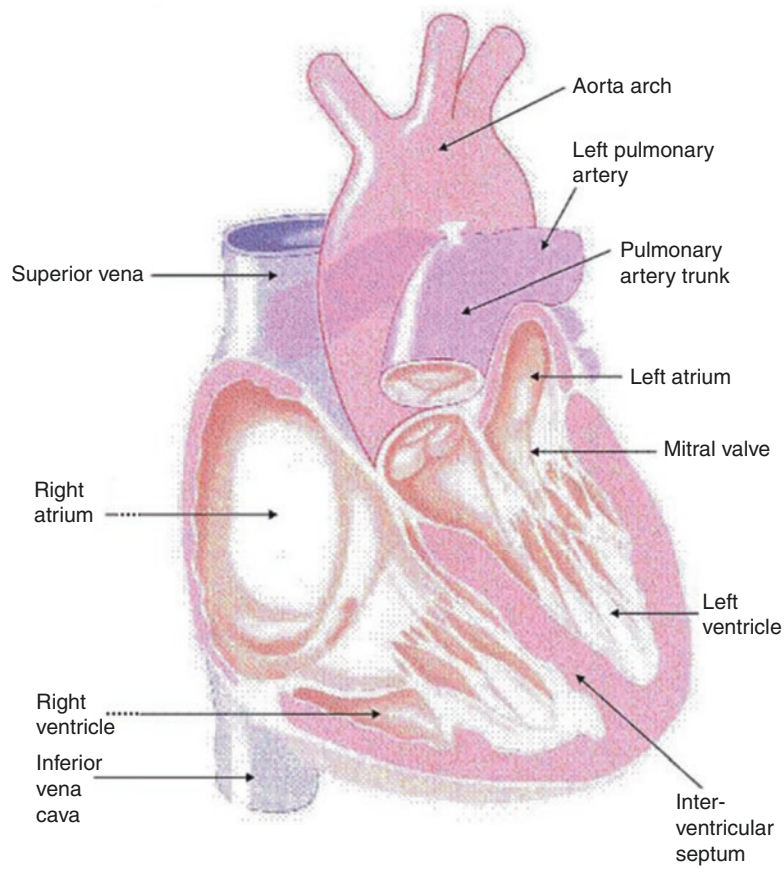

Fig. 9.1 Cutaway view of the heart

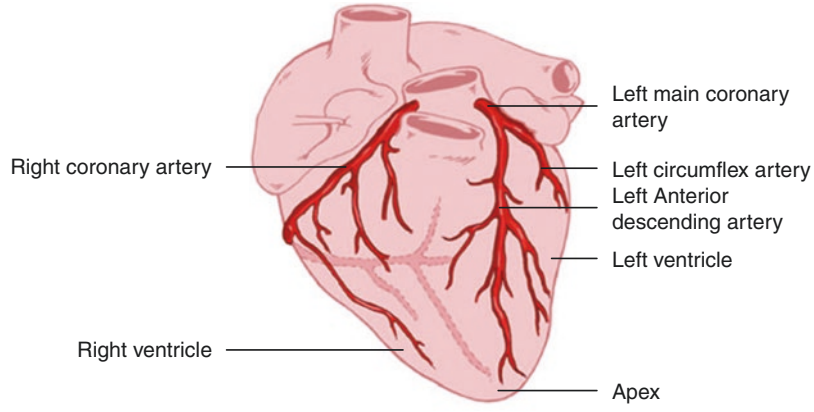

Fig. 9.2 Heart showing the origination of the coronary arteries from the left and right coronary sinuses of the aorta

The left circumflex artery (LCx) branches off from the left main artery and runs in the left atrioventricular groove. It then continues to the left and posteriorly. It supplies several posterolateral ventricular branches, which in turn supply the posterior lateral surface of the left ventricle and parallel the diagonal branches of the LAD. In most cases, the LCx continues as a small terminal posterior left ventricular branch.

The right coronary artery (RCA) arises from the right coronary sinus and descends in the right atrioventricular (AV) groove. Its first supply is to the proximal pulmonary conus and right ventricular outflow region. Normally, there are also two

or three large right ventricular branches that course diagonally over the right ventricle and supply the right ventricular myocardium. Most of the time the RCA continues along the diaphragmatic surface of the heart in the AV groove to reach the crux. At the crux, the RCA divides into a posterior descending artery (PDA) and posterior left ventricular branch. The PDA branch is usually a large artery that runs in an anterior direction in the inferior interventricular groove. The PDA supplies the inferior third of the septum. The PDA septal branches can provide a rich collateral pathway via septal perforating arteries of the LAD. The other terminal branch of the RCA, the posterior left ventricular branch, continues in the AV groove and communicates with the terminal branch of the Cx.

9.3 Physiological Considerations

9.3.1 Physiology of Coronary Blood Flow

The heart is continuously filled with blood throughout the whole life although blood within the cardiac chambers does not significantly contribute to the function, viability and maintenance of cardiac tissue. A specialized separate coronary circulation provides the myocardial tissue with oxygen and substrates to ensure normal function and viability.

Based on the demands for operating a constantly functioning contractile organ, the heart has the highest per gram oxygen consumption of any organ (50–100 μL O_2/min/g) and hence it extracts 70–80% of delivered oxygen even under resting conditions compared to skeletal muscle which utilizes only about 30–40% of delivered oxygen at rest [3, 4].

Coronary blood supply depends on coronary vascular resistance. Coronary vascular resistance depends on several factors (Fig. 9.3) and is continuously regulated to deliver sufficient quantities of oxygen supply to meet any change in the metabolic demand of the myocardial tissue (metabolism-perfusion matching) [3, 5, 6].

Regional myocardial blood flow can be currently measured noninvasively in the units of milliliters blood per minute per gram myocardium. These noninvasive measurements are achieved by positron emission tomography (PET) and can also be done using MRI and CT. Flow estimates with these different imaging modalities were found in animal experimental studies to correlate well with invasive flow estimates by the arterial blood sampling-microsphere technique which is considered the "gold standard" of blood flow measurements [7].

Measuring myocardial blood flow at rest provides limited diagnostic information as even in patients with advanced cardiovascular disease such as dilated cardiomyopathy, hypertrophic cardiomyopathy, or coronary artery disease, resting myocardial blood flows frequently are similar to those in normal individuals [7]. With pharmacologic or physiologic interventions, the response of coronary blood flow can uncover the presence of functional or structural disease-related alterations of the coronary circulation.

Changes in myocardial work and, consequently, in energy demand, are accompanied by proportional changes in coronary blood flow. This flow increase is initiated by a metabolically-

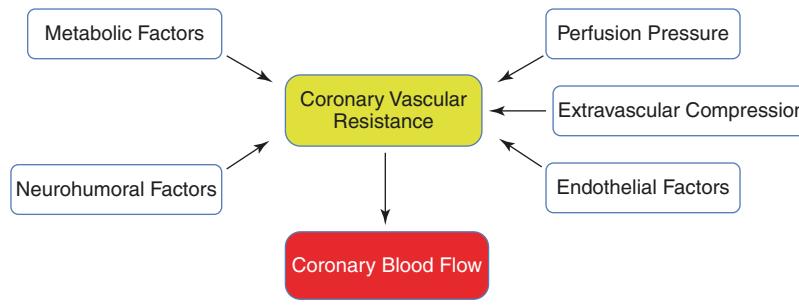

Fig. 9.3 Diagram illustrating factors affecting coronary vascular resistance, the main determinant of coronary blood flow

mediated decrease in microvascular resistance with vascular smooth muscle relaxation and hence to adjust the vessel diameter [7].

Seven to 15% of patients with acute coronary syndrome have nonobstructed coronary arteries and myocardial infarction is not accompanied with obstructed coronary arteries [8]. Quantitative measurements of myocardial blood flow identify functional rather than structural disturbances that may reflect adverse effects of coronary risk factors on endothelial function or early stages of developing coronary artery disease.

Measurements of myocardial blood flow in absolute units allows improved characterization of the extent and severity of coronary artery disease, its impact is likely to be the greatest in patients with microvascular disorders. It is in this particular disease entity where flow measurements offer a means for estimating the true ischemic burden of the myocardium and its associated cardiac risk. Furthermore, it aids to distinguish between functional and structural alterations and, at the same time, identifies potential reversibility and thus therapeutic strategies [9, 10].

The most useful application of measuring myocardial blood flow is in cases with coronary disease confined to microvasculature with angiographically nonidentifiable coronary disease. In other words, there is coronary disease affecting microvessels with no apparent macrovascular alterations. This condition may also show diffuse luminal narrowing without discreet coronary stenosis [7]. This condition is now known to be associated with several conditions such as diabetes and cardiomyopathy (Table 9.1) [11–13]. In addition to normal agiography or a finding of diffuse narrowing, myocardial perfusion studies can also be normal even in the presence of symptoms [7]. However, myocardial blood flow is typically diminished in response to vasodilator stress, although it is most likely be in the range of normal in resting status.

Table 9.1 Major causes of microvascular coronary disease

Diabetic microangiopathies
Hypertrophic cardiomyopathy
Systemic vasculopathies associated with inflammatory disorders
Transplant vasculopathies

9.3.2 Myocardial Contractility

Cardiac muscle has two essential properties: electrical excitability and contractility.

9.3.2.1 Electrical Excitation

The conduction system is composed of modified cardiac cells. The sinoatrial and atrioventricular nodes have cells with high electrical impulse automaticity, while the His bundle and the Purkinje system cells have higher rapid impulse conductivity. The contraction of the heart is normally initiated by an impulse in the sinoatrial node and then spreads over the atrial muscles to the atrioventricular node. The impulse then runs through the His bundle and the Purkinje system to reach all areas of both ventricles at approximately the same time [1, 14].

9.3.2.2 Contraction

The ability of myocardial muscles to shorten and generate the force necessary to maintain blood circulation is a fascinating property of the heart. This is achieved primarily through the unique contractile function of two proteins of the sarcomere (actin and myosin) of the syncytially arranged myocardial fibers. The two main mechanisms that can alter cardiac muscle performance are a change in initial muscle length (Frank-Starling mechanism) and a change in contractile state. In the intact heart, these are determined by preload status, afterload status, the contractile state under a given set of loading conditions, and the heart rate. There is a passive exponential relationship between the length and the tension of muscle fibers. Cardiac muscle tissue, like other body tissue, is not entirely elastic. Thus, this relationship does not exist beyond certain muscle stretch limits. Additionally, there is an active proportional relationship between the initial length of myocardial muscle and the force generated by this muscle, again up to certain length limits [1, 2, 14].

Unlike skeletal muscles, cardiac muscle cells are connected to each other by intercalated disks

and do not run the length of the whole muscle. Also, heart muscle has a rich supply of the high-energy phosphate needed for the contraction. Therefore, it may not easily develop an oxygen deficit as skeletal muscle does when its work exceeds its oxygen supply. Cardiac sarcomeres are limited by the fact that they can be extended only to a certain limit (the optimum length of 2.2 μm), whereas sarcomeres of skeletal muscles can be stretched out beyond that. Finally, cardiac muscle has all-or-none twitch contraction and cannot be physiologically tetanized as skeletal muscle can.

9.3.2.3 Left Ventricular Performance

Left Ventricular Function Curve

The left ventricular function curve usually refers to plotting of some of the LV performance measurements such as stroke volume or work against some of the preload indices such as pulmonary capillary wedge pressure [2, 15]. This analysis requires invasive measurements and is useful not only for providing prognostic information in acute cardiac conditions but also for monitoring response to therapeutic interventions.

Ejection Fraction

The ejection fraction is the most useful single number of the LV performance, defined as the stroke volume divided by the end-diastolic volume. This functional index can be measured by both invasive and noninvasive techniques. Ejection fraction is closely related to the LV function curve; however, it is very sensitive to loading conditions [2, 15].

Pressure–Volume Relationship Measurement

By studying the pressure–volume relationship, a stroke work index can be obtained [2, 15]. This is defined as stroke volume × (mean LV systolic ejection pressure − mean LV diastolic pressure). It is a very sensitive index since it is affected by all factors that may alter LV performance.

Regional Wall Motion Assessment

The assessment of regional wall motion is extremely useful in confirming and locating the site of coronary artery disease (CAD). As with LV ejection fraction measurement, it can be studied using both invasive and noninvasive methods.

Diastolic Function

Diastolic function is usually assessed by studying the relationship between LV passive pressure and volume and by examining the rate of relaxation after contraction. Several important measurements have been derived from various invasive and noninvasive techniques that can be used for both evaluating and monitoring the changes in diastolic function [15].

9.4 Pathophysiological Considerations

9.4.1 Heart Failure

Heart failure is considered a pathophysiological condition rather than a specific disease. In such a condition, the heart fails to supply enough blood to meet the metabolic demand of the tissues. Most cases of heart failure are due to primary myocardial dysfunction or intrinsic abnormalities, which include hypertensive myocardial hypertrophy, ischemic heart disease, valvular heart disease, pulmonary hypertension, pericardial disease, and other cardiomyopathies (Table 9.2). Various extrin-

Table 9.2 Major causes of heart failure

A. Systolic dysfunction:
1. Ischemic heart disease (e.g., chronic ischemia, myocardial infarction)
2. Valvular heart disease (e.g., mitral regurgitation, aortic regurgitation)
3. Dilated cardiomyopathy (idiopathic and nonidiopathic)
4. Chronic uncontrolled arrhythmia
B. Diastolic dysfunction:
1. Hypertension
2. Ischemic heart disease (e.g., acute ischemia)
3. Infiltrative myocardial disease (e.g., amyloid)
4. Left ventricular outflow tract obstruction (e.g., hypertrophic obstructive cardiomyopathy, aortic stenosis)
5. Uncontrolled arrhythmia

sic abnormalities can cause heart failure as well, despite normal ventricular function; this is referred to as secondary heart failure. Heart failure in this situation could have many reasons: inadequate blood volume as in hemorrhage, inadequate oxygen delivery as in anemia, inadequate venous return as in tricuspid stenosis, profound capillary vasodilatation as in toxic shock, and peripheral vascular abnormalities as in arteriovenous shunts.

Under normal conditions, the heart receives blood at low pressure in diastole, then ejects it at higher pressure during systole. Heart failure occurs when the heart fails to maintain adequate cardiac output (CO) to meet the body's metabolic demands. CO is the ejected amount of blood by the ventricle per minute. It is equal to the stroke volume (SV) multiplied by the heart rate (HR), i.e., CO = SV × HR. Stroke volume is the amount of blood ejected from the ventricle during systole, which is equal to the end-diastolic volume (EDV) minus end-systolic volume (ESV). SV depends on three determinants; preload, afterload, and contractility. Preload is the ventricular pressure at the end of diastole, while afterload is the pressure during ventricular systolic contraction. Myocardial contractility accounts for the change in contraction intensity. Ventricular SV increases when there is an increase in preload, a decrease in afterload, or enhanced contractility. When a cardiac muscle is passively stretched before contraction, and then stimulated to contract, the generated force depends on the length of the muscle fiber. The Frank-starling law explains how the SV increases if the preload is increased in relation to the myocytes stretching which results in increased systolic contraction. In other words, the more the ventricle is distended with blood during diastole, the more is the volume of blood ejected during systole. Ejection fraction (EF) is the portion of EDV ejected from the ventricle during each systole (EF = SV ÷ EDV). The normal EF range is between 55% and 75% [16].

Chronic heart failure occurs when the afterload increases, or ventricular contractility is reduced, a condition termed "systolic dysfunction." Essential causes of increased afterload are systemic hypertension and severe aortic stenosis. Significant causes of impaired contractility are coronary atherosclerosis, mitral regurgitation, aortic regurgitation, and dilated cardiomyopathies. Chronic heart failure may also result from impaired ventricular filling and diastolic relaxation which is known as "diastolic dysfunction." Causes include left ventricular hypertrophy, myocardial fibrosis, restrictive cardiomyopathies, and constrictive pericarditis or cardiac tamponade. Accordingly, heart failure has been categorized into two groups; heart failure with reduced EF, i.e., systolic dysfunction and heart failure with normal EF, i.e., diastolic dysfunction [17]. In heart failure with reduced EF, the incomplete ventricular emptying and increased EDV cause elevation of the LV pressure during diastole. This, in turn, is transmitted to the left atrium and the pulmonary vasculature. When pulmonary pressure is significantly elevated, i.e., more than 20 mmHg, pulmonary congestion and pulmonary edema will occur and generalized venous congestion and generalized edema will then follow. On the other hand, in heart failure with normal EF, diastolic filling occurs at a higher pressure due to reduced ventricular compliance. This elevated ventricular pressure is retrogradely transmitted to the left atrium, pulmonary and systemic venous circulation with similar consequences as described in heart failure with reduced E.F.

Compensatory mechanisms in heart failure include the Frank-Starling mechanism. When LV contractile function is impaired, this results in incomplete emptying and increased LV pressure. Myocardial fibers act through the Frank-Starling mechanism, increase stretch to induce a greater stroke volume which helps to empty the enlarged LV and maintain a normal cardiac output. The second compensatory mechanism is neurohormonal activation which comprises increased adrenergic activation, renin-angiotensin-aldosterone system, and increased antidiuretic hormone. The third (space)mechanism includes ventricular hypertrophy and remodeling. All such compensatory mechanisms can be beneficial within limits, but eventually fail to maintain adequate cardiac output [18].

All the physiological principles described in heart failure are essentially applied to both left-

sided and right-sided failure. However, the right ventricle is highly compliant compared to the left ventricle and therefore can accept larger volumes of blood with little changes in its filling pressure. Apart from the fact that left-sided heart failure is the commonest cause of right-sided heart failure, as a result of increased pulmonary vascular pressure, isolated right ventricular failure may occur following chronic obstructive pulmonary disease, reflecting the increased right ventricular afterload. The most common cause of acute right-sided heart failure is massive pulmonary embolism due to sudden increase of right ventricle afterload [16].

Heart failure may occur due to ventricular dysfunction as a result of various causes which include systemic hypertension, ischemic heart disease, cardiac valve disease, cardiomyopathies, chronic pulmonary disease, pericardiac disease, among other conditions. Other conditions may also lead to heart failure despite of normal ventricular function, such as hypovolemia, anemia, distribution shock, among other causes [19].

9.4.2 Systemic Hypertension

Blood pressure (BP) is the result of cardiac output (CO) and peripheral resistance (PR), i.e., $BP = CO \times PR$. There are four structures that are responsible for regulation of BP. These include the heart or the pump that creates the ejecting pressure; blood vascular tone which is responsible for peripheral resistance; the kidneys which control the intravascular volume; and neurohormones that moderate the previous three structures. However, a fourth short-term regulatory mechanism of BP is through the baroreceptor reflex, which plays a significant role in momentary changes in BP. Such receptors are present in the walls of the aortic arch and carotid sinuses. Whenever BP rises, baroreceptors are stimulated and transmit impulses to the brain stem medulla, which sends negative feedback signals through the autonomic nervous system, causing inhibition of the sympathetic nervous system and stimulation of the parasympathetic system with a consequent fall in BP. Contrarily, baroreceptors transmit fewer impulses to the medulla following a transient fall in BP, resulting in restoration of BP [20].

Hypertension increases the workload of the heart and damages the systemic arterial vasculature. It increases the afterload and can cause systolic dysfunction, left ventricular hypertrophy, which if uncontrolled, can eventually end in diastolic dysfunction. All of such effects can lead to left ventricular failure. Increased afterload will, in turn, increase the myocardial oxygen demands, which can lead to chronic myocardial ischemia. In addition, hypertension causes vascular endothelial damage, the most significant triggering mechanism for the initiation of atherosclerosis [21]. Hence, the role of hypertension as a risk factor for atherosclerosis cannot be overstated. In addition to its atherogenic role, hypertension contributes to many arterial pathological complications, which include tissue ischemia, thrombosis, embolism, aneurysm, and hemorrhage. Such effects may influence important and vital target organs, such as the heart, brain, kidneys, and the eyes.

The increased arterial peripheral resistance raises pressure inside the LV with increased afterload. As a compensatory mechanism, LV hypertrophy ensues in the form of concentric hypertrophy, mostly without dilatation. Increased LV muscular rigidity results in diastolic dysfunction [2, 22]. In such conditions, HF is manifested with a normal ejection fraction (EF). It follows that LV hypertrophy in such cases will result in pulmonary congestion and will eventually cause RV hypertrophy and congestive heart failure. Clinically, increased LV mass as a result of hypertrophy can be manifested by heaving LV impulse on chest palpation, and a fourth heart sound (S4) is present, since the left atrium is contracting into a rigid LV. In hypertensive patients, cardiac morbidity is proportionate to the extent of LV hypertrophy. This is valid in many cardiac illnesses, such as acute coronary syndrome, congestive heart failure, arrhythmias and, unsurprisingly, sudden death.

In patients with advanced hypertension, however, the increased LV pressure outweighs the LV mass built up throughout LV hypertrophy. This

will result in LV systolic dysfunction, with low CO and reduced EF, pulmonary congestion, and congestive HF. Myocardial ischemia, due to the likely associated coronary atherosclerosis, and the increased LV mass due to LV hypertrophy, plays a significant contributory role to LV systolic dysfunction.

9.4.3 Pulmonary Hypertension

The degree of pulmonary blood flow is affected mainly by the lumen size of the pulmonary vessels [23].

Furthermore, the pulmonary vascular resistance is defined as the difference of mean alveolar pressure and left atrial (LA) pressure divided by pulmonary blood flow. A change in any of these factors may therefore give rise to pulmonary hypertension. Pulmonary hypertension can be either primary or secondary to many other causes. In congenital heart diseases, increased medial thickening and atherosclerotic changes of the pulmonary vasculature are observed [24]. Such changes are also seen in patients with systemic to pulmonary collateral circulation. The sudden rise of PA pressure with irreversible RV failure and the usual significant decrease in LV systolic function association in acute pulmonary embolization are the cause of high mortality within the first hour in these patients [25]. Conversely, intimal fibrosis due to thrombus organization is the reason behind the cor pulmonale in chronic pulmonary embolization [26].

Pulmonary hypertension can also develop due to a rise of pulmonary venous pressure caused by LV diastolic dysfunction or high LA pressure. If such a condition persists long enough, medial thickening and arterialization of pulmonary veins will develop, which results in pulmonary fibrosis and destruction of alveolar capillaries [23]. The most common chronic lung disease associated with cor pulmonale is chronic bronchitis. The increased pulmonary vascular resistance in this case is caused by a reduction in the total area of the pulmonary vascular tree as well as mild thickening of the pulmonary arterioles [27, 28].

Unlike the LV, the RV is a high-volume, low-pressure pump. Consequently, as pulmonary vascular resistance increases, a decrease in RV stroke volume and EF is observed [29].

An increase in heart rate does not usually provide enough compensation, and a decrease in cardiac output is inevitable. Additionally, signs and symptoms of systemic venous congestion are seen due to high-pressure transmission from the RV. Diastolic LV dysfunction due to RV failure could be caused by the decrease in both the LV distensibility and the myocardial blood flow from the accompanied elevation in coronary venous pressure [30].

9.4.4 Atherosclerosis

Currently, atherogenesis is largely viewed as a chronic inflammatory process. Several decades back, it was regarded as a simple imbibition of elevated plasma lipoproteins through permeable vascular endothelium. The evolution of early atheromatous lesions, i.e., fatty streaks, may commence as early as during infancy [31]. Atherogenesis is a complex and incompletely understood multifactorial procedure. There are two adopted theories of atherogenesis; the first is the response to Injury, which probably contributes to the build-up of atherosclerotic lesions during the early stages of the disease. The second, thrombogenic theory, possibly participates in the progression of a pre-existing plaque that undergoes thrombotic formation (Fig. 9.4), with healing by organization and reendothelialization, and further progressive narrowing of the arterial lumen. The current view of atherogenesis incorporates elements of both theories and includes the recognized modifiable and unmodifiable risk factors [32].

The response to injury theory entails dynamic interaction between (1) endothelial dysfunction, (2) subendothelial inflammation, and (3) vascular smooth muscle cells response [33].

Endothelial dysfunction can be initiated by a number of risk factors, which include sheer mechanical stress related to hypertension, oxi-

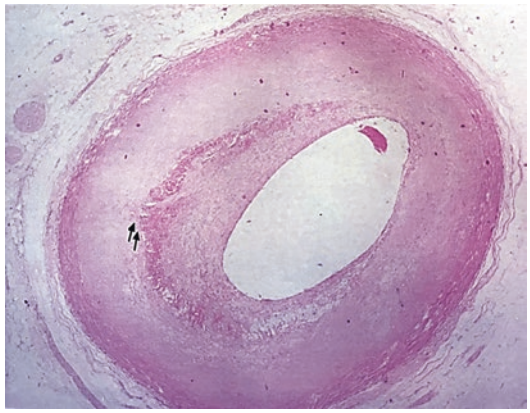

Fig. 9.4 Coronarynatherosclertic plaque showing an organized thrombus (arrows) building up the atheromatous growth

dized low-density lipoprotein (OxLDL), diabetes mellitus, smoking, elevated homocysteine levels, infectious agents, among others. Such physical and chemical stressors impair endothelial permeability, promote the release of inflammatory cytokines, increase monocytes adhesion, alter the release of vasoactive substances (e.g., prostacyclin and nitric oxide), and interfere with normal antithrombotic properties. Dysfunctional endothelium leads to (a) increased permeability to lipoproteins and (b) promoting passage of monocytes across the endothelium. The low-density lipoprotein (LDL) trapped in the subendothelium undergoes oxidation (OxLDL). The resultant inflammatory reaction involves incorporation of OxLDL in the subendothelium into the modified macrophages, forming foam cells that represent the earliest lesions known as fatty streaks or the precursor lesions. Fatty streaks are observed in the aorta and coronary arteries of most individuals by 20 years of age. The intimal thickening in fatty streaks is due to the accumulation of monocyte-derived macrophages filled with lipid (cholesterol esters) forming foamy cells [34].

Some fatty streaks, especially those involving the coronary arteries, have been shown to progress to the classic atherosclerotic plaques, as because of progressive lipid accumulation and migration and proliferation of smooth muscle cells. Some fatty streaks may regress, while others remain unchanged.

The pathogenesis of the atherosclerotic plaque involves the entry of LDL into the intima, where it binds to receptors of macrophages to form foam cells as described before. Once within the intima, LDL becomes chemoattractant to more blood monocytes and also causes macrophage aggregation, as well as further injury to the endothelium [34, 35].

Monokines from the activated macrophages also attract migration of smooth muscle cells from the media into the intima where they proliferate under the influence of platelet-derived growth factor (PDGF) and other cytokines released by endothelial cells, activated macrophages, and the smooth muscle cells themselves [36, 37].

Smooth muscles then modify into collagen fibers to form the fibrous component of the atheromatous plaque. By this fashion, fatty streaks progress into fibrofatty lesions or plaques. Instead of following a sequential pathway, the cells constantly interact and modify each other's behavior, forming plaques in one of many possible configurations.

The proportion of fibrous and fatty elements within the plaque varies from one lesion to another, i.e., some lesions are predominantly soft and fatty (with a thin fibrous cap and necrotic core), while others are largely hard and fibrous (with a thick fibrous cap). Beneath the cap is an accumulation of smooth muscle cells and macrophages containing lipid (foamy cells), as well as areas of necrosis (due to the toxic effects of oxidized extracellular lipid) and pools of lipid consisting of soluble cholesterol (cholesterol crystals). There is usually an associated chronic inflammatory infiltrate of lymphocytes and plasma cells. In large arteries (e.g., aorta), the lesions may appear as isolated or confluent plaques which eventually cover the entire intimal surface. In smaller arteries, however, e.g., coronary and cerebral, the involvement of the intima may be eccentric, reducing and pushing the lumen to one side, or it may be circumferential and concentric with a narrowed central lumen depending on the extent of intimal thickening. It is noteworthy that eccentric plaques may undergo outward plaque remodeling, which

can partly compensate for progressive growth of atherosclerotic lesions. However, such outward remodeling can possibly conceal angiographic diagnosis of large-sized plaques, and may be associated with an increased risk of plaque rupture [38].

Advanced or complicated plaques(space) may show ulceration, superimposed thrombosis (Fig. 9.5), or dystrophic calcification within the necrotic material in the intima. The size of the plaque determines the extent to which blood flow in the vessel is reduced. In the coronary artery, a plaque occupying >75% of cross-sectional area of the vessel (or >50% reduction of the lumen diameter) would cause significant interference with blood flow manifested as chronic ischemia in stable angina. Dynamic changes within the plaque may trigger fissuring or "rupture" of a thin fibrous cap (as in the vulnerable soft lipid plaque), thus exposing the circulating blood to potentially thrombogenic contents of the plaque. The clinical consequence of coronary plaque rupture depends upon a variety of elements. The site, i.e., proximal or distal, and caliber of the ruptured artery are crucial factors. Type of coronary circulation, i.e., right or left dominant circulation, will also influence the outcome. The nature of the composition of the ruptured plaque, i.e., soft fatty or hard fibrous, is another significant determinant factor. Finally, the presence of adequate collateral circulation at the area supplied by the ruptured vessel plays a very important role in such context.

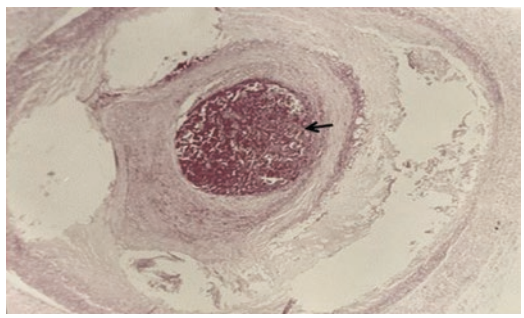

Fig. 9.5 Occluding recent thrombus (arrow) in a severely narrowed coronary artery by a predominantly fatty concentric atherosclerotic plaque

Ruptured plaque may result in luminal thrombus formation, with partial occlusion manifested by unstable angina or total (or near-total) occlusion leading to myocardial infarction or sudden death. Alternatively, a ruptured cap may admit blood inside the plaque causing intimal hemorrhage and/or intimal (intramural) thrombosis. Either of these may lead to rapid plaque enlargement, with the potential to occluding the lumen, partially or completely, as a result of pressure from inside the plaque. Ruptured plaque and subsequent intraluminal thrombosis may be also followed by organization of the thrombus and its incorporation within the plaque with further progressive arterial stenosis (thrombogenic theory). Furthermore, plaque erosion, or a small plaque fissuring may predispose to sudden coronary spasm without thrombosis, and the recognized manifestations of variant or Prinzmetal angina.

Extracellular matrix fortifies the fibrous cap(space) and (space) separates the thrombogenic plaque (space)core(space) from coagulating substrates within the circulation [39]. Macrophages, T-cells and their mediators play an important role in the pathogenesis of plaque rupture. Inflammatory signals alter collagen metabolism by reducing the synthesis and promoting the breakdown of collagen throughout the overproduction of matrix metalloproteinases (MMPs). In such conditions, the consequent thin and friable fibrous cap renders the plaque vulnerable to rupture and thrombotic complications. These inflammatory signals not only alter collagen synthesis and breakdown, but also increase the potential for thrombosis through excessive production of tissue-factor procoagulant. Such dual actions elucidate the strong association between inflammation and thrombosis in atherosclerosis [40].

Meanwhile, favorable effects of lipid lowering include reduction of the inflammatory signaling in plaques, with consequent reduction of the expression of MMPs, and increasing endothelial nitric oxide synthase. Coupled with the well-known anti-inflammatory effects of statins, low lipid levels seem to have a beneficial impact in stabilizing atherosclerotic plaques and reducing thrombotic potential [41].

Although it is essentially an intimal disease, atherosclerosis is frequently associated with thinning, atrophy and weakening of the media. This is due to indirect consequences of the intimal changes and can predispose to aneurysm formation. This is best seen in large arteries, e.g., abdominal aorta and iliac arteries. The adventitia also demonstrates neovascularization, arising from vasa vasorum, in addition to chronic inflammatory changes as a response to oxidized lipids within the plaque.

In summary, one or more of the risk factors, such as hypertension, diabetes mellitus, smoking, dyslipidemia, and others, can induce injury to the arterial endothelium, which promotes entry of LDL and monocyte-derived macrophages into the intima. This initial step is followed by a cascade of events that lead to the formation of the atherosclerotic plaque. Further evolution of changes within the plaque leads to increased intimal thickening with further arterial stenosis and chronic ischemic effects or acute plaque events resulting in acute ischemic episodes. Stages of atheroma include fatty streaks, atheromatous plaque, and complicated lesions, namely ulceration, thrombosis, and calcification. Diseases commonly associated with atherosclerosis result either from acute ischemia, e.g., myocardial infarction, stroke, and sudden death, or prolonged ischemic effects such as angina, chronic ischemic heart failure, vascular dementia, chronic renal ischemia, intermittent claudication, gangrene, among other chronic health impediments. Consequences of large-size arterial lesions, e.g., aorta, include aneurysm formation, which may lead to rupture or thrombo-embolic complications.

9.4.5 Ischemic Heart Disease

Ischemic heart disease (IHD) is a group of closely related syndromes due to myocardial ischemia, which means an imbalance between coronary blood supply and metabolic demands of the heart for oxygenated blood. In normal individuals, if the myocardial metabolic requirements are increased, even following forceful physical exertion, the oxygen supply to the heart matches such an upsurge, in order to maintain this balance [42].

Myocardial oxygen demand is proportionate to both the heart rate and myocardial contractility; when demand is increased both the rate and contractility are increased as well. Commonly referred to as coronary artery disease (CAD), IHD in the vast majority of cases, probably more than 98%, is due to advanced coronary atherosclerosis. Other minor causes include congenital ostium stenosis, arteritis, aneurysm, and thromboembolism. Two factors influence coronary artery flow: (a) coronary perfusion pressure and (b) coronary vascular resistance. The greatest coronary perfusion occurs during diastole, i.e., during myocardial relaxation to allow adequate coronary filling, which is unlike other arterial systems in the body. Hence, conditions that impair the aortic pressure, such as hypotension and aortic regurgitation, can have a negative impact on coronary perfusion.

Normally, physical or mental stress are associated with coronary vasodilatation. This is regulated by activation of the sympathetic nervous system, with enhanced blood flow and release of endothelial-derived vasodilators, such as nitric oxide (NO). The relaxation effect of NO seems to outweigh the direct constricting effect of catecholamines on arterial smooth muscle. Risk factors for atherosclerosis, such as hypertension, diabetes mellitus, smoking, and hypercholesterolemia, are associated with the diminished release of NO into the arterial wall, either because of impaired synthesis or due to excessive oxidative degradation. Diminished NO bioactivity may cause constriction of coronary arteries during physical or mental stress, thus contributing to myocardial ischemic injury. Additionally, diminished NO may facilitate vascular inflammation, thus promote oxidation of lipoproteins and foam cell formation in the pathogenesis of atherosclerosis [43].

In patients suffering from atherosclerosis, coronary perfusion is influenced by fluid mechanics, as well as the anatomy of the affected arteries. Fluid mechanics are essentially determined by the degree of coronary stenosis. From the anatomical point of view, distal intramural small-

caliber arteries are less affected by atherosclerosis, compared to proximal epicardial large coronaries, which display more frequent extents of atherosclerotic narrowing. Nevertheless, such small coronary vessels can play a significant compensatory role, by vasodilatation, in cases of proximal atherosclerotic narrowing. Thus, the hemodynamic impact of coronary stenosis is dependent upon the degree of epicardial proximal coronary stenosis, as well as the vasodilatation capability of the distal arteries. However, remodeling of plaques with outward expansion of the arterial wall allows sizable atheromatous lesions to reside in the walls of affected arteries without causing significant narrowing of the lumen. Thus, such plaques are undetectable on arteriograms and conceal warning symptoms or signs to both the patients and clinicians [41].

Although atherosclerotic plaques are usually developed over many years or even decades, they frequently produce clinical manifestations suddenly and without warnings. IHD may be manifested by a variety of presentations. The most popular form is through chest pain or "angina"; (Angina Pectoris = chest pain). Angina pectoris in its broad term is an uncomfortable feeling in the chest and neighboring anatomic structures produced by myocardial ischemia. Clinical presentation of coronary atherosclerosis can be gradual, as a result of progressive flow-limiting stenosis and exertional angina, or dramatic, with plaque rupture and thrombosis triggering unstable angina, myocardial infarction, (Figs. 9.6 and 9.7) or even sudden death. "Stable angina" is associated with stable coronary plaques of more than 75% cross-sectional stenosis and without acute coronary pathology, e.g., plaque rupture or thrombus formation. In such patients, pain occurs following physical exertion, i.e., increased demands. "Unstable angina," on the other hand, is a consequence of acute coronary lesions, mainly plaque rupture and subsequent thrombosis. However, the myocardial ischemia in such patients is not severe enough to cause permanent death of the myocardial cells. The third, less common form of anginal chest pain, is due to transient ischemia as a result of short-term coronary spasm and is known as "variant" or "Prinzmetal angina." A more severe clinical form of IHD is the "acute myocardial infarction" (MI). This follows severe, commonly occlusive, coronary thrombosis that results in an everlasting

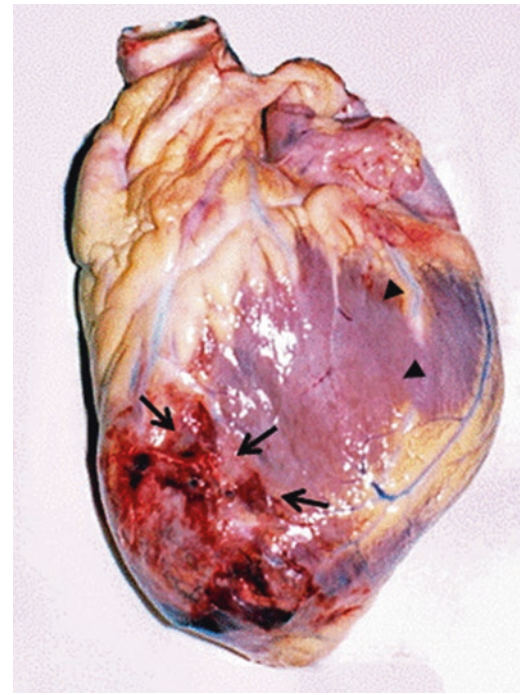

Fig. 9.6 Acute MI (Arrows) note the discoloration of the cardiac muscle with bloody spots compared to the adjacent viable muscle (arrow heads)

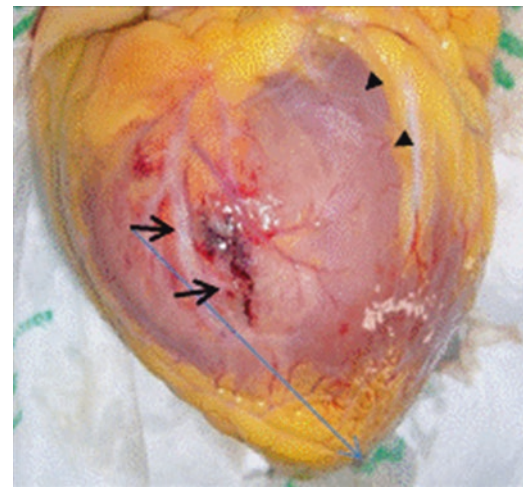

Fig. 9.7 Ruptured MI (arrows) of the anterior wall of the left ventricle. Note the adjacent viable cardiac muscle (arrowheads)

myocardial cell necrosis. Therefore, plaque rupture underlies most unstable angina, myocardial infarction, and sudden death due to IHD. Chronic IHD with CHF is the consequence of either chronic myocardial ischemia, in which there is scattered focal myocardial fibrosis following focal necrosis, or as secondary to the healing of an acute MI with replacement fibrosis [39].

9.4.6 Cardiomyopathies

Cardiomyopathy entails a diverse group of disorders with a primary myocardial dysfunction. Secondary myocardial changes, e.g., ischemic, hypertensive, valvular, etc., can lead to extrinsic cardiomyopathy, i.e., myocardial dysfunction with the primary pathology is not within the myocardium.

9.4.6.1 Dilated Cardiomyopathy

Dilated cardiomyopathy (DCM) is the most common form and accounts for almost 90% of cases. The etiology can be idiopathic and is possibly related to genetic, viral, or immunologic factors. DCM may also follow viral myocarditis with Coxsackie B virus, child birth, exposure to toxins or drugs e.g., cocaine, cobalt, or alcohol. The four cardiac chambers are markedly dilated, although areas of ventricular hypertrophy may be shown. Ventricular dysfunction is systolic as a result of impaired contractility. Thrombo-embolic complications are not uncommon. Functional mitral and tricuspid regurgitation are frequent consequences due to valve annular dilatation [44].

9.4.6.2 Hypertrophic Cardiomyopathy

Hypertrophic cardiomyopathy (HCM) is almost exclusively genetic [45].

It is characterized by asymmetric myocardial hypertrophy, particularly of the left ventricle. Thickness of the interventricular septum exceeds that of left ventricle free wall, and may cause obstruction of the blood flow in one third of the cases; a condition termed hypertrophic obstructive cardiomyopathy (HOCM). Diastolic dysfunction is due to ventricular stiffness and impaired compliance [46].

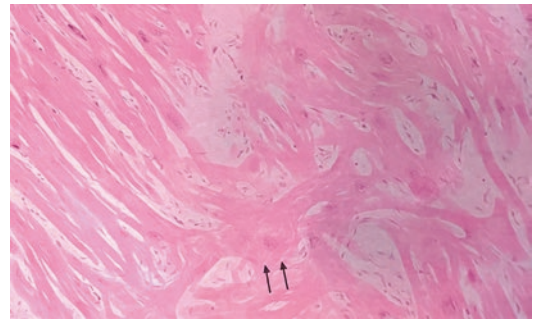

Fig. 9.8 Microphotograph of the myocardium illustrating the disarray of hypertrophied myocytes (arrows) in a case of HCM

Microscopically, the hallmark is the disorganized alignment or disarray of hypertrophied myocardial fibers (Fig. 9.8). Massive ventricular hypertrophy, high left ventricular pressure, and intramural coronary dysplasia (medial thickening and luminal narrowing) can lead to ischemic effects with anginal pain in the absence of coronary atherosclerosis.

9.4.6.3 Restrictive Cardiomyopathy

The restrictive cardiomyopathies are less common than DCM and HCM. The ventricles are abnormally rigid, but not necessarily thickened. This results in impaired cardiac filling with diastolic dysfunction, although the systolic function is usually normal [47].

There are two forms of restrictive cardiomyopathy; the first comprises a group of rare endomyocardial diseases which are of poorly understood etiology, including endomyocardial fibrosis (EMF), hypereosinophilic syndrome, and endocardial fibroelastosis (EFE). In EMF, the endocardium and the subendocardial layer of the myocardium display thickening with fibrotic plaques of variable extents. The second form is the infiltrative cardiomyopathy, with infiltration of the myocardium by an abnormal substance. The commonest cause of this form is amyloidosis. Other causes include sarcoidosis, radiation fibrosis, and hemochromatosis.

9.4.7 Pericardial Effusion

The pericardium is a sac surrounding the heart, composed of two layers, a layer on the heart (visceral pericardium) which is mesothelium, while the external portion (parietal pericardium) is mesothelium internally and fibrous externally. Normally, 15–35 mL of serous fluid surrounds the heart. The pericardium prevents the displacement of the heart and large vessels, prevents sudden dilatation of the heart, and the spread of infection or cancer from the pleura or lung as well as minimizes friction between the heart and surrounding structures [48]. Pericardial effusion is considered to be present when the amount of fluid in the pericardial space exceeds 50 mL. It may be presented as an incidental finding to a life-threatening emergency. Pericardial effusion can be associated with generalized processes not related to the pericardium, as the pericardium may be involved in a large number of systemic diseases (space) such as congestive heart failure, hypoalbuminemia, volume overload, and pulmonary hypertension or may be diseased, as an isolated process. The numerous causes of pericardial effusion can generally be divided into inflammatory and non-inflammatory etiologies (Table 9.3) [48, 49].

The most common causes are neoplastic, uremic, infectious, and idiopathic pericarditis. The hemodynamic consequences of pericardial effusion depend on the rate at which the effusion is developing and the compliance of both the pericardium and the ventricles. With significant increase in the pericardial fluid pressure, the filling pressure of both ventricles may decrease, which subsequently leads to a decrease in cardiac output. This condition is called pericardial tamponade and in severe cases is associated with a high mortality. Echocardiography is an excellent tool for the diagnosis and follow-up of pericardial effusion. The condition is also invariably seen with equilibrium radionuclide angiography (ERNA); however, an effusion of more than 400 mL is usually needed to be well recognized. The identification of pericardial effusion is important to be able to start an appropriate workup for this potentially lethal condition.

Table 9.3 Causes of pericarditis

A. Infectious
Viral (common), bacterial, parasitic, or fungal
B. Non-infectious
Auto immune diseases
Cancer
Metabolic conditions (e.g. end stage renal disease)
Trauma, direct and indirect (e.g. post-myocardial infarction, post-pericardiotomy, penetrating injury)
Drugs (e.g. chemotherapy)
Miscellaneous: amyloidosis, chronic heart failure. Idiopathic

[49–51]

9.5 Correlative Scintigraphic Evaluation of Cardiac Diseases

9.5.1 Evaluation of Ventricular Function

Radionuclide techniques including first pass, equilibrium blood pool, gated myocardial SPECT provide both accurate and noninvasive means of evaluating cardiac function with simple indices, such as left ventricular volumes and ejection fraction (LVEF). It provides diagnostic and prognostic implications in the spectrum of cardiac diseases [52].

Although most ventricular function studies are performed with the patient at rest, exercise functional studies can also be done to assess regional and global myocardial contraction changes with stress. The cardiac information obtained by these methods is summarized in Table 9.4 [53].

Nuclear medicine techniques are accurate and reproducible for cardiac function evaluation.

Table 9.4 Information obtained by radionuclide evaluation of ventricular function

1. Global left and right ventricular ejection fraction
2. Regional right and left ventricular function
3. Absolute ventricular volumes
4. Systolic emptying and diastolic filling rates
5. Detection and quantitation of cardiac shunts

They provide important information that is useful in the diagnosis and management of the following clinical situations: assessment and prognosis of congestive heart failure, monitoring drug therapy and exposure to cardiotoxins and also for diagnosis of coronary artery disease. Echocardiography made the utilization of gated blood pool studies more limited [54].

The left ventricular (LV) ejection fraction is the preferred parameter applied for the noninvasive evaluation of LV systolic function in clinical practice. It has an established and important extensive role in the clinical management of numerous cardiac conditions.

9.5.1.1 Equilibrium Radionuclide Angiography

Radiopharmaceuticals. Studies with radiopharmaceuticals require the use of an intravascular tracer that equilibrates within the blood pool. The ease with which ^{99m}Tc-pertechnetate can be attached to the patient's own red blood cells (RBCs) makes labeled RBCs the preferred technique over labeled pooled human serum albumin. The usual adult dose is about 30 mCi. Three methods of labeling the RBCs are commonly used: in vivo, modified in vitro, and in vitro. The characteristics of each method are described below. All three methods allow the ^{99m}Tc to bind irreversibly to the hemoglobin and remain in the intravascular space, allowing serial studies to be performed for up to 6–8 h following labeling of the RBCs [55].

In Vivo Technique. The patient first receives stannous pyrophosphate intravenously. The stannous ion (tin) enters the RBCs and creates the optimal oxidation-reduction environment for reduction and binding of the ^{99m}Tc-pertechnetate, which is injected intravenously 15–20 min later. Once the ^{99m}Tc-pertechnetate is in the RBCs, it is trapped inside by strong binding to the beta chain of the hemoglobin. Approximately 70–80% of the ^{99m}Tc is attached to RBCs, but in some patients as little as 50% or less may be attached. This makes identifying the edges of the blood pool during processing and analysis more difficult. In some laboratories, this method is used only when a first-pass study precedes ERNA or the patient has limited venous access. The major advantages of this method are the simplicity of use, shorter labeling time, and lower cost.

Modified In Vitro Technique. This technique is used by many laboratories because it is easier to perform than the in vitro technique and results in a higher labeling efficiency than the in vivo method. As in the previous method, stannous pyrophosphate is first injected intravenously. The blood is then drawn from the patient into an anticoagulant acetate dextrose solution (ACD) or a heparin-treated, lead-shielded syringe containing ^{99m}Tc-pertechnetate. Subsequently, the syringe is placed in a mechanical rocker or rotated slowly by the technician for 10–15 min, and the RBCs are then reinjected into the patient. Labeling efficiency is usually greater than 90%. This method offers the best compromise between ease of use and high labeling efficiency. Total labeling time averages 30 min.

In Vitro Technique. The labeling efficiency of this method approaches 100%. Patient blood is drawn and the RBCs are separated, washed with saline, and incubated first with stannous pyrophosphate and then with ^{99m}Tc-pertechnetate. The cells are washed with normal saline before and after each step to eliminate unbound material. Finally, the labeled cells are reinjected into the patient with very little or no free ^{99m}Tc-pertechnetate. The average labeling time is slightly more than 30 min. This technique also requires handling blood during multiple steps and using needles to inject blood into sealed vials.

RBCs from patients receiving heparin therapy are sometimes difficult to label, and in such cases the use of ACD as an anticoagulant is preferred to increase the labeling efficiency. Inadequate anticoagulation or too aggressive shaking of cells may cause thrombus formation and result in hot spots in the lungs. Likewise, stannous pyrophosphate can be oxidized by water in glucose solutions, and this may lead to poor RBC labeling.

Image Acquisition

Assessing ejection fraction and regional wall motion requires measurement of volume changes and wall motion at different intervals throughout

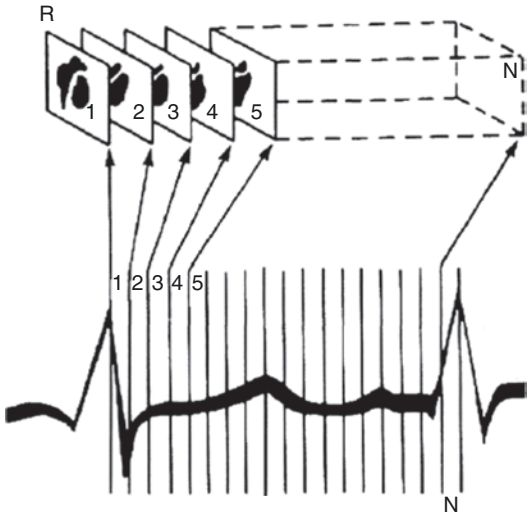

Fig. 9.9 Method by which the computer generates multiple gated images. The cardiac cycle is divided into a preselected number of frames of equal duration. Scintigraphic data from successive beats are placed into separate parts of the computer memory, depending on the temporal relation of the scintigraphic data to the R-wave marker (R). For each frame (*1*…*N*), scintigraphic data from successive beats are accumulated either until a preset time is reached (e.g., 2 min for exercise scintigraphy) or until the average cardiac image contains a predetermined number of counts (e.g., 200,000 counts for typical resting studies). (Reproduced with permission from Berman et al. [56])

the cardiac cycle. Acquisition of multiple timed images of the blood pool activity in the heart will then be triggered by each R wave (Fig. 9.9). The duration of every frame may be 1–60 ms. Multiple beats are acquired to obtain adequate counts in each frame, and typically a complete radionuclide ventriculographic study will consist of 200–800 summed beats for each of the three planar views [53] (Fig. 9.10).

A minimum of three different views of the heart are needed to assess all walls of the LV as well as all four cardiac chambers. The best septal views are left anterior oblique (LAO), anterior (ANT), which is 45° to the right from LAO, and left lateral (LLT), which is 45° to the left of LAO. Following labeling of the RBC pool, the LAO view is obtained first, as this view allows the best quantitation of the ejection fraction. In the LAO view, the camera is positioned so that the RV and LV are well separated. The other views are obtained for a similar number of counts as the LAO view. The closer the head of the camera is to the patient, the better the spatial resolution of the images. A 10° caudal tilt is used in the LAO view to minimize overlap of the left atrium (LA) and LV counts. Alternatively, a slanted hole collimator may be used to give optimal separation while allowing the camera head to be closer to the patient on the LAO view. The general all-purpose (GAP) collimator offers a compromise between the high-resolution and high-sensitivity collimators and is the one most frequently used in clinical imaging. A dedicated computer system is required to acquire, store, and process the information.

Studies may be acquired for a fixed number of heartbeats or for the total counts in the complete study. Fixed-beat studies usually acquire 200–800 individual beats, and the time of acquisition is dependent on the heart rate. Fixed-count studies usually require six million counts for the entire study or they may be acquired until a fixed number of counts are reached within each image or in the LV region.

Modes of Acquisition

There are three possible modes of acquiring ERNA: list, frame, and dynamic arrhythmia filtration. Each method has its advantages and disadvantages, as described below and summarized in Table 9.5.

List Mode. During acquisition the computer records the spatial location of each photon, the ECG gating signal, and rimming markers, usually every millisecond. Following acquisition, each individual beat can be reviewed to eliminate atrial or ventricular premature beats that exceed a determined R-R interval duration (arrhythmia rejection). The acceptable beats can then be framed in the most appropriate timing interval for the type of analysis that is needed.

Frame Mode. Prior to starting frame mode acquisition, the patient's heart rate is sampled for 10–20 s, and the mean R-R interval is used to set the time limits or window for acceptable sinus beats. For clinical studies, beats 10% shorter or longer than the mean R–R interval are rejected as possible premature beats. The beat following the early rejected beat is also rejected, as it has a pro-

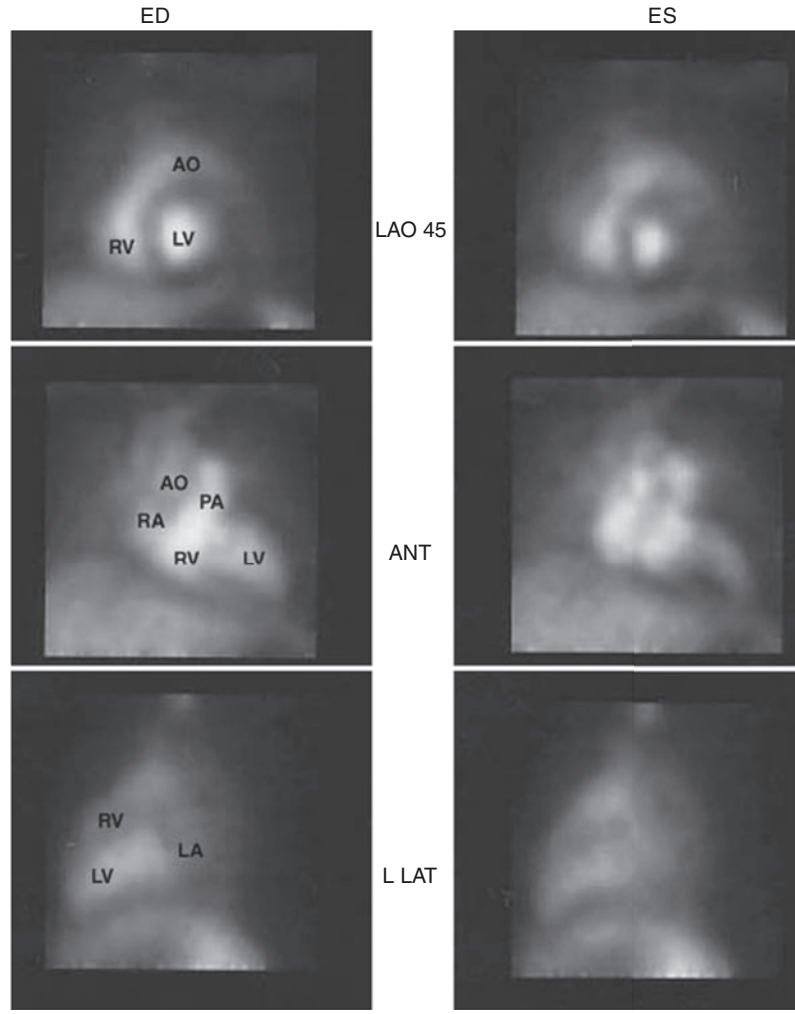

Fig. 9.10 Example of a normal gated blood pool study. The pictures on the *left* represent end-diastolic (*ED*) frames, while the images on the *right* represent end-systolic (*ES*) frames. The main structures are identified in each projection: *AO* aorta, *RV* right ventricle, *LV* left ventricle, *RA* right atrium, *PA* pulmonary artery, *LA* left atrium

longed filling interval and will result in a higher ejection fraction. Frame mode studies are generally acquired for 16–32 frames. It is extremely important that patients be in a resting state during the heart rate sampling prior to starting acquisition and throughout acquisition. Major shifts in heart rate will cause many beats to be rejected and prolong the acquisition.

Dynamic Arrhythmia Filtration. This technique allows the acquisition parameters (duration of each frame, percent R-R variability allowed for beat rejection, and total number of frames) to be set at the beginning of acquisition. Once acquisition starts, each beat is placed in a temporary memory buffer where it is examined with regard to the preset parameters. If it meets all criteria, it is accepted and included in the final data set. If it does not meet all the criteria, it is rejected. Thus, greater flexibility in beat selection is possible than with frame mode, but without the memory requirements and longer processing time required by list mode acquisition.

Regardless of the method of acquisition used, it is important to confirm that only the R wave from the ECG signal is detected as the trigger signal and as appropriately gating the acquisition. This can be done by examining an ECG rhythm strip and identifying the triggering signal. Gating may sometimes occur incorrectly on the P-, T-, or R-wave signal as well as muscle artifact and pacing spikes from artificial pacemakers. If this occurs, the lead placement needs to be changed

Table 9.5 Comparison between the different modes of computer acquisition

Mode of acquisition	Advantages	Disadvantages
List mode	Optimal temporal resolution	Intensive memory requirement
	Excellent arrhythmia rejection	Longer processing time
Frame mode	Easy setup	Count drop-off
	Minimum memory	Fixed temporal resolution
		Poor arrhythmia rejection
Dynamic arrhythmia (buffered beat) mode	Flexible temporal resolution and arrhythmia rejection	Longer setup for greater options
	Less memory than list	
	Accurate systole/diastole	

or the voltage amplitude adjusted to avoid inappropriate gating [56].

Simple LV ejection fraction calculations (Fig. 9.11) usually require time intervals of 40–50 ms to adequately define the end-systolic point in the heart cycle, where the heart has the smallest volume. For analysis of diastolic function, timing intervals of 10–20 ms give the most reliable information for the ventricular filling portion of the heart cycle. Even with list mode and dynamic arrhythmia filtration, there is still slight R-R interval variability that can lower the counts and distort the last few frames of the time-activity curve. This count drop-off does not affect ejection fraction calculation but is deleterious for diastolic function analysis. This limitation can be overcome by generating separate forward and backward time-activity curves and combining them in a final curve for analysis.

Patients in atrial fibrillation have variable diastolic filling intervals, and this results in a different ejection fraction for each beat. LV ejection fraction measurement by ERNA during atrial fibrillation has been shown to be an accurate reflection of the summed ejection fraction of each of the individual bats. Thus, it is an accurate reflection of overall ventricular systolic function [55].

Contrast ventriculography and echocardiography will sample only a few beats for ejection fraction calculation and may be less representative of true function.

9.5.1.2 ECG-Gated Myocardial Perfusion SPECT

Gated myocardial perfusion SPECT studies provide information on both myocardial perfusion and ventricular function. Quantification of gated SPECT images provides a global LVEF, plus indices of regional wall motion and wall thickening, useful in the evaluation of ventricular function and LV dyssynchrony that occurs with primary contractile dysfunction [57] (see later). Recently, a low-dose SPECT (as low as 8 mci) gated bloodpool SPECT for quantification of LV function was used [58, 59]. The low-dose ^{99m}Tc-RBC imaging method was proved to provide precise quantification of LV function and resulted in the most consistent assessment of LV function compared with the gold standard high-dose ERNA method, along with excellent inter-observer reproducibility with a greater than 67% reduction in radiation dose [58].

9.5.2 Evaluation of Myocardial Perfusion

9.5.2.1 Myocardial Perfusion SPECT Imaging

Clinical manifestations of coronary artery disease include angina pectoris, myocardial infarction, congestive heart failure, and sudden death. It may be asymptomatic until advanced in severity or complications. Most diagnostic methods, both invasive and noninvasive, depend on the detection of luminal narrowing of the epicardial coronary vessels. Vessel narrowing of up to 75% of the cross-sectional area (or <50% of luminal narrowing) does not affect the resting coronary flow. Increase of coronary flow caused by exercise or pharmacological stress exaggerates flow nonuniformity, through either increased metabolic demand or vasodilation [60].

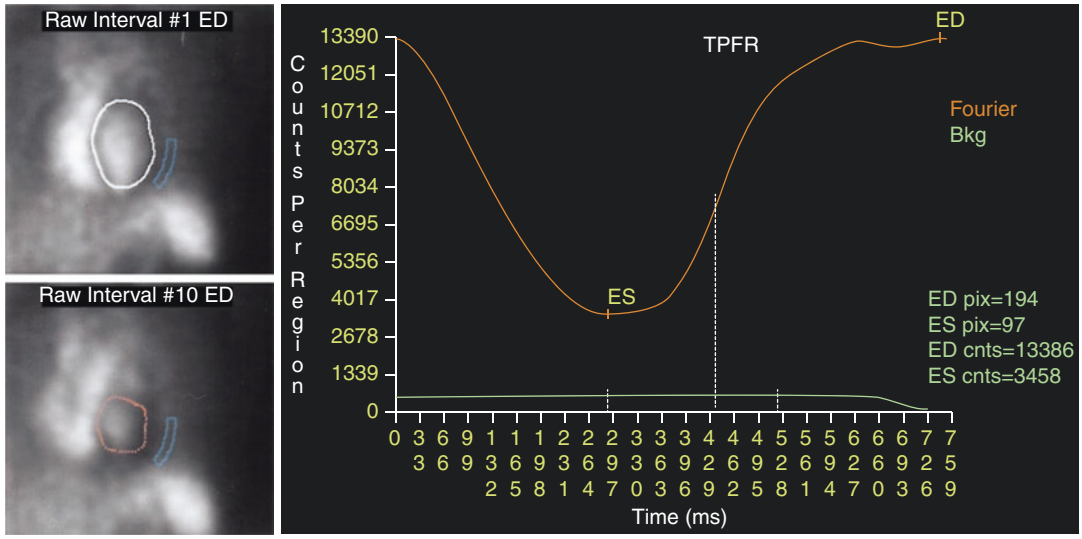

Fig. 9.11 Ejection fraction calculation of an LAO radionuclide ventriculogram. Shown are left ventricular edges as determined by an automated computer algorithm for end diastole (*top left*) and end systole (*bottom left*), chosen area for background subtraction, volume curve (*right*), and ejection fraction (60%) of the left ventricle. Specific information on heart rate and time/frame is also provided

The easiest method of increasing coronary flow is physical exercise, using a motorized treadmill or a stationary bicycle. In patients who are unable to exercise adequately, pharmacological agents are used for transient elevation of coronary flow.

SPECT Radiotracers

The ideal tracer of coronary flow would be extracted by the myocardium with 100% efficiency, like microspheres. Its myocardial uptake would be linearly related to coronary flow, and the tracer isotope would have optimal emission photon energy for imaging with a gamma camera. Currently, this ideal tracer is not present and two classes of tracers are widely used for conventional MPI: thallium-201 and the Tc-99m-labeled tracers.

Thallium-201

Thallium-201 (Tl-201) has been in clinical use for decades. Tl-201 is a metal in group III-A of the periodic table and, as an isotopic cationic tracer, has properties similar to those of potassium. Tl-201 is extracted with a high extraction fraction by the ATPase-dependent Na^+/K^+ channels (Table 9.6). Diagnostic and prognostic data on Tl-201 are extensive. An advantage of Tl-201 is the ease of use since one injection only is needed (Fig. 9.12). Tl-201 is the preferred radiotracer for evaluation of myocardial viability among the conventional SPECT agents. Major drawbacks of Tl-201 include low energy of its principle X-ray photons (69–80 keV) and its long half-life (72 h), which limits the injected dose, due to its relatively higher radiation dose to the patient. The limited dose leads to suboptimal image quality due to noise [61].

Tc-99m Sestamibi and Tc-99m Tetrofosmin

Tc-99m sestamibi (MIBI) and Tc-99m tetrofosmin have shorter physical half-life of Tc-99m (6 h) allowing the use of higher tracer doses (up to 50 mCi/day) (Table 9.6). Combined with the more optimal photon energy for gamma camera imaging (140 keV) compared with Tl-201, image quality is less noisy, and frequency and severity of attenuation artifacts are decreased. Negligible washout of Tc-99m-based tracers [62] requiring the use of two separate tracer injections: one for rest imaging and one for stress imaging. SPECT imaging is usually started 20–60 min after tracer injection. The delay is needed for blood pool

Table 9.6 Radiotracers for SPECT myocardial perfusion imaging

	Thallium-201	Tc-99m sestamibi	Tc-99m tetrofosmin
Brand name	N/A	Cardiolite	Myoview
Class	K^+ analog	Isonitrile	Diphosphine
Preparation	Cyclotron	Kit (heated)	Kit (cold)
Charge	Cation	Cation	Cation
Lipophilicity	Low	High	High
Redistribution	Yes	Minimal	Minimal
Tissue clearance	50%/4 h	>6 h	>6 h
Excretion	Renal	GI (renal)	GI (renal)
Time of imaging (min)	5–10	20–60	10–45
Completion time (h)	4–6	3–4	3–4
Counts	Adequate	High	High
SPECT	Yes	Yes	Yes
Extraction	0.85	0.39	0.24
Gating	±	Yes	Yes
Heart-liver (1 h)	2.6	1.2	1.4
TEDE (rem/3.5 mCi)	2.1	1.1	0.8
Clinical use			
Diagnosis	Yes	Yes	Yes
Prognosis	Yes	Yes	Yes
Viability	Yes	Yes	Yes

[a] *N/A* not applicable

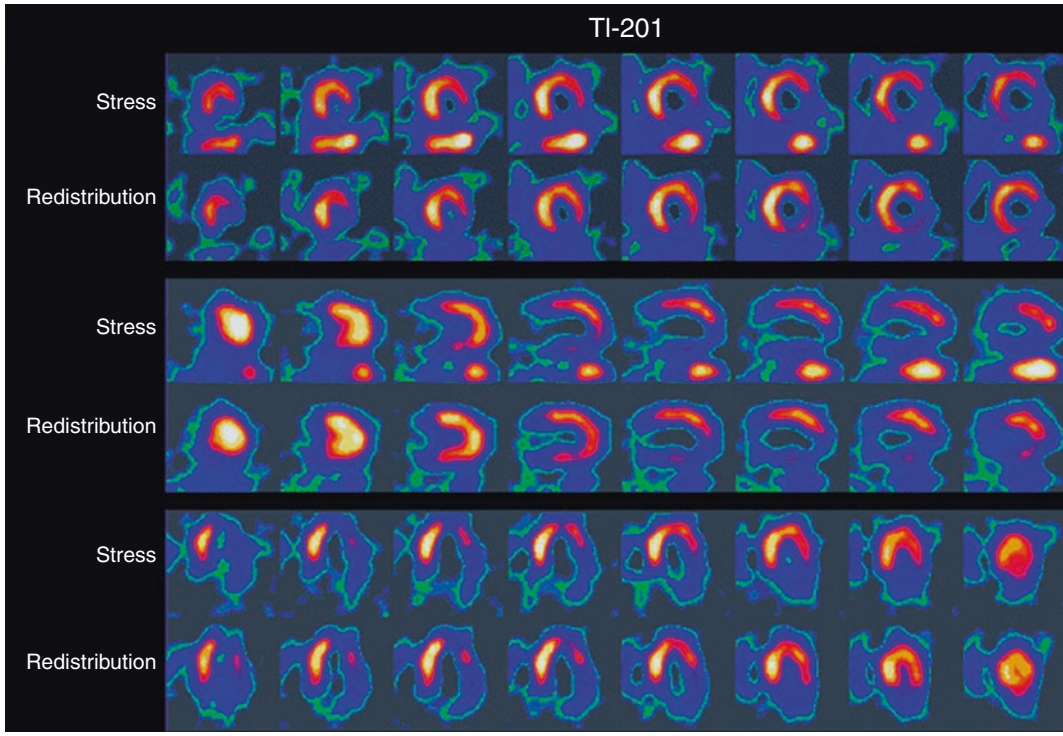

Fig. 9.12 Thallium-201 stress and redistribution images of a patient showing a severe fixed inferolateral defect; a severe, partially reversible basal inferolateral defect; a reversible basal inferoseptal defect; and a mild to moderate reversible anterolateral defect

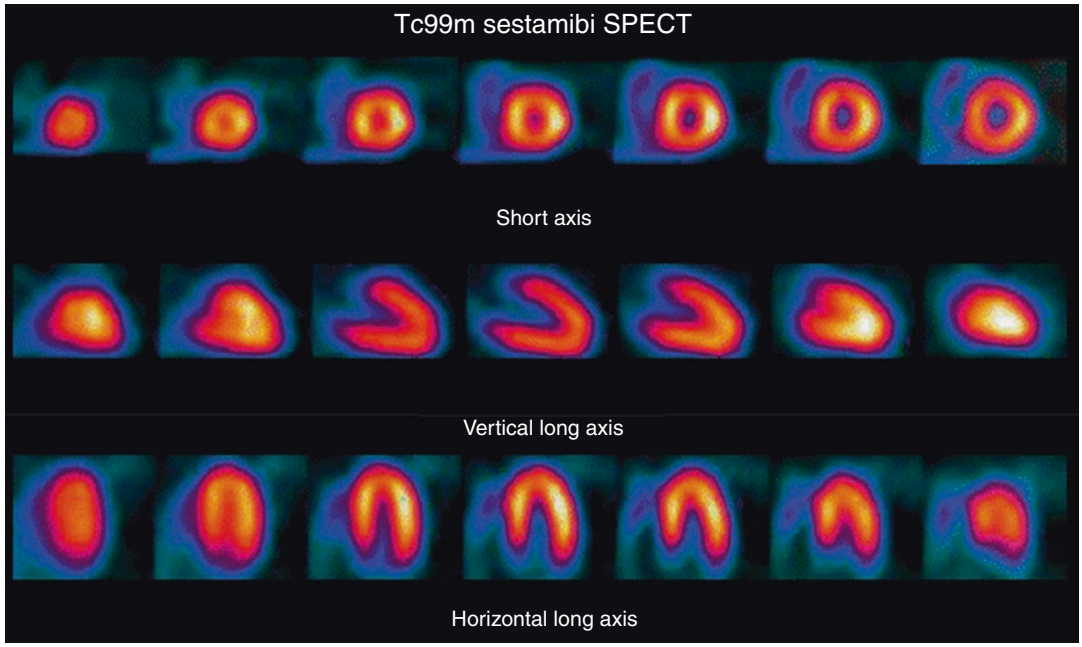

Fig. 9.13 Normal stress Tc-99m sestamibi myocardial perfusion SPECT images in short axis, vertical axis, and horizontal long. There is homogeneous distribution of the radiotracer in the left ventricular wall. The short axis views have a doughnut shape distribution of radioactivity, while the horizontal and vertical long axis views are like a horse shoe. These views depict different parts of the left ventricle: apex, anterior wall, septum, lateral wall, and inferior wall, as well as the right ventricle. Gated images show uniform motion and thickening of ventricular walls with left ventricular ejection fraction (LVEF) greater than 50%. Left ventricular end-diastolic and end-systolic volumes were within normal limits. There is mild uptake in the normal right ventricle

clearance and partial liver clearance (Fig. 9.13). Gating of Tc-99m sestamibi or Tc-99m tetrofosmin images made possible because of the high photon flux, allows simultaneous evaluation of perfusion and function.

Excretion of the Tc-99m tracers is through the hepatobiliary and, to a lesser extent, renal systems. High subdiaphragmatic uptake in the liver or intestines occasionally interferes with the evaluation of cardiac perfusion.

In an attempt to utilize advantages of both types of tracers, dual-tracer protocols were developed: Tl-201 is injected at rest, and rest imaging is started within 15 min. Exercise or pharmacological stress is followed by Tc-99m MIBI or Tc-99m tetrofosmin injection at peak stress. The test is completed in less than 3 h [63].

A drawback from the different pharmacokinetic properties of the tracers results in nonparallel flow-uptake relationships and different spatial contrast due to different isotope energies.

Tc-99m teboroxime was another perfusion agent that was marketed. This highly lipophilic agent readily crosses myocardial cellular membranes but, unlike MIBI, rapidly diffuses out of the cells in 6–10 min, allowing only a few minutes for imaging [64].

It requires separate rest and stress injections. There is some evidence that the differential washout rate of Tc-99m teboroxime obtained from stress-redistribution images can differentiate between ischemic and infarcted myocardium [65].

One advantage of teboroxime is its very high extraction fraction, which is higher than any of the other conventional SPECT agents at high flow rates during pharmacological vasodilation. Due to the demanding rapid imaging protocol required, its use never became extensively applied, in spite of examples of good quality images obtained with either multiheaded or single-headed gamma cameras in some laborato-

ries. Its commercial availability has been stopped for years.

99mTc-3SPboroximine is a newer perfusion radiotracer since its cardiac uptake is largely relies on the regional blood flow. It can be used for the detection of perfusion abnormalities, accurate quantification, and determination of regional blood flow rate [66–68].

Methods of Stress

Exercise Stress

Exercise stress is the most frequently used test for noninvasive diagnosis of coronary artery disease (CAD). This form of stress is usually performed with exercise protocols using either a treadmill or bicycle. Exercise is associated with sympathetic stimulation and changes in coronary vasomotor tone which affects coronary blood flow through dilatation of coronary arteries. Exercise results in increase in myocardial oxygen demand and coronary vasodilation allowing increased oxygen delivery which is crucial to myocardial perfusion to prevent ischemia. This hyperemic effect is behind the identification of ischemia, as stenotic vessels do not vasodilate efficiently [69].

Sensitivity of a symptom-limited exercise treadmill test (ETT) for the diagnosis of CAD is 65–70% [70].

When combined with myocardial perfusion imaging, the sensitivity increases to 85–90%, while specificity is increased as well [61]. This combination of results also provides the best prognostic value and risk stratification for patients with coronary artery disease [71].

ETT evaluates the hemodynamic changes and provides independent prognostic information including total exercise time and capacity, heart rate response, blood pressure response, and symptoms during stress [71]. Systolic blood pressure is expected to increase during stress to maintain adequate cardiac output. Any drop in blood pressure during exercise may indicate the presence of coronary artery disease and, therefore, poor prognosis and outcome [72, 73]. Heart rate is also expected to increase during the exercise preferably up to 85% of the maximum age predicted heart rate (MPHR) which can be calculated by subtracting the patient age from 220 [74]. However, achievement of 85% of MPHR is not an indication for termination of the test and ETT should rather be symptom-limited. Slow heart rate during exercise can be normally seen in athletes. On the other hand, heart rate that is slow to return to baseline during recovery may indicate inability of the heart to recover from this increased demand resulting in exercise intolerance. This can be seen in patients with coronary artery disease and congestive heart failure and is considered as an independent predictor of risk for major cardiac events [71]. Metabolic equivalent (MET) is another parameter that is routinely recorded during exercise. One MET equals about 3.5 mL of oxygen/kg of body weight [72]. This parameter can be used to assess the functional status of patients and help in treatment options by categorizing patients into three classes. Class I patients can exercise beyond 7 or 8 METs, class II patients get symptom-limited exercise at 5 or 6 METs, while class III patients get symptom-limited exercise at 3–4 METs. Healthy people can usually exercise beyond 10–11 METs [71].

The single most powerful prognostic predictor in both men and women is the exercise capacity (length of the exercise) [75].

Pharmacological Stress

Patients who cannot exercise for noncardiac reasons (e.g., orthopedic, neurological, peripheral vascular) or are unable to exercise adequately (for a meaningful period of time and/or to an adequate heart rate) are candidates for pharmacological stress testing. Five agents are currently approved for use in conjunction with MPI: adenosine, dipyridamole, regadenoson, dobutamine, and arbutamine. Adenosine, dipyridamole, and regadenoson are coronary vasodilators. Dobutamine and arbutamine are beta-adrenergic agonists and increase myocardial oxygen demand; they also have some direct vasodilatory effect [76].

Pharmacological stress makes possible evaluation of patients unable to exercise for noncardiac reasons, including sick and debilitated patients. However, physiologically useful param-

eters derived from an exercise test, valuable for a comprehensive evaluation, are lost.

Adenosine

Adenosine is an endogenous coronary vasodilator produced from ADP and AMP in myocardial and vascular smooth muscle cells. Adenosine affects two kinds of receptors: A1 and A2. Activation of the A1 receptor slows AV conduction. Activation of the A2 receptor leads to coronary vasodilation (Fig. 9.14, Table 9.7). The half-life of adenosine is extremely short (seconds only). Perfusion tracers are therefore injected during continuous adenosine infusion (140 μg/kg/min for 6 min). Side effects of adenosine include flushing in 37% of patients, chest pain in 35%, shortness of breath in 35%, and gastrointestinal symptoms in 15%. Chest pain is not indicative of myocardial ischemia. Vasodilation causes a modest blood pressure drop, usually accompanied by compensatory tachycardia, although transient second-degree AV block is seen in 3–4% of patients and third-degree AV block in <1% of tested patients. All side effects and hemodynamic changes are transient and reversible. Use of an antidote (IV aminophylline) is very rarely needed. Most situations can be controlled by decreasing the infusion rate and/or by shortening the duration of the infusion. Adenosine may trigger bronchospasm and should not be used in patients with bronchospastic disease, particularly those who have clinical asthma and/or are being treated with bronchodilators. Caffeine, theophylline, and their metabolites competitively block adenosine receptors. Therefore, patients should abstain from caffeine-containing beverages and medication for 12–24 h prior to the test [74].

Dipyridamole

Dipyridamole is an indirect vasodilator: It increases intravascular concentration of endogenously produced adenosine by blocking its cel-

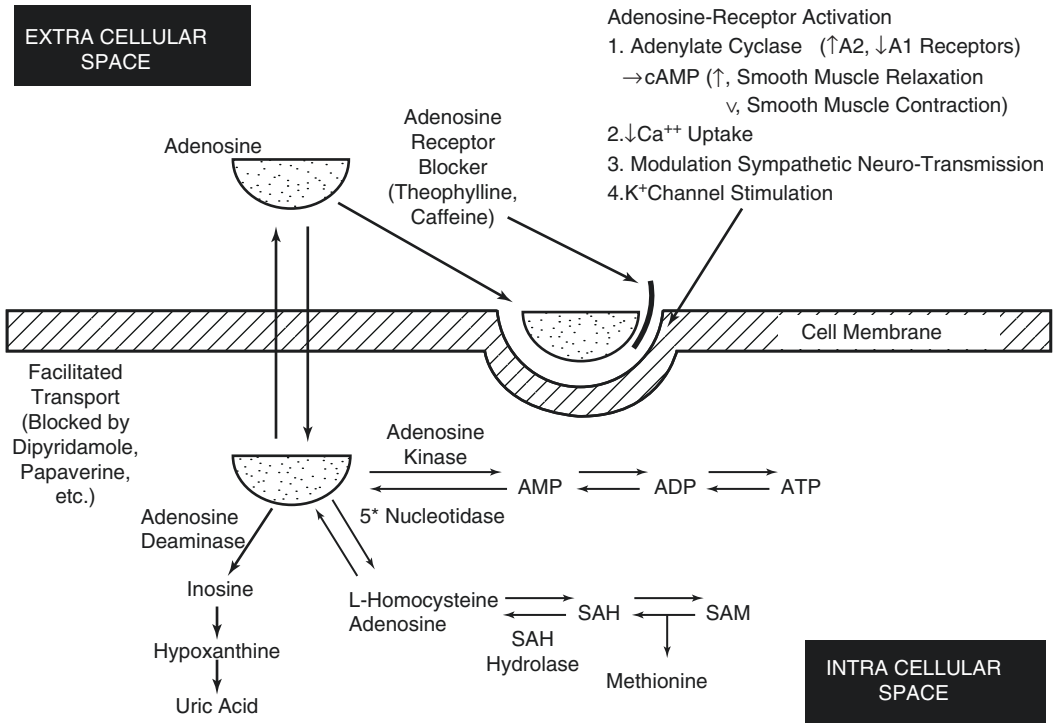

Fig. 9.14 Mechanisms of the vasodilating stress agents. Adenosine is synthesized intracellularly and leaves the cells to act on surface membrane receptors. Dipyridamole blocks adenosine reentry into the cell, increasing extracellular adenosine that can bind to the receptor. Methylxanthines, such as theophylline and caffeine, competitively block the receptor sites. (Reproduced from Iskandrian et al. [77] with permission)

Table 9.7 Main coronary vasodilators

	Adenosine	Regadenoson	Dipyridamole
Effect	Direct	Direct	Indirect
Half-life	<10 s	8.5 min	Minutes
Onset of action	Seconds	Seconds	Minutes
Time to peak effect	ca. 1 min	20–40 s	ca. 7 min
AV block	7%	3%	0%
Diagnostic utility	Inability to exercise	Inability to exercise	Inability to exercise
Contraindications	Bronchospasm		Bronchospasm
	Unstable/severe ischemia	Unstable/severe ischemia	Unstable/severe ischemia

lular reuptake (Fig. 9.14). Dipyridamole has a longer half-life than adenosine and does not affect AV conduction. Dipyridamole is usually infused for 4 min. The perfusion tracer is injected at 7 min. In some laboratories, the patient is asked to perform low-level exercise or handgrip exercise to enhance its effects. Contraindications for dipyridamole use are similar to those for adenosine, although chest pain is less frequent. An effective antidote is IV aminophylline (50–100 mg IV), which can be used to normalize hemodynamic changes, relieve ischemia, and/or treat side effects [74].

Dipyridamole potentiates the effects of exogenously infused adenosine. Therefore, oral dipyridamole, when being taken for its antiplatelet effects, should be discontinued on the day of the stress test.

Regadenoson

The first historically available vasodilator stress agents, dipyridamole and adenosine, are effective and useful, but they do have significant side effects, making stress testing an unpleasant experience in many patients, and are contraindicated in patients with bronchospastic disease. It has been established that there are four adenosine receptor subtypes distributed in various locations: A_1, A_{2A}, A_{2B}, and A_3. The selective activation of A_{2A} receptors leads to coronary vasodilation, while A_1 are responsible for decreased AV conduction and chest pain, while the stimulation of A_{2B} receptors leads to peripheral vasodilation, mast cell degranulation, and bronchiolar constriction, and the stimulation of A_3 leads to ischemic preconditioning and mast cell degranulation [78].

Regadenoson is an A_{2A} receptor agonist that is a coronary vasodilator with very weak affinity for A_1, A_{2B}, and A_3 receptors that are associated with adenosine's unpleasant side effects. It is supplied in prefilled syringe doses of 0.4 mg in 5 mL of solution. It is administered as a single-dose bolus (less than 10 s), which leads to increased coronary blood flow to more than twice baseline levels within 30 s, with maximal vasodilation 1–4 min after injection, and decreases to less than twice baseline within 10 min. This is accompanied by decrease in systolic and diastolic blood pressure and increase in heart rate [79].

In the ADVANCE MPI multicenter trial comparing myocardial perfusion imaging with regadenoson compared to adenosine pharmacological stress, it was demonstrated that regadenoson was similar to adenosine for the detection of ischemia [79].

Methylxanthines block the effects of regadenoson, as for adenosine. Patients should be instructed to avoid consumption of any products containing methylxanthines, including caffeinated coffee, tea, and other caffeine-containing beverages of drug products for at least 12 h prior use. In clinical trials conducted during regadenoson's development, where side effects were compared to adenosine, 80% of subjects had some kind of adverse reaction, including dyspnea (28%), headache (26%), flushing (16%), chest discomfort (13%), angina or ST segment depression as evidence of myocardial ischemia (12%), dizziness (8%), chest pain (7%), and nausea (6%). In most categories, this profile was similar to side effects from adenosine, except for a lower rate of chest discomfort (13% vs. 18%) or evidence of ischemia (12% vs. 18%). There was a

similar rate (26% vs. 30%) of rhythm or conduction abnormalities, but a lower rate of first-degree block (3% vs. 7%) or second-degree AV block (0.1% vs. 1%). There was a higher rate of respiratory adverse reactions, such as dyspnea or wheezing compared to placebo (12.9% in the asthma group and 19% in the COPD patient group), but most respiratory adverse reactions resolved without therapy. Aminophylline was used 3% of the time to treat side effects from regadenoson, versus 2% for adenosine. As for dipyridamole and adenosine, serious ischemia, leading to myocardial infarction, ventricular arrhythmias, and cardiac arrest, has occurred following regadenoson injection [80].

Dobutamine and Arbutamine

Dobutamine is a synthetic catecholamine with predominantly β1 affinity and short plasma half-life (approximately 2 min). In the presence of significant epicardial coronary artery stenosis, the increase in oxygen demand caused by positive inotropic and chronotropic effects of dobutamine can induce myocardial ischemia. Additionally, dobutamine at higher doses induces coronary vasodilation. The infusion rate used for diagnostic imaging (40–50 μg/kg/min) is higher than the customary therapeutic infusion rate of dobutamine (10–20 μg/kg/min) used for inotropic support in the intensive care units. The side effects of dobutamine in our patient series included supraventricular and ventricular arrhythmia (6% of patients), palpitations (40%), chest pain (20%), shortness of breath (17%), headache (15%), and GI symptoms (5%). Dobutamine was used mostly in patients who are unable to exercise and have bronchospastic disease [81], but its use has decreased since the introduction of the selective A_{2A} vasodilator agonist regadenoson.

Arbutamine is also a synthetic catecholamine. It has been marketed with a computerized feedback system between arbutamine infusion rate and the heart rate. This approach attempts to minimize the time required to reach a selected peak heart rate. However, added complexity and expense of this approach limited its widespread use [81].

Combined Exercise and Pharmacological Stress

Many laboratories have found it useful to combine low-level treadmill exercise with either adenosine, regadenoson, or dipyridamole. This has been found to reduce the unpleasant side effects of flushing, headache, dizziness, or nausea due to either stressor. Image quality is also improved through a decrease in hepatic and gut uptake of the technetium-99m perfusion tracers, which is more common with adenosine or dipyridamole, compared to exercise [82].

On the other hand, the incidence of stress-inducible ischemia is more common due to increased myocardial demand, leading to a higher prevalence of ischemic chest pain and ischemic ECG changes. The combination of adenosine or regadenoson and symptom-limited exercise in patients who can exercise but where it is not certain that they can attain maximal heart rate has been found safe and useful to achieve maximal level of stress [83].

Combined exercise with pharmacological stress should be avoided in patients with left bundle branch block or RV pacemaker, since the likelihood of false-positive myocardial perfusion stress images is increased with exercise.

Methods of SPECT Imaging

SPECT

Single-photon emission computed tomography (SPECT) has by now been well standardized and optimized for either thallium-201 or Tc-99m sestamibi or Tc-99m tetrofosmin imaging as well as optimized for each imaging system manufacturer. This includes timing of acquisition, choice of collimators, choice of step-and-shoot versus contiguous acquisition, circular versus elliptical orbits, filtered versus iterative reconstruction, filtering, display, quantification, and correction for movement artifact. The greatest area of concern and therefore undergoing the greatest evolution is the challenge of addressing inaccuracies in diagnoses and inefficiencies in patient management arising from mistaking soft tissue attenuation artifacts from true perfusion defects.

Solutions to the problem of soft tissue attenuation include training in recognition by the technologist and the interpreting physician and the utilization of various compensation strategies, such as prone imaging, ECG gating, image quantification, and the use of attenuation correction hardware and corrective reconstruction.

The inspection of the original multiplanar images allows one to detect movement artifact, as well as ascertain the presence of overlapping soft tissue likely to cause attenuation artifact, either due to an overlapping diaphragm, causing inferior wall defects, or in women and obese men, overlapping breast tissue, causing anterior, anteroseptal, or anterolateral defects. This allows the interpreting physician to properly evaluate the obtained images and avoid an unnecessarily false-positive reading.

If an inferior wall defect is recognized early, while the patient is still in the laboratory, it has been demonstrated that inferior wall defects due to attenuation artifact seen in the standard supine position resolve after repeat imaging in the prone position, which improves diagnostic accuracy. Limitations of this approach include the creation of a new anterior wall attenuation defect and the apparent lack of efficacy in anterior wall attenuation artifacts [84, 85]. This strategy is useful when other means are not available or in combination with gated SPECT imaging.

Gated SPECT

ECG gating of the SPECT myocardial perfusion images provides, independently from the perfusion information, important information on global LV and RV function, LV ejection fraction, and regional wall motion and thickening. This information provides information that incrementally add to the value of myocardial perfusion imaging alone. It can also help enhance the accuracy of perfusion imaging. When there is a wall motion abnormality corresponding to a perfusion abnormality, the presence of disease can be made with greater confidence, resulting in enhanced accuracy [86].

However, normal wall motion associated with a reversible perfusion defect does not exclude reversible ischemia. Normal wall motion in the presence of mild to moderate fixed perfusion abnormality could be due to non-transmural wall injury, insufficient to cause a discernible wall motion abnormality.

Quantification of gated SPECT images provides a global LVEF, plus indices of regional wall motion and wall thickening, useful in the evaluation of function. Whereas its original use was applied in planar gated blood pool imaging, it has been applied to three-dimensional SPECT gated blood pool images to overcome problems of overlap of adjacent cardiac structures and inaccurate localization of left ventricular and right ventricular abnormalities [87], which was subsequently applied to myocardial perfusion imaging [88].

This technique has been found useful in patients with advanced systolic heart failure and evidence of dyssynchrony on ECG due to conduction abnormalities, single ventricle pacing, in predicting which patients would benefit from cardiac resynchronization therapy [89].

Clinical Uses of Myocardial Perfusion Imaging

Initially, myocardial perfusion imaging was a primarily diagnostic method for noninvasive detection of coronary artery disease (Figs. 9.15 and 9.16). Later applications have extended to evaluation of prognosis to assess the patient risk and outcome (Table 9.8) [90, 91].

Advances in surgical, percutaneous, and medical therapy of CAD have fundamentally changed the natural history of the disease. Thus, appropriate identification of high-risk patients, followed by appropriate therapy, favorably modifies prognosis. Conversely, the identification of low-risk patients with a benign prognosis reduces the need for costly and potentially detrimental invasive testing and therapy. A normal SPECT myocardial perfusion imaging study has been shown to be extremely effective in predicting a good prognosis in a variety of settings.

Diagnosis

Appropriate candidates for stress testing with MPI are patients with intermediate pretest

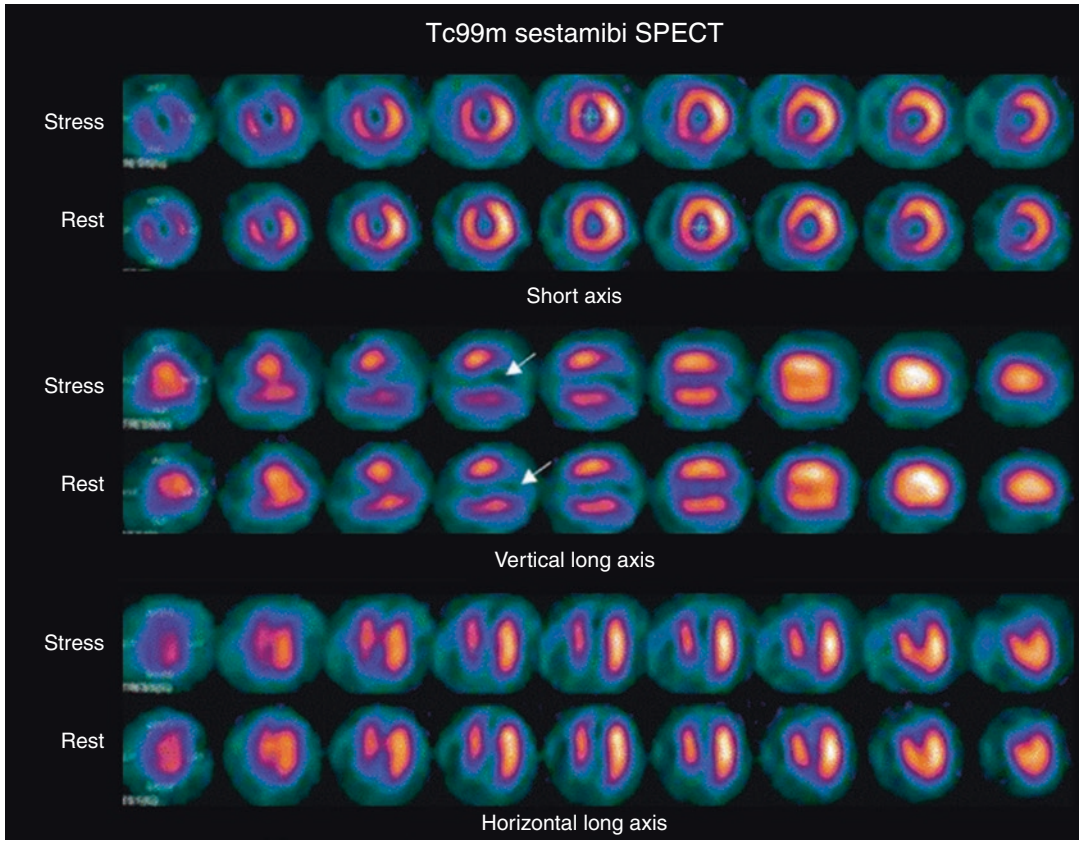

Fig. 9.15 Stress and rest Tc99m sestamibi myocardial perfusion SPECT images in short axis, vertical long axis, and horizontal long axis. SPECT images demonstrate fixed perfusion defect in the apex (arrows). There was also akinetic wall motion in this region. Findings are consistent with apical scar/infarct with possible aneurysm suggested by slight divergence of left ventricular walls as they approach the apex, instead of normal convergence on horizontal long axis images

probability for the presence of coronary artery disease. The pretest probability is determined from easily obtained parameters: age, gender, symptoms, and rest ECG [92]. Such patients might be chronically symptomatic with some atypical features at presentation. MPI is inappropriate for patients with a low pretest probability due to the high rate of false-positive results in such patients. Patients with several risk factors for CAD and typical symptoms with a high probability of CAD do not gain so much from MPI for diagnosis, as the diagnosis is nearly certain on clinical grounds. However, such patients would benefit from MPI for risk stratification. Exercise stress testing without MPI is inadequate for diagnostic purposes in patients who are unable to exercise adequately and in those with nondiagnostic baseline ECG, such as LBBB, paced rhythm, left ventricular hypertrophy, or users of digoxin [93].

In other patients, MPI adds to the diagnostic accuracy of ECG stress testing alone.

Average sensitivity and specificity of MPI for diagnosis of CAD have been reported close to 90 and 70%, respectively. The gold standard for diagnosis of CAD remains coronary angiography, despite its known limitations and likely systematic underestimation of the extent of disease. True sensitivity and specificity with each new tracer and each new imaging protocol have been difficult to ascertain because of posttest angiographic referral bias. Patients with negative results on MPI are rarely referred for coronary angiography, except where clini-

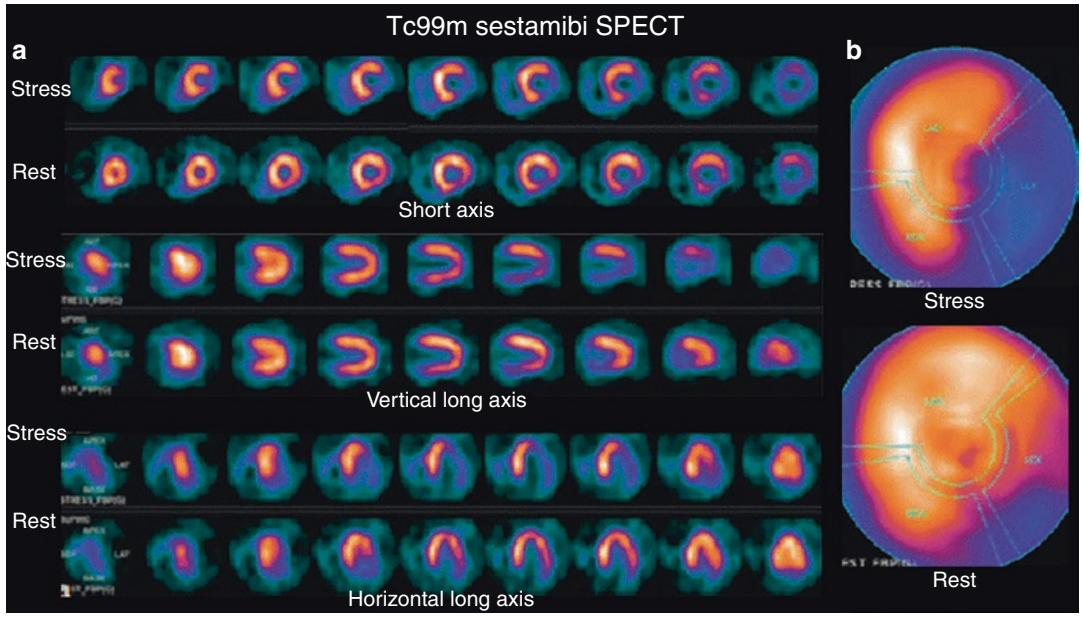

Fig. 9.16 Sixty-year-old male with history of hypertension and CAD and currently complains of shortness of breath**.** Stress and rest myocardial perfusion SPECT images in short axis, vertical long axis, and horizontal long axis (**a**) and stress and rest bullseye polar maps (**b**). There is a large area of significant reversible perfusion defect involving the lateral wall, and inferolateral regions, which is consistent with stress-induced ischemia. A small fixed defect in the inferolateral base

Table 9.8 Candidate patients for MPI for prognostic and risk stratifications

1. Stable CAD evaluated for prognosis
2. Acute chest pain syndromes
3. Post-acute myocardial infarction
4. Post-revascularization procedures (CABG, PTCA, coronary stenting)
5. Before noncardiac surgery
6. Post-cardiac transplantation

cal ECG responses or clues in the MPI images suggest possible global "balanced ischemia." This practice is justified because of the known excellent prognosis of patients with a normal MPI study [94].

Nevertheless, this referral bias limits the usefulness of retrospective validation studies using a clinical test population.

Prognosis

Several distinct patient groups are commonly referred for MPI for prognostic assessment.

1. **Prognosis Assessment in Stable CAD**

Current guidelines recommend that the care for ishemic heart disease patients is driven by risk assessment. Structural and functional information provided by different imaging techniques aids the physician in assessing different aspects of the disease. The recent shift in the management of these patients from an anatomical to a functional gold standard which further emphasized the importance of functional imaging techniques. Recent technological advances in image acquisition and processing such as tomographic imaging (SPECT), gating, attenuation correction, and Tc-99m-based tracers allow for more accurate simultaneous evaluation of myocardial perfusion and function. Perfusion abnormalities can be classified according to size, localization, severity, and reversibility. Left ventricular volumes, systolic wall thickening, segmental wall motion, and ejection fraction can be quantified. Right ventricular size and function can be assessed.

Retrospective and prospective observations have defined patterns which are compatible with high-risk prognosis as well as benign prognosis. A normal perfusion pattern in patients with an adequate level of stress and with high-quality study is consistent with an excellent short-term prognosis, regardless of coronary anatomy [94]. The extent of perfusion abnormalities characterized by number of abnormal segments, severity of defects, and extent of reversibility (ischemia) defines prognosis. When integrated with results of the exercise stress test and parameters of left and right ventricular function, combined information has a prognostic value which exceeds prognostication based on performance of coronary angiography [91]. The average annual cardiac event rate in patients with abnormal images is 12-fold than in patients with normal images. Both fixed and reversible defects are prognostically significant. Fixed defects are a predictor of death, whereas reversible defects are an important predictor of nonfatal myocardial infarction [95].

The event rate is significantly greater in patients with severe than in those with mild abnormalities (10.6% annual hard event rate vs. 3.5%) [93]. Incorporation of other SPECT variables, such as stress-induced LV dilation, LVEF, and LV volumes, further enhances the prognostic power of SPECT imaging [93, 96].

A high likelihood of multivessel (hence surgical) CAD is indicated by the presence of perfusion defects in each of the three coronary artery territories, diffuse slow washout of Tl-201, prominent pulmonary Tl-201 activity, transient stress-induced LV dilation, fall in LVEF on the gated stress SPECT MPI images, and the "left main pattern" of anterior, septal, and posterolateral defects [97].

2. **Prognosis Assessment in Acute Chest Pain Syndromes**

Acute chest pain may be due to myocardial ischemia as a result of a coronary artery plaque rupture and may be potentially life threatening. However, in only 40% of emergency department (ED) visits for chest pain the pain of cardiac origin. Rapid and reliable triage is needed for speedy diagnosis of acute myocardial infarction and to prevent unnecessary hospitalizations and inappropriate discharges from the ED [98].

Current diagnostic tools include clinical observation, serial ECGs, ST segment monitoring, serial measurements of serum markers of myocardial necrosis (such as CK-MB, troponins), and noninvasive cardiac imaging. Some centers perform MPI at rest. Abnormal results lead to hospital admission. Others perform stress testing, with or without MPI, 6–12 h after a negative workup for an acute MI [99, 100]. Based on the results of MPI, a patient's short-term prognosis can be determined.

3. **Prognosis Assessment After an Acute Myocardial Infarction**

The purposes of early or predischarge MPI evaluation after an acute myocardial infarction are (a) to assess the extent of sustained damage, including determination of the ejection fraction, and (b) to detect residual ischemia, both in the infarct-related territory and in the other vascular territories using either exercise MPI or pharmacological stress. In the era of acute interventions (i.e., thrombolysis, PTCA, stenting), the urge to perform invasive assessment (by angiography) is often irresistible. However, recent reports support a less aggressive approach: Patients with a limited amount of ischemia after an acute myocardial infarction can be risk stratified noninvasively and, if found to have a low-risk profile, treated medically with the same results as those treated with interventions [101, 102].

4. **Prognosis Assessment After Revascularization Procedures**

In view of the possibility of restenosis after percutaneous revascularization and of aorto-coronary bypass graft closure after coronary artery bypass surgery, and the frequent absence of reliable symptoms, MPI is an efficient means to determine the need for additional and/or repeat interventions, especially when the clinical symptoms are vague or nonspecific [103].

5. **Risk Assessment Prior to Noncardiac Surgery**

   Preoperative evaluation for noncardiac surgery depends partly on a patient's risk factors. These include severity and/or stability of known heart disease; the presence of concomitant conditions such as diabetes mellitus, peripheral vascular disease, renal insufficiency, and pulmonary disease; urgency of the surgery (emergency vs. elective); and type of surgery planned. Several principles for preoperative evaluation are summarized in the 2002 AHA/ACC Task Force guideline update recommendations [104].

   There is currently no evidence that preoperative revascularization alters the outcome of noncardiac surgery. However, risk stratification based on preoperative testing can help the patient and physician choose the best type and timing of surgery, perioperative care, and long-term postoperative management.

6. **Prognosis Assessment After Cardiac Transplantation**

   Long-term survival after heart transplantation, in excess of 80% after 1 year, is now common [105, 106].

   Immunologically mediated obstructive coronary vasculopathy has emerged as the most devastating late complication. Pain symptoms of myocardial ischemia are absent because of denervation of the transplanted heart. Frequent invasive (angiographic) evaluation is not practical. MPI and perhaps stress echocardiography are emerging as surveillance methods for detection of asymptomatic myocardial ischemia [107, 108].

9.5.2.2 PET Myocardial Perfusion Imaging

Currently, PET is considered the gold standard for noninvasive quantitative assessment of myocardial perfusion and metabolism although the availability is still limited. Although the role of SPECT MPI in the diagnosis and management of ischemic heart disease is well established and its qualitative or semi-quantitative assessment of regional perfusion is most used in clinical practice, it has limitations in determining the extent of the disease particularly in patients with multivessel disease and its inability to delineate the extent and severity of diffuse atherosclerosis and microvascular dysfunction. On the other hand, PET enables better assessment of disease by analyzing myocardial perfusion, function, and metabolism (Table 9.9).

Table 9.9 Advantages of PET imaging in heart disease

Offers reliable attenuation correction
Higher resolution
Ability to reliably detect coronary disease down to about 50% occlusion
Ability to delineate the extent and severity of diffuse atherosclerosis and microvascular dysfunction
More reliable in obese patients
Absolute perfusion quantitation
Lower radiation than SPECT MPI

Myocardial Perfusion PET imaging

The tracers used most commonly are 82Rb-chloride and 13N-ammonia [109]. Less commonly used are and O-15 water and F-18flurpiridaz (Table 9.10). Each has specific features that make one preferable over another in individual situations.

The perfusion tracer is injected intravenously at rest, followed by a PET acquisition, and again during pharmacological stress with either intravenous regadenoson, dipyridamole, adenosine, or dobutamine/arbutamine.

The rest and stress perfusion studies can and should be gated, if possible, providing valuable information about LV function at rest and during stress. With a PET-CT scanner, a CT transmission scan with each of the rest and stress perfusion scans is performed. For N-13 ammonia or F-18 flurpiridaz, it is possible to perform either exercise or pharmacological stress, although pharmacological stress is been used in most patients. In the USA, regadenoson is the agent utilized most commonly for inducing coronary vasodilation [110]. Exercise stress is challenging technically because of the short half-lives of PET radiotracers, size of PET gantry for supine bicycles, and motion artifacts with exercise [109].

Table 9.10 Positron-emitting tracers for myo cardial perfusion

Tracer	Physical half-life	Mean range (mm)	Production	Scan duration	Mechanism	Require on-site cyclotron
N-13 ammonia	9.8 min	0.7	Cyclotron	20 min	Metabolic trapping in myocardium	Yes
Rubidium-82	75 s	2.4	Generator	6 min	Free diffusion, metabolically inert	No
F-18 flurpiridaz	110 min	0.2	Cyclotron	20 min	Metabolic trapping in myocardium	Yes
O-15 water	2.0 min	1.1	Cyclotron	6 min	Metabolic trapping in myocardium	No

1. **N-13 Ammonia**

In the bloodstream, N-13 ammonia consists of the neutral NH_3 molecule in equilibrium with NH_4^+. At normal pH, NH_4^+ is the predominant form. The neutral, lipid-soluble NH_3 readily crosses cell membranes by diffusion. Inside the cell, the NH_3 converts into $NH_4^+$and is trapped in the cell as glutamine in a reaction catalyzed by glutamine synthase [111].

Egress from the cell is slow, mostly through catabolism of proteins and amino acids. N-13 ammonia has been used as a PET myocardial perfusion agent since 1972 [112] with either pharmacological or exercise stress. Its extraction fraction remains high even with high flows during pharmacological vasodilation, although under severe metabolic derangement, the glutamine synthase pathway can be blocked and the uptake of N-13 ammonia can become low [113].

Its half-life allows high-quality image acquisition and gating. In dogs, Gould et al. demonstrated that coronary stenoses of 47% or greater can be detected by perfusion imaging with N-13 ammonia in conjunction with IV dipyridamole [114].

In human beings, Schelbert et al. correctly identified 52 of 58 stenosed vessels (90% sensitivity per vessel) and correctly diagnosed the presence of CAD in 31 of 32 patients (97% sensitivity) [111]. Tamaki et al. [115] demonstrated a sensitivity of 95% for N-13 ammonia rest and exercise stress imaging (Fig. 9.17).

2. **Rubidium-82**

Rubidium-82 is a potassium analog. Like Tl-201, Rb-82 is transported into cells by the Na^+/K^+ ATPase pump. Like Tl-201, Rb-82 extraction decreases at high blood flow and can be altered by drugs, severe acidosis, hypoxia, and ischemia [116, 117].

With ischemia, segmental reduction of Rb-82 uptake can persist following exercise, even after symptoms and ECG abnormalities have resolved, for up to 30 min. Owing to its short half-life (75 s), Rb-82 is injected at a high dose (30–60 mCi); this is followed by a short acquisition lasting 4–6 min. The imaging sequence can be fast and efficient. An example of rest and stress Rb-82 PET myocardial perfusion images and gated resting images is shown in Fig. 9.18. In chronically instrumented dogs, Gould et al. detected coronary stenoses of 50% or greater with Rb-82 imaging and dipyridamole stress [118].

Gould et al. [119] compared Rb-82 rest and dipyridamole-handgrip stress imaging with a validated quantitative flow reserve index obtained from contrast angiograms. The results showed a sensitivity of 95% and a specificity of 100% for impaired flow reserve. Studies performed to study the accuracy of Rb-82 PET perfusion MPI for the detection of CAD showed a sensitivity from 85 to 93% and a specificity of 50–90% (Fig. 9.19).

The normal myocardial distribution of Rb-82 is similar to Tc-99m-labeled SPECT tracers, but the image resolution is better (Fig. 9.18).

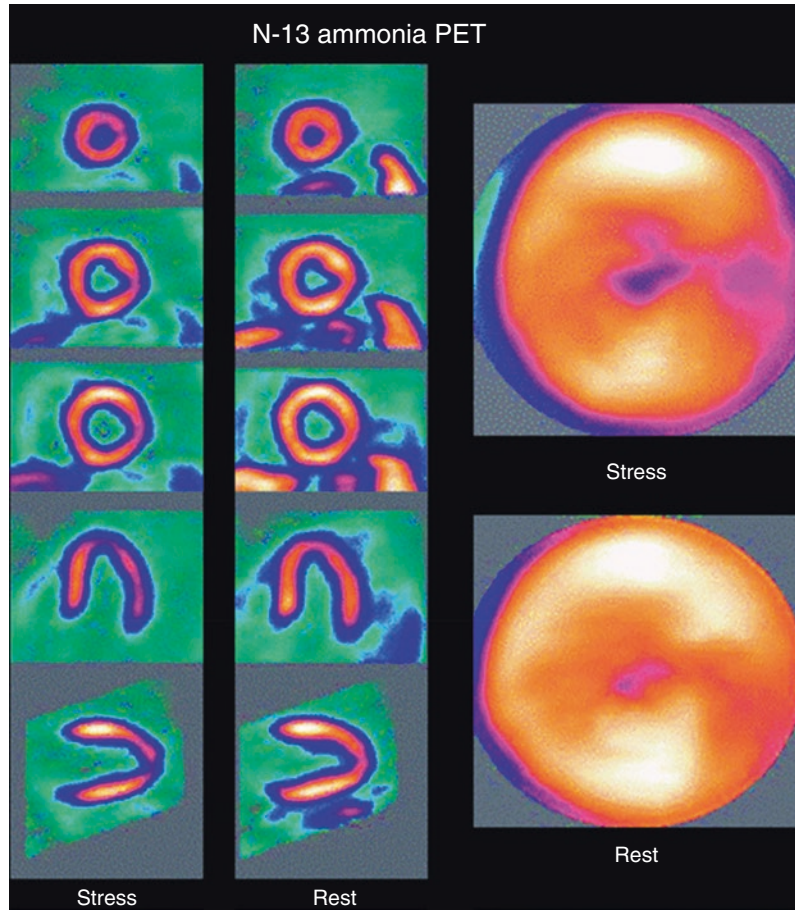

Fig. 9.17 Stress and rest N-13 ammonia PET images demonstrating a mild lateral wall defect during stress, with normal distribution at rest

3. **Oxygen-15 Water**

   The use of O-15 water is limited to quantification of coronary blood flow. Water enters all cells by diffusion, with a high extraction fraction even at high myocardial flow. Owing to the very short half-life of O-15, the tracer must be produced by an on-site cyclotron.

4. **Fluorine-18 Flurpiridaz**

   F-18 flurpiridaz is lipophilic and, like Tc-99m sestamibi, binds to mitochondria with high affinity. Preclinical studies showed that the extraction fraction of F-18 flurpiridaz was greater than that of N-13 ammonia, R-82, thallium-201 (201Tl), or technetium-99m (Tc-99m) sestamibi and was in fact found to be greater than 90%. Both sensitivity and absolute quantification of MBF would be expected to be more suitable with this high-extraction-fraction tracer because there is significantly less roll-off in extraction at high flows than there is with other tracers [119]. In Phase I trials, the heart exhibited high and sustained retention of F-18 flurpiridaz from the earliest images through approximately 5 h after injection [120].

   Similar to the Tc-99m perfusion agents, one administers a slightly lower for resting study dose (approximately 74–111 MBq (2–3 mCi)). After waiting for approximately 50–70 min, perform exercise or pharmacological stress, and administer a higher (approximately 240 MBq (6.5 mCi)) during stress for stress study (Fig. 9.20). In a Phase II study comparing F-18 flurpiridaz MPI to Tc-99m sestamibi SPECT MPI in the same 143 subjects in 21 centers, a higher percentage of images was rated as excellent or good on PET versus SPECT imaging, with a higher diagnostic certainty. In 86 patients who underwent coronary angiography, sensitivity of

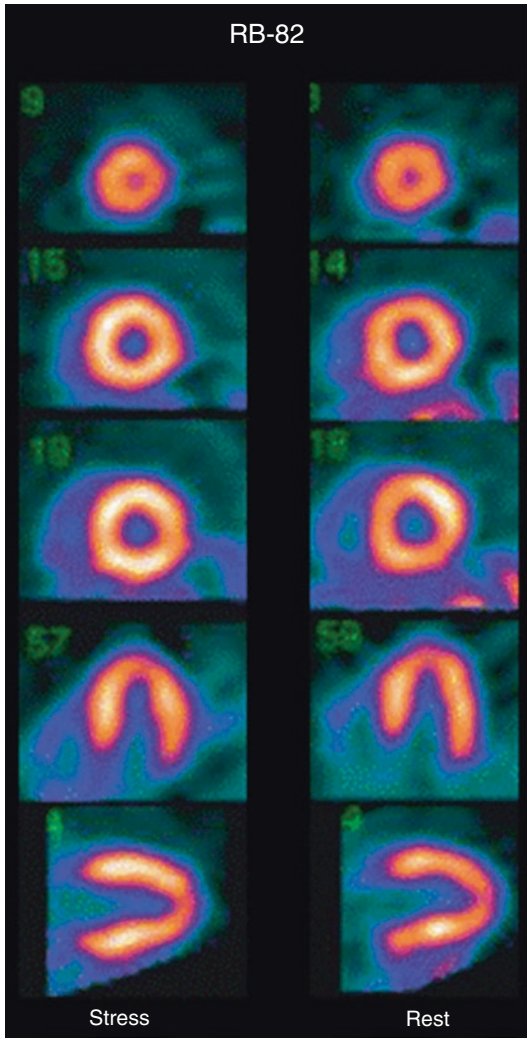

Fig. 9.18 Stress and rest selected Rb-82 short axis and horizontal and vertical long axis images demonstrating normal perfusion

F-18 flurpiridaz PET for individual coronary vessel disease was higher than SPECT MPI, 79% versus 62%, with similar specificity, and a normalcy of 90% with F-18 flurpiridaz PET versus 97% with SPECT. In patients with CAD on angiography, the magnitude of reversible defects was greater with PET compared to SPECT [121].

Myocardial Metabolism FDG PET Imaging

The major source of ATP in a normal heart is oxidation of free fatty acids, rather than of carbohydrate. With ischemia, reversible metabolic adaptation will occur to enable myocytes to survive in a low oxygen environment. Mitochondrial oxidation is supressed and anaerobic metabolism may occur. Exogenous glucose uptake and glycogen breakdown are increased with stimulation of glycolysis and ATP production from the anaerobic catabolism of glucose. Accordingly F-18 FDG is the radiotracer used for PET metabolic imaging [122].

FDG is a glucose analogue that is transported into the myocyte by the same carriers (GLUT-1 and GLUT-4) as glucose and phosphorylated to FDG-6-phosphate by hexokinase. PET imaging of regional glucose uptake reflects overall cell glucose uptake. FDG uptake may be increased in hibernating but viable myocardium; uptake in regions with reduced blood flow at rest has become a marker of hibernation.

Clinical Uses of PET in Heart Diseases

Positron emission tomography is increasingly used in the diagnosis and risk stratification of patients with ischemic heart disease (Table 9.11). PET myocardial perfusion imaging has a mean sensitivity and specificity of around 90% for the detection of angiographically significant coronary artery disease, and is also highly accurate for assessing the prognosis of patients with ischemic heart disease. Based on the tracer used, it can provide information not only on myocardial perfusion but also on myocardial metabolism, which is important for myocardial viability evaluation. The value of this imaging technique has been further enhanced with the introduction of hybrid scanners (PET/CT and PET/MR), offering integrated morphological and functional information and consequently comprehensive assessment of atherosclerosis effect on the myocardium [123].

PET in the Diagnosis of Ischemic Heart Disease

FDG-PET has several advantages including higher sensitivity and specificity over perfusion tracer, reliable attenuation correction, thus avoiding the attenuation artifacts seen frequently in SPECT imaging, although caution needs to be exercised to recognize and correct for PET emis-

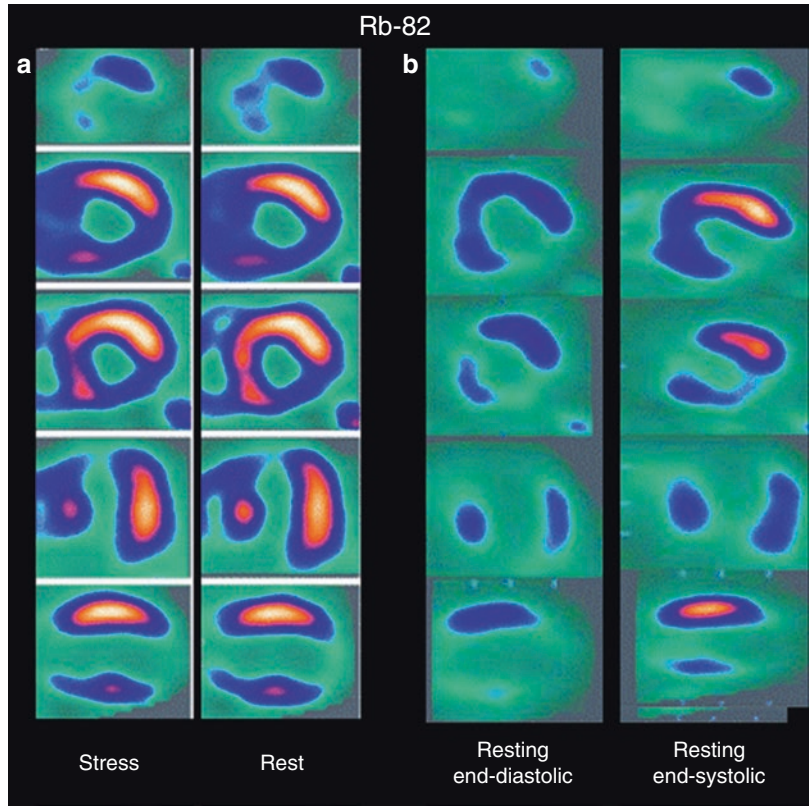

Fig. 9.19 (**a**) Stress and rest of Rb-82 PET images demonstrating severe extensive apical, septal, and inferior scarring and only minimal basal septal ischemia. (**b**) Resting end-diastolic and end-systolic gated images, showing poor or absent contractility in the scarred regions and poor overall LV function

sion-transmission misregistration artifacts. PET imaging also offers higher resolution. A number of studies have shown a higher accuracy of coronary disease detection by stress PET imaging compared with SPECT imaging [111, 120, 124, 125]. The high extraction fraction of the PET tracers, especially N-13 ammonia and O-15 water, assures higher sensitivity for disease at high flows during pharmacological stress, resulting in the ability to reliably detect coronary disease down to about 50% occlusion [124, 126]. Comparisons of sestamibi and PET perfusion imaging showed that adenosine stress MIBI SPECT imaging significantly underestimates ischemia and defect severity compared with N-13 ammonia PET [127, 128].

Many studies indicate that PET imaging consistently yield higher diagnostic accuracy for detection of coronary artery disease compared to gated Tc-99m sestamibi SPECT imaging, both with and without SPECT attenuation correction [129–135]. One study performed head-to-head comparison of 208 adults of coronary computed tomography angiography, single-photon emission tomography, $[^{15}O]H_2O$ positron emission tomography, and hybrid imaging for the diagnosis of myocardial ischemia [133]. demonstrated highest diagnostic accuracy for Positron emission tomography compared with single-photon emission tomography and coronary computed tomography angiography.

The gating of MPI at rest and during stress with PET imaging allows the additional diagnostic and prognostic relevant information about the severity of disease. During gated vasodilator stress Rb-82 PET imaging, LVEF increases with vasodilator stress in patients without significant stress-induced perfusion defects or severe left main/3-vessel CAD. A high LVEF reserve appears to be an excellent tool to exclude left main/3-vessel CAD noninvasively [136].

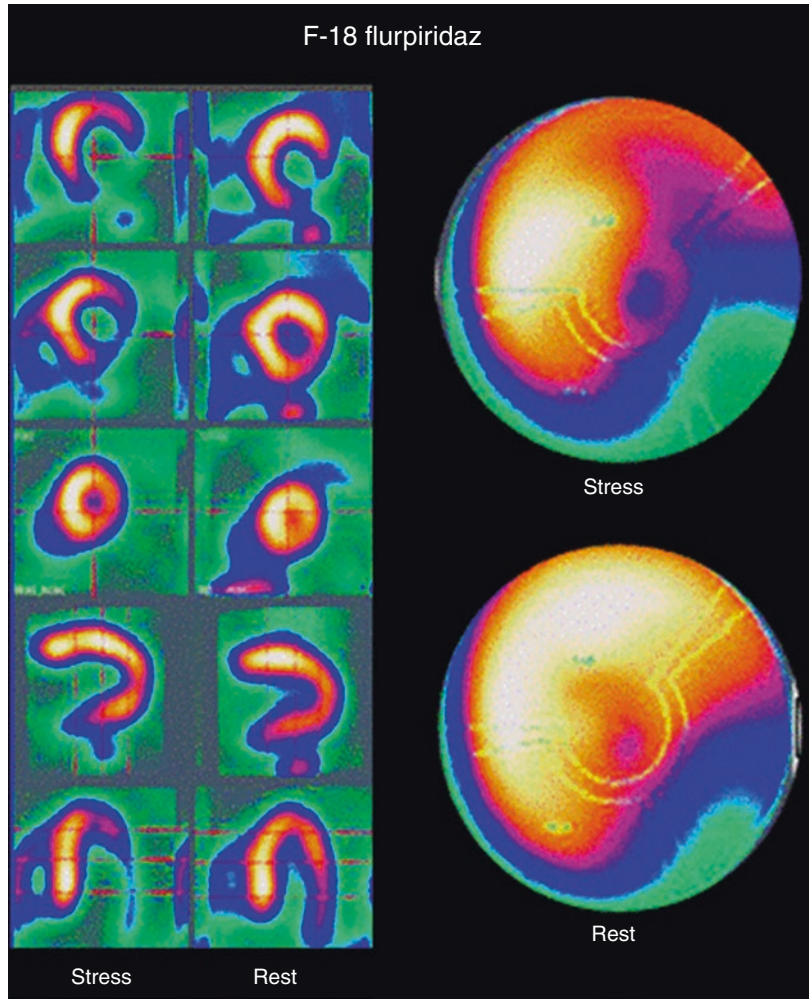

Fig. 9.20 Stress and rest PET images with F-18 flurpiridaz, demonstrating severe inferolateral and mild anterolateral and apicolateral defects with stress, with complete improvement in the anterolateral and apicolateral wall and partial improvement in the inferolateral wall

Table 9.11 Clinical applications of PET in heart diseases

1. Perfusion assessment
2. Absolute quantification of myocardial blood flow
3. Assessment of myocardial viability
4. Prognostic assessment
5. Assessing ventricular function
6. Cardiovascular prosthetic infection
7. Cardiac sarcoidosis, amyloidosis

Quantation of myocardial perfusion in absolute units by PET further improves its diagnostic accuracy. Patients with multivessel disease, microvascular disease, and obese patients may benefit most from this quantitative assessment [137, 138].

Quantification of Myocardial Blood Flow

In addition to qualitative and semi-quantitative grading, PET enables absolute quantification of perfusion. Absolute quantification of myocardial blood flow expands the scope of conventional relative MPI from identifying only end-stage epicardial IHD to the earlier identification and characterization of abnormalities in coronary endothelial function and subclinical stages of IHD (microvascular dysfunction) [139]. Quantitation of myocardial perfusion offers an objective parameter which is more reproducible than visual interpretation. PET has become the noninvasive imaging modality of choice for the quantification of MBF. In conclusion, it adds not

only to diagnostic certainty but also provides prognostic value (see later).

PET in Prognosis Assessment

PET MPI, similarly to SPECT MPI, has great prognostic value in patients with known or suspected IHD. Marvick et al. noted that defect severity with PET was related to outcome [140, 141]. Normal ribidium-82 PET MPI have good prognosis, regardless of ECG changes during stress including patients whose diagnosis was uncertain after SPECT MPI and in obese patients [142–144]. A multicenter observational registry in 7061 patients from 4 centers underwent a clinical indicated rest-stress Rb-82 PET MPI, with a mean follow-up of 2.2 years. The investigators found that the risk-adjusted hazard of cardiac death increased with 10% with abnormal stress PET, compared to normal PET results. The model worked even better when clinical risk factors were combined with PET MPI findings [145]. In a related work, Rb-82 PET findings were particularly helpful in identifying high-risk, older women [146]. Similarly, perfusion findings on 256 N-13 ammonia PET MPI studies were shown to be strong predictors of clinical outcome [147]. Dorbala et al. [148] demonstrated that not only vasodilator stress Rb-82 PET MPI provides incremental prognostic value to historical/clinical variables to predict risk of cardiac events and all-cause death, but also the left ventricular ejection fraction reserve provides significant independent and incremental value to Rb-82 MPI for predicting the risk of future adverse events. The extent and severity of PET perfusion defect, rest left ventricular (LV) ejection fraction (LVEF), stress LVEF and LVEF reserve (stress LVEF - rest LVEF), LV volumes and myocardial flow reserve provide valuable prognostic information [144–146, 149]. Even in the presence of angiographically significant IHD, normal findings on stress MPI are generally associated with a low risk of CV events (around 1% per year) [150].

The risk of cardiac events, however, must consider all factors besides imaging information. Ceratin groups of patients such as diabetics, those with known IHD, old age group were found to have higher annual event rate (1.4–1.8%) despite normal MPI. The warranty period of a normal PET MPI in is around 2 years [151] depending on risk factor control.

Myocardial flow reserve was found to independently augment clinical outcome prediction. The quantification of blood flow at rest and during maximal pharmacological stress allows measurement of flow reserve in various hypertrophies and cardiomyopathies, post-transplant CAD [152], syndrome X, and other vascular endothelial disorders and to study the effects of smoking, diabetes, various medications [153–156], and lipid control [157–159].

Multiple studies documented the greater prognostic value of PET-derived myocardial flow reserve (MFR) compared to clinical factors and perfusion defect size and severity in patients with known or suspected IHD [160, 161]. Addition of PET derived MFR, led to correct reclassification of estimated risk categories in 35% of patients with previously intermediate risk of death [162]. Since MFR indirectly reflects microvascular disease, it also has prognostic value in diabetic patients with diabetes and in patients with chronic kidney disease [163].

In viability imaging, FDG PET has the greatest sensitivity for predicting global LV functional recovery following revascularization, compared with SPECT, dobutamine stress echocardiography, and cardiac MRI [164–166].

The amount of tissue of scarring as well as hibernating myocardium on FDG PET has also been shown to be an important predictor of improvement in LVEF following revascularization [167–169]. Additionally, compared to scar, dysfunctional myocardium diagnosed as hibernating or stunned by PET has a high chance of functional improvement following revascularization [169].

PET in Assessment of Myocardial Viability

PET is very valuable in assessing viability in stunned myocardium (Delayed functional recovery myocardium) and hibernating myocardium (chronically depressed function of hypoperfused myocardium). Demonstration of preserved glucose metabolism by FDG is a marker of myocardial viability (Fig. 9.21) While matching defect on perfusion and FDG indicates non-viable myocardium (Fig. 9.22). The detection of viable myo-

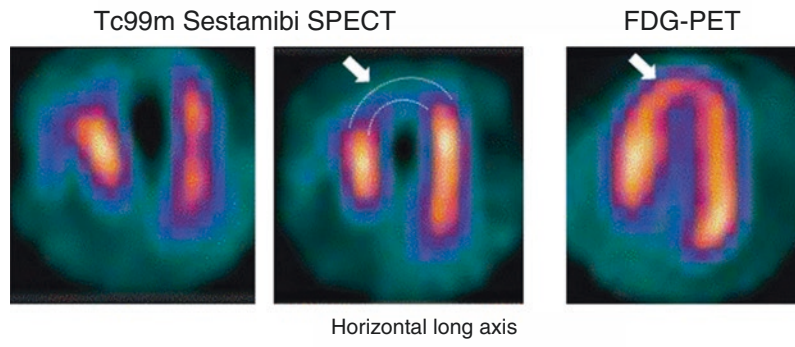

Fig. 9.21 Viable myocardium pattern

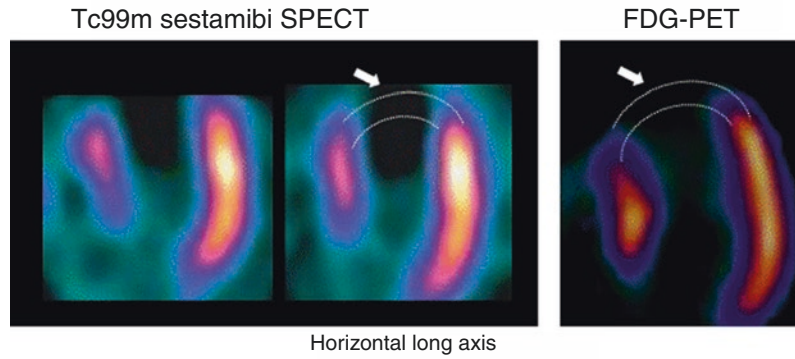

Fig. 9.22 Pattern of non-viable myocardium

cardium is accurately estimated by referencing the level of myocardial glucose metabolism to the level of MBF [123, 169]. Sequential perfusion-metabolism imaging gives the most complete information, yielding different interpretation scenarios. See later more details.

PET in Assessing Ventricular Function

Gated first-pass ^{18}F-FDG PET has also been introduced for assessing ventricular function [170].

PET in Endocarditis and Cardiovascular Prosthetic Infection

Cardiovascular prosthetic infection is a difficult condition to diagnose. PET has a major role in the diagnosis of endocarditis and prosthetic infections (Pathophysiology and diagnosis is presented in Chap. 4).

PET in Assessing Ventricular Function

Gated first-pass ^{18}F-FDG PET has also been introduced for assessing ventricular function [170].

PET in Endocarditis and Cardiovascular Prosthetic Infection

Infective endocarditis is among the most severe infectious diseases. Patients with damaged or artificial heart valves and heart defects are at greatest risk for endocarditis. Cardiovascular prosthetic infection is a difficult condition to diagnose. PET has a major role in the diagnosis of endocarditis and prosthetic infections Fig. 9.23 (see details in Chap. 4).

PET in Cardiac Sarcoidosis and Amyloidosis

Sarcoidosis and Amyloidosis are both multiorgan systemic diseases. Diagnosis of cardiac involvement is particularly important because it can be fatal. Sarcoidosis is a multisystem granulomatous disorder affecting the heart in up to 25% of patients. Cardiac involvement is often associated with a poor prognosis [171] as it may lead to advanced heart block, cardiomyopathy, arrhythmias, or death. PET may be essential in the diagnosis, risk stratification, and patient management [172, 173]. When sarcoidosis involves the heart it affectst left ventricular subepicardial regions,

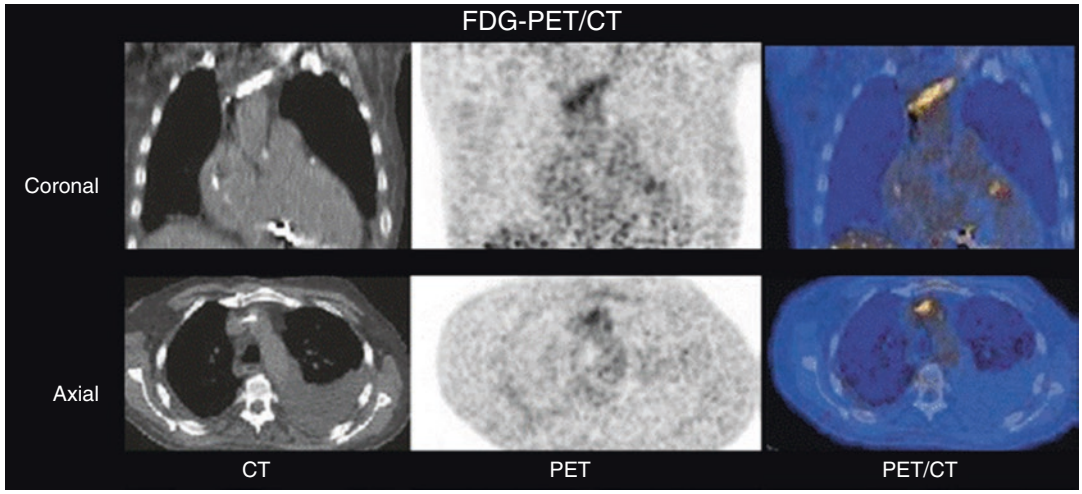

Fig. 9.23 FDG PET/CT study for a 68-year-old male with bacteremia and questionable infectious endocarditis. There is increased FDG accumulation around electrode in the left subclavian vein near superior vena cava. Findings are consistent with infection. Note successful suppression of normal cardiac uptake of FDG after 6–12 h fasting and unfractionated iv heparin administration

septal, and right ventricular free wall in >90% of cases [174]. F-18 FDG PET and 18-FDG PET/MRI are useful in the diagnosis of cardiac involvement of sarcoidosis [175, 176]. Cardiac sarcoidosis may be an incidental finding cardiac MR or PET show similar accuracy in the diagnostic workup of CS compared with autopsy studies. Combining 18F-FDG-PET/CT study with SPECT/CT perfusion is particularly useful, as the finding of multiple uptake areas associated with the matching perfusion abnormalities seen in SPECT/ CT indicate high probability of an accurate diagnosis 18F-FDG-PET/CT may also be useful to assess the therapeutic and prognostic factors [177].

Amyloidosis is the clinical condition caused by the deposition of unstable misfold proteins as amyloid fibrils. Cardiac amyloidosis is the condition in which the primary interstitial protein deposition occurs in the extracellular space of the heart. Systemic amyloidosis represents a debilitating, under-diagnosed but increasingly recognized group of disorders characterized by the extracellular deposition of these misfolded proteins in one or more organs. Cardiac amyloid deposition leads to an infiltrative or restrictive cardiomyopathy and is the major contributor to poor prognosis in patients with systemic amyloidosis. Many proteins can form amyloid fibrils, but the two main types that can infiltrate the heart are monoclonal immunoglobulin light-chain amyloid and transthyretin amyloid. Cardiac amyloidosis is classified into amyloid immunoglobulin light chain (AL) and amyloid transthyretin (ATTR) types [178]. These two most common types of cardiac amyloidosis have distinct therapeutic management and prognosis. Cardiac amyloidosis can be acquired in older individuals or inherited from birth. Early and accurate diagnosis of cardiac amyloidosis is crucial for the implementation of appropriate patient care and is now more important than ever given the availability of new therapies [179].

Cardiac amyloidosis is currently diagnosed more frequently than in the past owing to the advanced diagnostic modalities. Echocardiography and Cardiac MRI play a crucial role in the diagnostic workup of cardiac amyloidosis; however, the differentiation between the subtypes of cardiac amyloidosis is still difficult [177]. Scintigraphy is valuable in the diagnosis and follow-up of the disease. Radiotracers for amyloidosis include (1) bone tracers including PYP, (2) amyloid-directed molecules, (3) PET amyloid agents, and (4) I-123-

MIBG. Bone tracers are particularly sensitive in the detection of ATTR type amyloidosis, whereas PET amyloid agents show a higher affinity for the AL type. An important limitation of ^{18}F-FDG is the physiologic uptake in the myocardium, which may remain in approximately 20% of patients even after proper preparation [178]. This fact limited the FDG PET scan's sensitivity for detection of cardiac involvement to 62.5% [180]. ^{11}C-Labeled Pittsburgh compound B (^{11}C-PiB), a radio-labeled derivative of thioflavin-T that is used to detect Aβ amyloid deposition in Alzheimer's disease [181]. The findings of ^{11}C-PiB PET were found to correlate well with post-mortem histopathological samples [180]. Finally, 123I-MIBG scintigraphy is capable of detecting cardiac sympathetic denervation in cardiac amyloidosis [181].

9.5.2.3 Hybrid Myocardial Perfusion and CT Imaging

CT Attenuation Correction

Combining PET and CT imaging as a single combined PET-CT unit has become the preferred approach for PET imaging in oncology. For cardiac PET imaging, the scout CT checks the position of the patient in a few seconds. The CT transmission scan, lasting 10–30 s, saves a significant amount of time compared to transmission imaging using radiation pin-sources. The CT transmission scan is relatively noise free, compared to the dedicated PET transmission scan. It enables one to perform an entire rest and pharmacological stress PET perfusion imaging study with rubidium-82 in 30–40 min, compared to 45–60 min for a dedicated PET scanner.

Calcium Scoring

Another application of PET-CT and SPECT-CT is the possibility of obtaining coronary calcium scores in the same imaging session as the PET or SPECT MPI, which is feasible with an 8-, 16-, or 64-slice multidetector CT scanner. Calcium scoring requires gating and a higher current from the CT scanner than a transmission scan, resulting in higher patient radiation exposure, but still lower than diagnostic CT imaging [182–185].

CT Coronary Angiography

The possibility of performing CT coronary angiography performed together with PET or SPECT MPI in selected patients can be very valuable.

9.5.2.4 Assessment of Myocardial Viability

Nonfunctioning but viable myocardium includes stunned and hibernating myocardium and also remodeling.

1. Stunned myocardium reoresents reversible regional decreased contractility after an episode of prolonged ischemia, but intact blood flow at the time of observation [169]. Oxygen-derived free radicals contribute to postischemic dysfunction [186]. Stunned myocardium generally improves without further intervention. In most cases of exercise-induced ischemia, this may take a few minutes or, uncommonly, several hours. Following an acute coronary occlusion and thrombolysis, most of the improvement takes place over 7–10 days, but it may take longer in the presence of residual stenosis and/or repeated stunning [187]. Patients may experience repeated episodes of ischemia, often silent, in the same territory, and the stunned myocardium may not be able to recover, leading to a quasi-permanent state of stunning [188, 189] and progressing to hibernation [190]. When superimposed on an already severely dysfunctional heart, it may become dangerous, and the patient may require hemodynamic support. Recovery of myocardial function is spontaneous provided that myocardial perfusion remains normal. The duration of stunning is directly proportional to the duration of the preceding ischemia.
2. Hibernation occurs in myocardium that has undergone a downregulation of contractile function, thus reducing cellular demand for energy, in response to chronic or repetitive ischemia [123]. Hibernation may represent a spectrum, with chronic repetitive stunning showing normal or near normal resting perfusion and impaired MFR at one end and reduced rest MBF at the other. In most cases, the impair-

ment is only detected through reduced MFR, with reduced rest MBF only being seen in the most advanced cases [123]. Hibernation, by definition, requires the restoration of blood flow in order to improve function. Benefit also may be expected from reduced metabolic demand via hemodynamic support.

3. Remodeling may result in dysfunctional myocardium in the area adjacent to an infarct or hibernation also that may or may not improve with revascularization [169].

Normal myocardium uses several different metabolic substrates (predominantly glucose or fatty acids) for its energy needs. In the fasting state, the myocytes predominantly use fatty acids, whereas in the post-prandial state, they switch to use glucose [191]. The majority of dysfunctional but viable segments are in fact due to stunning (72%), with only a minority (28%) due to hibernation [192]. The definition of either stunning or hibernation includes the recovery of function, either spontaneously or after intervention. Other potential benefits from the reversal of stunning or hibernation, including prevention of remodeling or arrhythmias.

Dysfunctional but viable myocardium is not uncommon. Up to 50% of patients with previous infarction may have areas of dysfunctional viable myocardium mixed with scar tissue, even in areas with Q waves on the ECG [191].

Resting wall motion imaging identifies myocardium which is thickening and moving well and that which is not. It cannot differentiate dysfunctional viable myocardium from permanently scarred myocardium, except by documenting serial changes in function over time. Stimulation by exercise, catecholamines, or nitrates and post-exercise and post-PVC potentiation are all evidence of viability, but with limited sensitivity. Low-dose dobutamine (LDDE) and high-dose dobutamine echocardiography (LDDE) showed that both biphasic response (improvement at low dose and deterioration at high dose) and sustained improvement of wall motion (improvement at both low dose and high dose) in dysfunctional segments were highly predictive of reversible dysfunction [193], with a combined sensitivity of 84% and specificity of 81% [193–196].

The uptake and retention of myocardial perfusion agents is good evidence of myocardial viability. However, impaired retention of perfusion tracers can be seen in dysfunctional, stunned myocardium, while decreased uptake due to decreased perfusion is often seen in hibernation [195]. Simple stress-redistribution imaging with Tl-201 has been shown to underestimate the presence of viability. Augmentation with late (12–24 h) imaging and/or resting reinjection was found to increase sensitivity for viability [196–199]. The latter approach yielded a combined mean sensitivity of 86% but at the cost of a lower specificity [194] (Table 9.12). In patients who cannot exercise owing to poor LV function and clinical CHF, rest-redistribution Tl-201 imaging has shown a combined sensitivity of 90% and specificity of 54% [194]. Comparisons showed LDDE to be slightly less sensitive but more specific.

Myocardial perfusion imaging with Tc-99m sestamibi has yielded a slightly lower sensitivity of 83% but higher specificity of 69% [202]. Tc-99m sestamibi imaging combined with nitrate administration has yielded an improved sensitivity of 91% and specificity of 88% [194]. Gated Tc-99m sestamibi imaging with nitroglycerin (NTG) administration can be used successfully as an alternative to rest-redistribution Tl-201 SPECT imaging [203]. Tc-99m tetrofosmin showed performance similar to that of Tl-201 stress-redistribution imaging and slightly lower sensitivity than rest-late redistribution Tl-201 imaging [204].

Table 9.12 Sensitivity and specificity of various methods of imaging for myocardial viability

Method	Patients	Sensitivity	Specificity
Dobutamine stress echocardiography	1869	76	81
Tc99m	695	83	69
Tl-201	1067	87	51
F-18 FDG PET	930	90	68
Dobutamine cardiovascular magnetic resonance (Db CMR)	247	81	91
Late gadolinium-enhanced cardiovascular magnetic resonance (LGE-CMR)	331	95	51

Data extracted from [193, 200, 201]

Myocardial perfusion can be imaged with N-13 ammonia or Rb-82 with PET imaging or Tl-201, Tc-99m sestamibi, or Tc-99m tetrofosmin imaging using SPECT (Figs. 9.24, 9.25, and 9.26).

Stunned myocardium shows relatively preserved flow and either matched or excessive FDG accumulation. At times, stunning results in impaired FDG accumulation, producing an underestimation of viability [205]. Hibernation

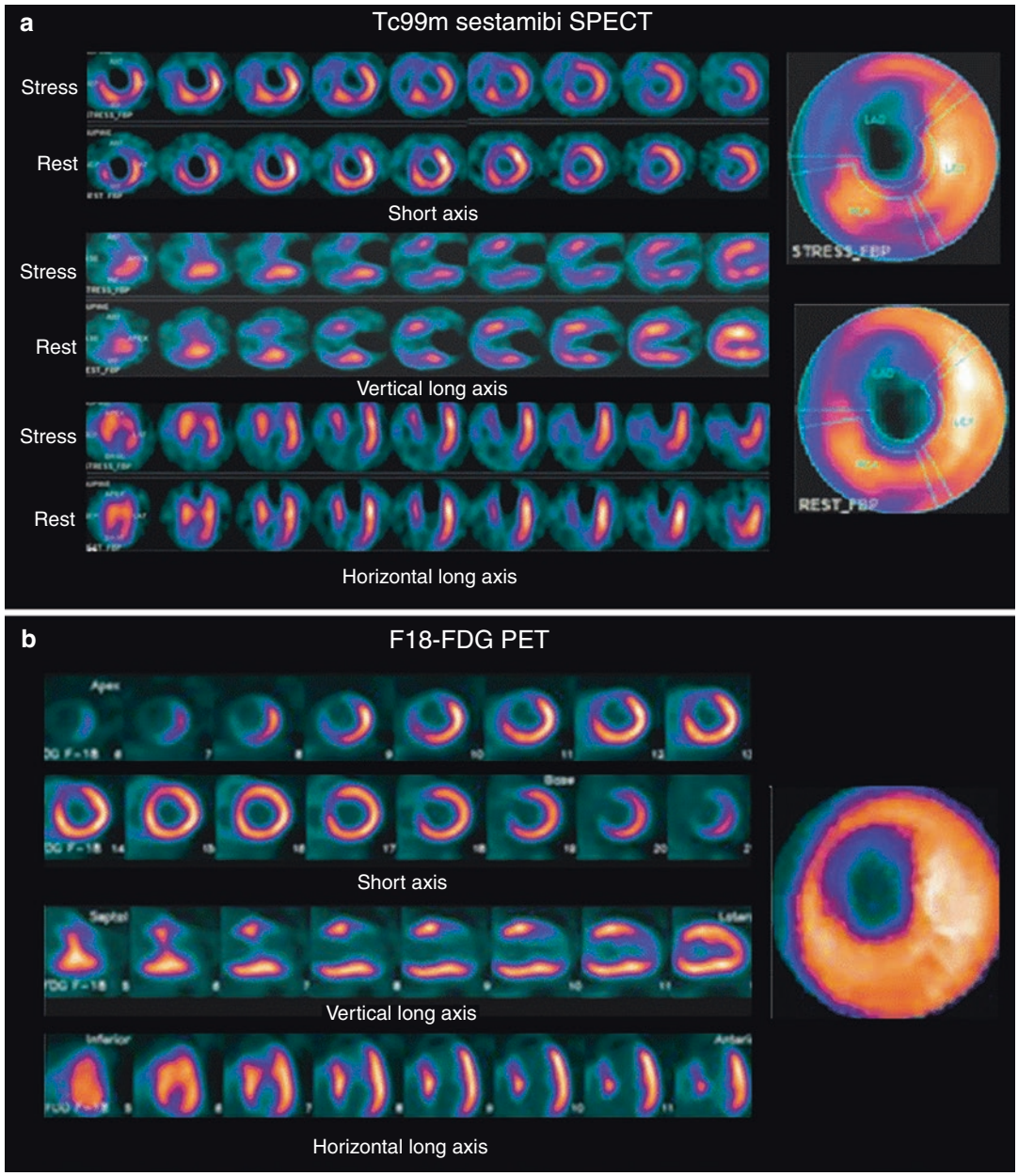

Fig. 9.24 Tc-99m sestamibi stress and rest myocardial perfusion SPECT images and polar maps (**a**) and F-18 FDG studies (**b**) for a 62-year-old male with dyslipidemia, smoking, and fixed perfusion defect on myocardial perfusion SPECT. The patient was referred for viability study. Tc-99m sestamibi SPECT images (**a**) demonstrate a large area of fixed perfusion defect involving apex and mid-anteroseptal region with stress-induced ischemia in the anteroseptal base. FDG PET images (**b**) demonstrate absent glucose metabolism in the same region. Findings are consistent with nonviable/scar tissue in the apex/mid anteroseptal region

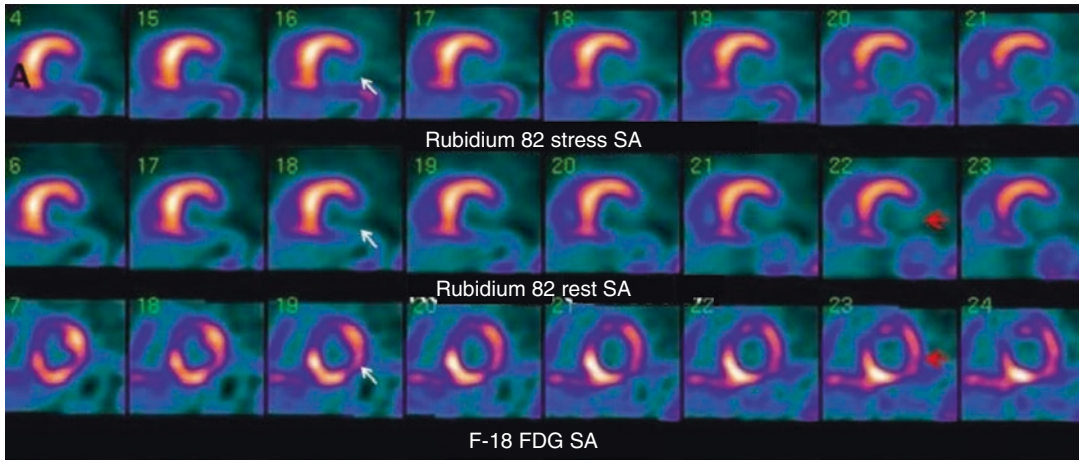

Fig. 9.25 Selected short axis frames of Rubidium-82 and F-18 FDG are shown. Viable myocardium is indicated by filling of the inferior-lateral defect by activity on FDG images (arrows) while is fixed on the perfusion study obtained utilizing Rubidium-82

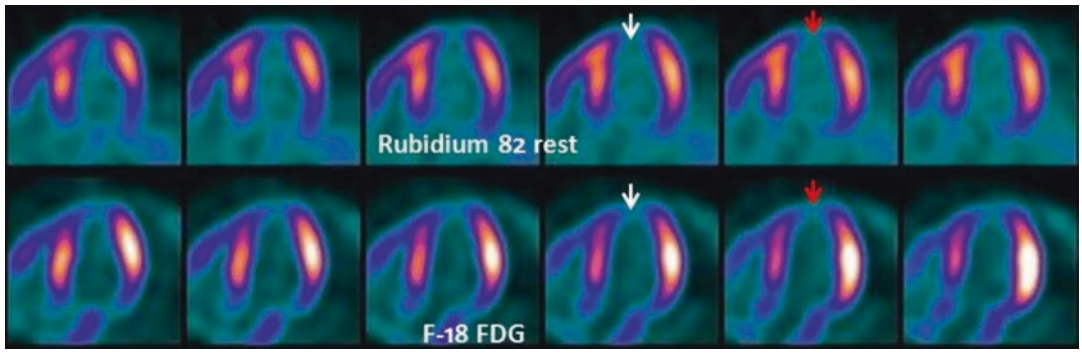

Fig. 9.26 Rubidium-82Perfusion (upper) and FDG metabolic (lower) images show no difference in an apical defect indicating a scar with no viability

has been shown to demonstrate decreased perfusion and relatively preserved or disproportionately increased FDG accumulation [202, 206]. Infarcted myocardium shows a matched decrease in both perfusion and FDG uptake (Figs. 9.25 and 9.26) while ischemia shows a mismatched pattern.

Addition of metabolic imaging to perfusion imaging using analogs of either free fatty acids or glucose imaging is valuable. Injured myocardium frequently demonstrates impaired oxidative metabolism, impaired free fatty acid utilization, and an excess of glucose utilization relative to flow. Myocardial FFA uptake is proportional to blood flow. FFA beta-oxidation is reduced in the presence of ischemia, stunning, and hibernation, which increases the proportion of FFAs accumulating in the triglyceride pool. Myocardial imaging with iodine-123-labeled FFAs shows uptake and rapid clearance in the normal myocardium and delayed clearance or accumulation in the presence of impaired oxidation. Thus, impaired FFA clearance represents recoverable myocardium [207, 208]. Labeled FFAs are only investigational in the USA. BMIPP is approved for clinical use in Japan. Where FDG production and PET imaging equipment are unavailable, I-123-labeled FFA imaging is a feasible alternative to FDG imaging.

More recently, several studies tried to address the role of viability imaging in routine decision

making, with complex results. In the PARR-1 study, in 82 patients with severe LV dysfunction who had FDG PET perfusion imaging before revascularization, the amount of scar was a significant independent predictor of LV function recovery after revascularization. A combination of PET and clinical parameters predicted the degree of recovery [209]. In PARR-2 the investigators conducted a randomized trial to assess the effectiveness of FDG PET-assisted management in a patient with severe LV dysfunction followed for 1 year for cardiac death, myocardial infarction, or recurrent hospital stay. Two hundred and eighteen patients were randomized to management assisted by FDG PET or 212 randomized to standard care. The study did not demonstrate a significant reduction in cardiac events for FDG PET-assisted management versus standard care. Given that there was a substantial proportion where the recommendations based on FDG PET were not followed, a separate analysis of patients where management adhered to PET recommendations and in patients without recent angiography, significant benefits in event-free survival were observed, thus supporting the utility of viability FDG PET imaging [210]. The complexity of the relationship between clinical factors and viability imaging and management decisions was also illustrated in the STICH trial. Among 1212 patients with CAD and LV dysfunction enrolled, 601 were randomized to assessment of myocardial viability. Of these, 298 were randomized to medical therapy plus CABG, and 303 were randomized to medical therapy alone. While 37% of 487 patients have viable myocardium and 51% without viable myocardium, seemingly confirming utility of viability imaging, after adjustment for baseline variable, the association between mortality and viability was no longer significant. One potential weakness of the study was that the viability studies were a mixture of SPECT MPI and dobutamine stress echocardiography [211].

9.5.2.5 Imaging of Myocardial Metabolism

While gated myocardial perfusion SPECT imaging offers invaluable diagnostic and prognostic information for the evaluation of patients with suspected or known coronary artery disease, advances in the cellular and molecular biology of the cardiovascular system lead to molecular imaging, which can play a role in in the early detection of CAD at the level of the vulnerable plaque, the evaluation of cardiac remodeling, and monitoring of important new therapies including gene therapy and stem cell therapy [212].

Unlike skeletal muscle, cardiomyocytes sustain an everlasting cycles of contraction and relaxation in order to supply the body with blood and maintain the homeostasis of nutrients and metabolic gases [213]. Cardiomyocytes are specialized for aerobic metabolism of fatty acids and are packed with mitochondria performing oxidative phosphorylation and β-oxidation. Cardiac health is dependent on the heart's ability to utilize different substrates to support overall oxidative metabolism to generate ATP. In other words, it is a process that converts energy-providing fuels to ATP, the energy currency in the cell. ATP is largely used to maintain myocardial contraction and to regulate the membrane pumps and movements of ions in and out of the cell. Cardiac health is dependent on the heart's ability to utilize different substrates to support overall oxidative metabolism to generate ATP.

For a given physiologic environment, the heart consumes the most efficient metabolic fuel. In the normally oxygenated heart, fatty acids account for the majority of ATP production with glucose making only a small contribution to the ATP production, unless there is an insulin surge. During an acute increase in work load (for example, inotropic stimulation), the heart immediately mobilizes its metabolic reserve contained in glycogen (transient increase in glycogen oxidation) and meets the needs for additional energy from the oxidation of carbohydrate substrates (glucose and lactate). When the oxygen supply is decreased, the heart protects itself from an oxygen-deficient state by switching its energy source to glycolysis, downregulating mitochondrial oxidative metabolism, and reducing contractile function. A substrate preference is characteristic of a variety cardiac diseases such as diabetic heart disease, in which fatty acid metabolism predominates, and dilated cardiomyopathy, in which glucose metabolism predomi-

Table 9.13 Main conditions evaluated by molecular imaging for evaluating metabolic alterations

Radiotracer	Condition evaluated	Basis of uptake
F-18 FDG	Myocardial viability	Glucose metabolism
C-11 palmitate	Idiopathic dilated cardiomyopathy	Fatty acid metabolism
C-11 acetate	Hypertrophic cardiomyopathy	Tricarboxylic acid flux
F-18 FTHA	CAD	Fatty acid metabolism
F-18 FTP	Diabetes type-2	Fatty acid metabolism
F-18 FCPHA	CAD	Fatty acid metabolism

nates [214]. Thus, the tight coupling between metabolism and contractile function in the heart offers a unique opportunity to assess cardiac performance at different levels in vivo: coronary flow, myocardial perfusion, oxygen delivery, metabolism, and contraction [215].

Based of understanding the metabolic changes of several cardiac diseases, several tracers are used for evaluation such diseases. Table 9.13 summarizes the main tracers and conditions evaluated.

9.5.2.6 Cardiac Shunt Evaluation

Two distinctive types of studies can be obtained to both qualitatively and quantitatively evaluate cardiac shunts, depending on the type of shunt suspected.

Left-to-Right Shunt

A first-pass study should be performed to assess patients with this type of shunt. Subsequently, a time-activity curve is generated from a region of interest drawn in the lung field. The pulmonary transit time is normally shown as a narrow spike, with symmetric limbs that represent the pulmonary blood flow of the radioactivity. However, this curve, particularly the descending limb, is distorted in left-to-right shunts due to early recirculation of pulmonary blood from the shunt. Calculation of the pulmonary-to-systemic flow ratio can be obtained by subtracting the fitted shunt curve from the pulmonary one. This is a sensitive method for detecting pulmonary-to-systemic blood flow shunts between 1.2 and 3.0, provided that the patient has no pulmonary hypertension, congestive heart failure, or tricuspid regurgitation [53].

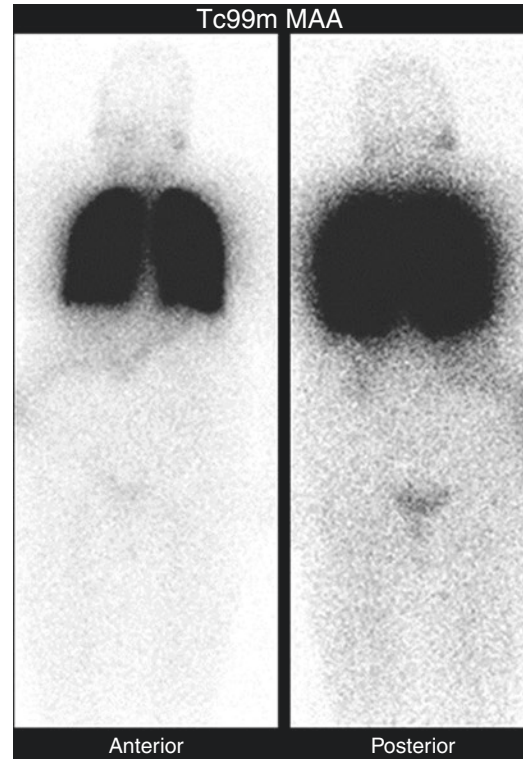

Fig. 9.27 Tc99m MAA shunt study illustrating normal findings. There is intense activity is een in the lungs, and no abnormal activity in the brain or kidney parenchyma. Mild activity in the kidneys is due to excreted activity in pelvicalyceal structures

Right-to-Left Shunt

This can be suggested from visual examination of a first-pass study, where there will be early visualization of the LV. A more accurate and quantitative method of assessing these types of shunt is to inject ^{99m}Tc-macroaggregated albumin (Fig. 9.27). The small particles of this radiopharmaceutical, used mainly in perfusion lung scan, are trapped in the capillary beds as they pass through the pulmonary arteries. However, in the presence of a right-to-left shunt, the pulmonary capillary system is bypassed and the particles enter the systemic circulation, where they are trapped in end organs such as the brain and the kidneys. Qualitative as well as

quantitative analysis of activity within the body can be accurately obtained. A significant right-to-left shunt is present if the organ counts are greater than 7% of the total lung uptake [55]. Complication because of capillary blockage is not a clinical concern with this procedure, as the number of particles used is very small compared with the number of capillaries in any organ.

9.6 Lymphatic System

9.6.1 Anatomic and Physiologic Considerations

The lymphatic system is the second vascular system, after blood circulation, in mammalian species. The function of the lymphatic system includes drainage of excess interstitial fluid, absorption of fat, and immune surveillance. Knowledge of the normal anatomy of the lymphatic system is crucial for predicting which lymph nodes may be the site of metastatic disease for primary tumors and for understanding the pathophysiological changes of lymphatic disorders such as lymphedema. The lymphatic system is composed of many structures including lymph nodes, tonsils and adenoids, bone marrow, thymus, and spleen, all of which are connected via a network of lymphatic vessels (Table 9.14) that run parallel to the venous circulation. Lymphatic vessels form a complex network that transport the ultrafiltrate of extracellular fluid back to the intravascular space. The lymphatic capillary network wraps around the surface of the body and also lines the internal surface of the gastrointestinal and respiratory tract. Normally, some fluid is forced out of the vascular space at the arterial end of the capillary bed but is reabsorbed at the venous end. Capillary egress, however, exceeds venous reabsorption by approximately 3 L/day (approximately 10% of capillary contents), leaving behind fluid in the interstitial tissue [99]. This fluid can contain protein and often fat, especially after meals. The peripheral lymphatic capillary collection site has a single layer of overlapping endothelial cells with a poorly developed basement membrane [216]. When the volume of fluid in the interstitial space increases, the intercellular gaps between the endothelial cells widen to allow the surplus of fluid to enter [216]. Lymphatic vessels coalesce into increasingly larger vessels that eventually contain smooth muscle and one-way valves to promote forward flow back toward the vascular space via the thoracic duct or the right lymphatic duct. Fluid travels through the lymphatic system at an average rate of 120 mL/h or 2–3 L/day, encountering numerous lymph nodes which serve as filters to remove foreign elements such as tumor cells and bacteria. Lymph enters the nodes through the afferent lymphatic vessel, filtering through the sinusoids of the node and subsequently leaving through the efferent lymphatic vessel. The lymphatic system plays an important role in the dynamic control of fluid volume, protein concentration, and, consequently, the pressure in the interstitial space.

Table 9.14 Components of lymphatic system

a. Organs
I. Primary lymphoid organs
1. Bone marrow
2. Thymus
II. Secondary lymphoid organs
1. Spleen
2. Lymph nodes
3. Tonsils and adenoids
b. Tissue
1. Peyer's patches
2. Vermiform appendix
c. Lymphatic vessels
d. Collecting ducts

The lymphatic system is distributed throughout the entire human body, except CNS (not including the dura mater), the bone marrow and cartilage [217], endomysium of muscle [216]. All human beings have similar lymphatic system anatomy; however, there can be considerable variation in the exact route of drainage from different locations of the body. The lymphatic vessels are usually located in close proximity to the venous system. Approximately 800 lymph nodes are present in the human body, with a short axis diameter that ranges from a few millimeters to 1 cm [218, 219]. Lymph nodes contain reticuloendothelial cells, primarily tissue phagocytes, that remove abnormal substances.

Lymphatic vessels have the capability of regeneration and can establish their own anastomoses within a short period (weeks) after organ transplantation [220, 221]. Additionally, new lymph tracts can develop and may subsequently reconnect to the main system. This occurs when small lymphatics are surgically transected or there is an attempt to circumvent flow obstruction.

Lymphatic vessels are divided into three categories according to their structural characteristics: lymph capillaries, pre-collectors, and lymph collecting vessels [222]. The lymph capillaries (between 20 and 70 μm in diameter) do not have a valvular structure. The lymph capillary begins with a blind ending. The endothelial cells that form the lymph capillary connect with each other loosely. A fibrous structure called an anchoring filament connects the endothelial cell with the surrounding tissue [223]. When the tissue increases in volume owing to extra interstitial fluid (edema), the anchoring filaments pull the endothelial cells outward so that the junctions between the cells open up to capture the extra interstitial fluid into the lumen [217].

The lymph capillaries connect to pre-collectors (70–150 μm in diameter) which have a valvular structure that regulates the direction of lymph flow unidirectionally. The pre-collectors connect to the lymph-collecting vessels, or collectors. These collectors (between 150 and 500 μm in diameter). The lymph-collecting vessels have a three-layered wall made of endothelial cells, smooth muscle cells, and collagen fibers with fibroblasts that contracts rhythmically to propel lymph flow [217].

The lymph node barrier theory postulates that each lymphatic vessel connects to at least one lymph node before connecting to the vein. Lymph nodes are classified as regional or interval, according to their location. Regional lymph nodes are groups of lymph nodes that form lymphatic basins into which lymph drains from different skin regions or organs. The regional lymph nodes are the target of lymph node dissection in cancer treatment to halt the spread of cancer cells, with neck dissection for tongue cancer, axillary dissection for breast cancer, and inguinal dissection for lower extremity melanoma. Interval lymph nodes are located in the limbs, and the lymph vessels pass through them on the way to the regional lymph nodes. The superficial lymphatic system in the upper extremities originates in the lymph capillaries in the fingertips and palm while the superficial lymphatic system in the lower extremities originates in the lymph capillaries in the toes and soles of the feet [217].

9.6.2 Pathophysiology of Relevent Lymphatic Disorders

9.6.2.1 Lymphedema

Lymph is a body fluid with low protein content, high fat level, and circulating lymphocytes. Lymph drains from peripheral tissues in blind-ended lymph vessels passing through lymph nodes and ending into the central venous circulation. Failure of lymph drainage from an area of the body results in lymphedema. Lymph drainage can be studied by following the movement of radiolabeled microparticles injected intradermally by scintillation camera imaging.

Lymphedema is the excess accumulation of protein-rich fluid in the interstitial space. It may develop due to excess production of lymph, obstruction of lymphatic drainage, or disruption of the integrity of the lymphatic system. Excess production occurs when there is (a) obstruction of the capillary or venous system with resultant increased pressure, (b) excessive fluid migration from the vascular space due to low oncotic pressure, or (c) a leak in the system. Obstruction of lymphatic drainage occurs secondary to scarring following trauma, radiation, surgery, and infection or when there is abnormal development of the lymphatic system or compression of a main lymphatic by a mass [224]. These conditions force fluid to travel back to the vascular space via the nearest accessible lymphatic route.

Lymphedema may be primary or secondary (Table 9.15). The primary type is uncommon, may be congenital or developmental, and usually causes only minimal disturbances in lymphatic flow. Primary lymphedemas have been subclassified on the basis of their onset into congenital, peripubertal (lymphedema Praecox) and late-

Table 9.15 Causes of lymphedema

Class	Pathogenesis
Primary	Defects in genes involved in lymphatic vessel development
Secondary	Damage or physical obstruction of lymphatic vessels or LNs due to Inflammation Malignancy Radiation therapy Filariasis Surgical dissection Trauma Recurrent dermatitis

onset lymphedema (Tarda). Many genes have been associated with different forms of primary lymphedemas including VEGFC-VEGFR3, CCBE1, PTPN14, FOXC2, and SOX18 [225]. The more common secondary type can be due to several factors including infection, trauma, and other venous disorders. Since lymph is rich in protein, it promotes a cycle of inflammation that may be followed by fibrosis, leading to progressive scar formation which can worsen lymphatic obstruction [224]. Lymphedema should not be confused with lipedema which is a chronically progressive accumulation of adipose tissue primarily in the lower extremities but can also affect arms. It affects almost exclusively woman and can be inherited. It is symmetrical (Lymphedema is assymetrical) and does not involve feet (affected by Lymphedema) [226].

Severe edema of the upper limb may complicate the effective treatment of breast cancer. The surgical removal and irradiation of the breast and associated axillary lymph nodes result in lymphedema in 4–49% of patients [224, 226].

The most dramatic example of secondary lymphedema is seen in lymphatic filariasis, a neglected tropical disease that affects about 40 million people in the endemic areas of Africa, South America, and South-East Asia. This disease is caused by mosquito-transmitted parasitic nematodes, such as *Wuchereriabancrofti* (in 90% of the cases), which targets and dwell in lymphatic vessels and LNs for years, resulting in extensive fibrosis. This may cause significant edema of the lower limbs and external genitalia that is so massive to be named elephantiasis [225].

Podoconiosis (endemic nonfilarial elephantiasis), another tropical secondary lymphedema visa noninfectious geochemical disease of the lower limb lymphatic vessels resulting from chronic barefoot exposure to red-clay soil derived from volcanic rock. Pathogenesis was suggested to be due to mineral particles in red-clay soils are absorbed through the skin of the foot and engulfed by macrophages in the lymphatic system of the lower limbs, inducing an inflammatory response in the lymphatic vessels resulting in fibrosis and vessel obstruction [227].

9.6.2.2 Lymph Nodes with Metastases

In general, tumors can metastasize by several routes including venous, arterial, lymphatic, and local invasion. It is believed that while most tumors initially spread through the lymphatic system, temporarily being retained at successive levels of lymph nodes by the body's defense system, some tumors may spread through both the vascular and lymphatic systems nearly simultaneously. Since lymph nodes are common sites of metastasis, knowledge of their involvement is crucial for patient management and prognosis. When small numbers of tumor cells (micrometastases) are found in lymph nodes, the architecture and physiological characteristics of the lymph node are not altered. Even with larger tumor loads, lymph nodes may remain normal in size, making them difficult to detect with anatomical imaging studies. Determination of focal defects within lymph nodes secondary to tumor infiltration is usually unreliable with all current imaging modalities.

9.6.2.3 Sentinel Node

The lymph node(s) that receives initial lymphatic drainage from a location harboring tumor has been termed the "sentinel node." There can be single or multiple nodes which may be located in one or different lymphatic beds [228]. Since determination of lymph node involvement is an integral part of tumor staging and management, lymph node excision with pathological evaluation is commonly performed. A complete nodal dissection (often involving large areas of tissue), however, can cause considerable morbidity, including lymphedema, and still fail to remove small diseased nodes [228, 229]. If the sentinel node(s) can be identified, extensive pathological examination of the node(s) can forecast whether

tumor dissemination has occurred, since it is the first filter that metastatic cells encounter. Identification of the sentinel node can be done by injections of blue dye around the tumor just before surgery or by using a radiopharmaceutical injected in a similar fashion.

9.6.3 Scintigraphy of Lymphatic System

Tracer is injected into a specific location, and imaging is then performed while the material crosses into the lymphatic system and migrates toward the vascular space. Agent movement will depend on the specific radiopharmaceutical used and the location of the injection. Particulate agents such as colloids are not transported into the peripheral collection sites as well because of their larger size. However, they are better retained in the lymph nodes because of their localization within RES cells. Nonparticulate agents travel much faster and efficiently but are not retained within a lymph node because they do not localize to any of the tissue components but are simply passing through. Because of the very rich supply of lymphatics in the skin, injections into this location will show very efficient uptake and movement of tracer, while breast injections move much slower due to a much sparser lymphatic system.

9.6.3.1 Detection and Follow-Up of Lymphedema

Lymphoscintigraphy can demonstrate (a) clearance of radiolabeled colloid from an interstitial injection and (b) flow to regional lymph node(s), along with some lymph node anatomical features. Several acquisition protocols can be used. The procedure usually consists of a 45-min dynamic acquisition followed by delayed imaging, usually at 90 min post injection. For lower extremity disease, if movement of the tracer through the lymphatic system is not seen on early images, patients may be instructed to exercise their calf muscles by walking. Interpretation of images includes visual assessment of the injection sites, lymphatic tracts, lymph nodes, and time-activity curves, along with review of the early dynamic acquisition via a computer-generated cine display. Several quantitative procedures have been advocated for use in detecting lymphatic flow disturbances, with some attempting to define the cause of the disease. These include determination of the timing as well as the amount of tracer uptake in the draining lymph nodes. However, care is advised when using such measures because there is a normal decrease in lymphatic flow parameters with age, and the use of different radiopharmaceuticals, different injection techniques, and additional procedures such as exercise can alter expected values.

Normally, there is rapid and fairly symmetrical transport of the radiotracer from foot injections through one or two lymphatic vessels in the calf and one lymphatic vessel in the thigh. Multiple pelvic lymph nodes should be clearly visualized within 1 h (Fig. 9.28) but may be seen within 6 min when a nonparticulate agent such as ^{99m}Tc-HSA is used [230]. Upper extremity findings in normal flow are similer (Fig. 9.29).

Scan findings in patients with lymphedema will depend on the cause of the swelling, the length of time that the process has been present, and compensatory mechanisms that have developed to circumvent the flow disturbance [231]. Figure 9.20 shows the pathological mechanisms that lead to lymphedema and the corresponding scan patterns. Figures 9.30, 9.31, and 9.32 illustrate a lymphedema studies.

9.6.3.2 Detection of Lymph Node Metastases

Since lymph nodes have reticuloendothelial cells that phagocytose foreign material, radiocolloids are used to visualize them. Direct determination of the presence of tumor is extremely difficult, since the desired space-occupying defects caused by tumor infiltration require a significant portion of the node to be involved. When lymphatic tissue is largely replaced by tumor, lymph nodes

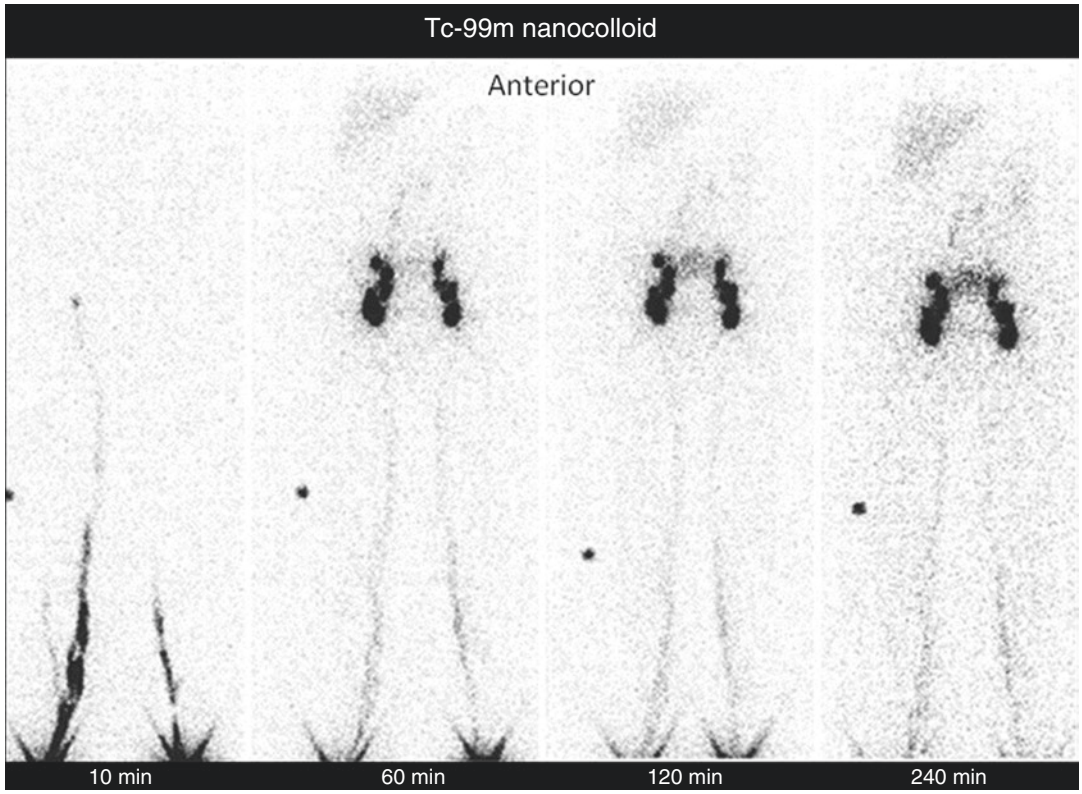

Fig. 9.28 Tc-99m nanocolloid images of the lower extremities. Anterior view images at 10, 60, 120, and 240 min. Images demonstrate normal ascend of activity throughout the lymphatic channels, particularly the medial band, and localization in the inguinal nodes bilaterally within 1 h. The lymph nodes are in symmetric appearance and similar number

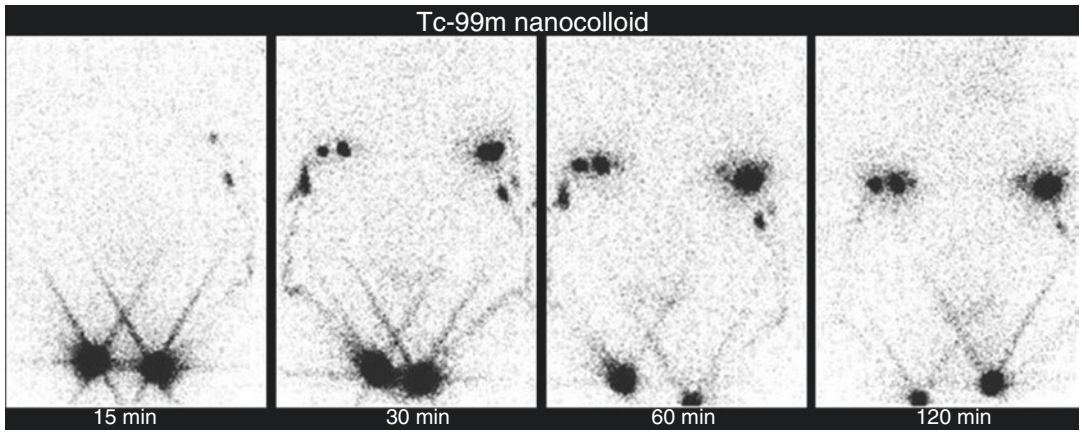

Fig. 9.29 Tc-99m nanocolloid lymphoscintigraphy images of the upper extremities. Anterior view images at 15, 30, 60, and 120 min. Normal upper extremity lymphoscintigraphy images demonstrate normal ascend of activity through lymphatic channels and localization in axillary lymph nodes bilaterally within 30 min. The lymph nodes are in symmetric appearance and similar number

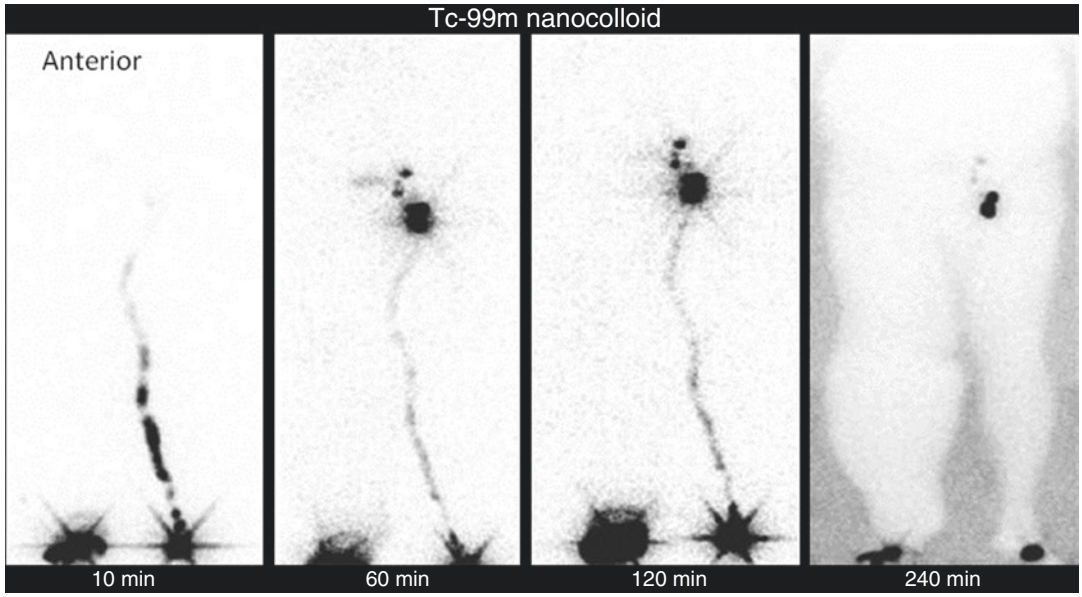

Fig. 9.30 Forty-seven-year-old male with severe right leg swelling. No lymphatic channels or lymph nodes are identified in the significantly swollen right leg and inguinal region (primary lymphedema). Findings are normal on the left side with normal visualization of lymphatic channels and inguinal lymph nodes which are in normal appearance

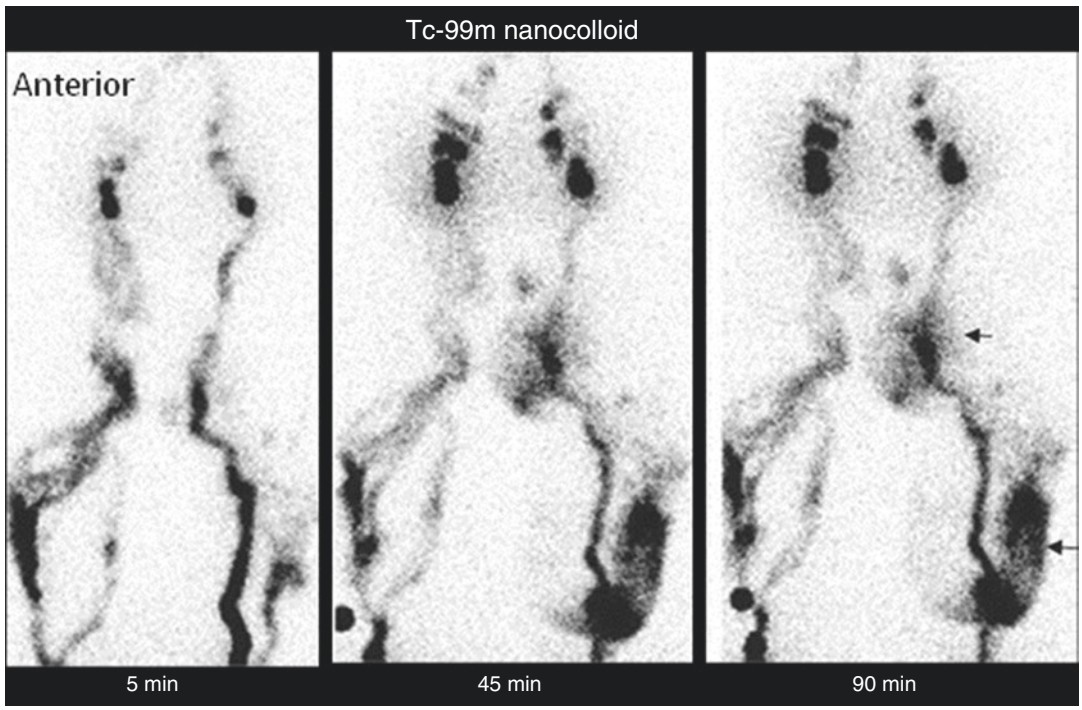

Fig. 9.31 Bilateral Lower Limb Lymphedema in a 65-year-old female with bilateral leg swelling for 2 years. Images were obtained at 5, 45, and 90 min and demonstrate prominent lymphatic channels and dermal backflow in the left lower and upper leg (arrows) indicating secondary lymphedema in bilateral legs

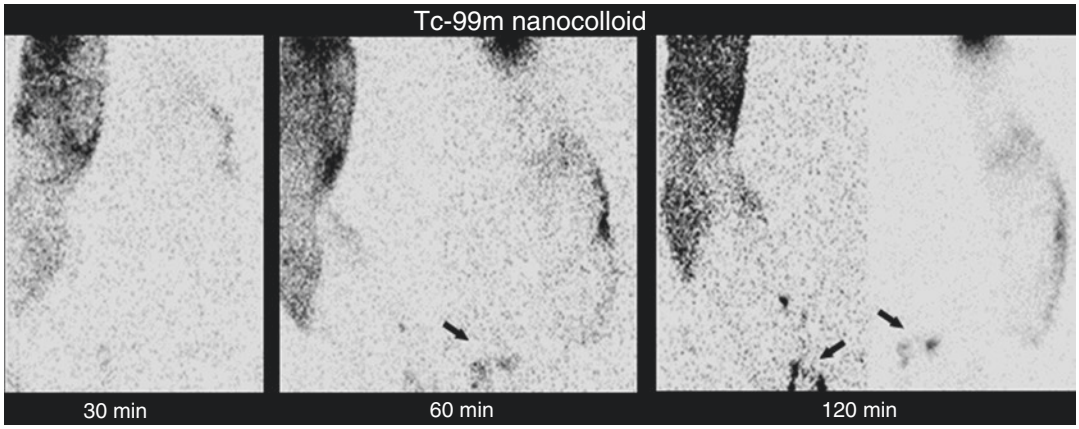

Fig. 9.32 Lymphoscintigraphy of the upper extremities for a 75-year-old woman with history of long-standing lymphedema in upper limbs. There is dermal backflow which is significant in the right arm and mild in the left arm. No lymphatic channels are identified in both arms. There is activity in few lymph nodes in both axilla (arrows)

may not be visualized because the tracer is blocked from entering. Tumor-involved nodes can even show more tracer uptake than normal nodes. This may be explained by reactive changes in the lymph node, with increased numbers of RES cells being present, possibly in reaction to the presence of tumor antigens.

Lymphoscintigraphy with radiolabeled anti-tumor antibodies such as anti-CEA has been used to detect occult tumor in lymph nodes. Contrary to radiocolloid lymphoscintigraphy, which depends on phagocytosis, radiolabeled antibody localization requires attachment of the antibody directly to tumor cells. Interstitial injection of these agents has the advantage of producing a higher concentration of tracer at the tumor site in the lymph node than when the antibody is injected intravenously. However, the presence of a definitive number of metastatic cells is required for detection, depending on the agent and the imaging technique used. More recently FDG PET is being used to detect more effectively lymph node metastasis of many tumors. It has proven useful in detecting lymph node metastasis of lung cancer changing the mode of therapy in a significant number of cases [232, 233].

9.6.3.3 Sentinel Node Detection

Radioactive sentinel nodes can be detected using imaging with a gamma camera and/or a gamma probe at surgery. Lymphoscintigraphy using dynamic and static imaging better defines the sequence of lymphatic flow from the tumor site to draining lymph nodes, especially the sentinel node (Fig. 9.33) SPECT/CT is much better in achieving accurate localization, (Fig. 9.34) (see Chap. 12 for more details).

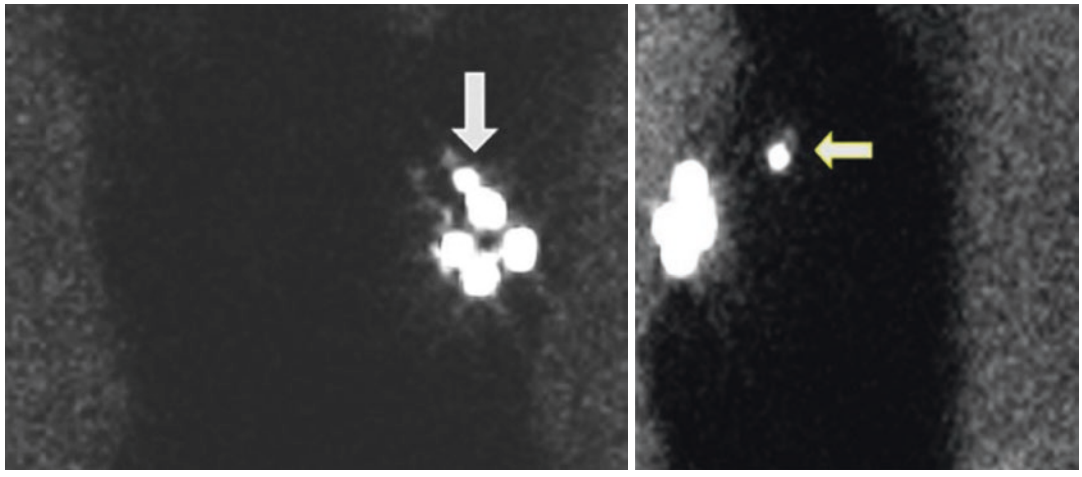

Fig. 9.33 A sentinel lymph node localization study in a patient with left breast cancer showing visualization of a sentinel lymph node in the anterior projection and more clearly in the left lateral projection (*arrows*)

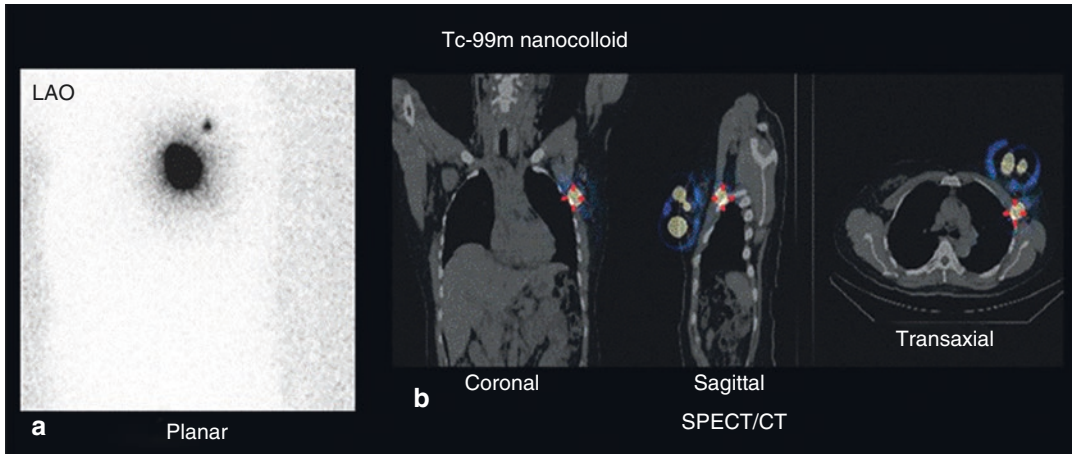

Fig. 9.34 Tc-99m nanocolloid sentinel node scintigraphy in a patient with breast cancer. Anterior oblique view of the left breast and axilla (**a**) and selected coronal, sagittal, and transaxial SPECT/CT fusion images of the chest (**b**). Breast lymphatic tracts, nodes, and their surgical classification. Images show intense activity at the injection site in the left breast as well as radiotracer accumulation in the left axillary sentinel lymph node. SPECT/CT better locates the lymph node in the axilla (level 1)

References

1. Parmley WW, Wikman-Coffelt J (1991) Physiology of cardiac muscle contraction. In: Parmley WW, Chatterjee K (eds) Cardiology. Lippincott, Philadelphia, pp 1–26
2. Parmley WW (1991) Ventricular function. In: Parmley WW, Chatterjee K (eds) Cardiology. Lippincott, Philadelphia, pp 1–20
3. Duncker DJ, Bache RJ (2008) Regulation of coronary blood flow during exercise. Physiol Rev 88:1009–1086
4. Tune JD (2014) Coronary circulation. Morgan & Claypool Life Sciences, San Francisco
5. Ardehali A, Ports TA (1990) Myocardial oxygen supply and demand. Chest 98:699–705
6. Goodwill AG, Dick GM, Kiel AM, Tune JD (2017) Regulation of coronary blood flow. Compr Physiol 7(2):321–382

7. Schelbert HR (2010) Anatomy and physiology of coronary blood flow. J Nucl Cardiol 17:545–554
8. Niccoli G, Scalone G, Crea F (2015) Acute myocardial infarction with no obstructive coronary atherosclerosis: mechanisms and management. Eur Heart J 36:475
9. Campisi R, Czernin J, Schoder H, Sayre JW, Schelbert HR (1999) L-arginine normalizes coronary vasomotion in long-term smokers. Circulation 99:491–497
10. Schindler TH, Nitzsche EU, Munzel T, Olschewski M, Brink I, Jeserich M et al (2003) Coronary vasoregulation in patients with various risk factors in response to cold pressor testing: contrasting myocardial blood flow responses to short- and long-term vitamin C administration. J Am Coll Cardiol 42:814–822
11. Gould KL, Nakagawa Y, Nakagawa K, Sdringola S, Hess MJ, Haynie M et al (2000) Frequency and clinical implications of fluid dynamically significant diffuse coronary artery disease manifest as graded, longitudinal, base-to-apex myocardial perfusion abnormalities by noninvasive positron emission tomography. Circulation 101:1931–1939
12. Cecchi F, Olivotto I, Gistri R, Lorenzoni R, Chiriatti G, Camici PG (2003) Coronary microvascular dysfunction and prognosis in hypertrophic cardiomyopathy. N Engl J Med 349:1027–1035
13. Neglia D, Michelassi C, Trivieri MG, Sambuceti G, Giorgetti A, Pratali L et al (2002) Prognostic role of myocardial blood flow impairment in idiopathic left ventricular dysfunction. Circulation 105:186–193
14. Bombardini T (2005) Myocardial contractility in the echo lab: molecular, cellular and pathophysiological basis. Cardiovasc Ultrasound 3:27. https://doi.org/10.1186/1476-7120-3-27
15. Dandel M, Hetzer R (2021) Ventricular systolic dysfunction with and without altered myocardial contractility: clinical value of echocardiography for diagnosis and therapeutic decision-making. Int J Cardiol 327:236–250
16. Miranda D, Lewis GD, Fifer MA (2016) Heart failure, Chapter 9. In: Lilly LS (ed) Pathophysiology of heart disease: a collaborative project of medical students and faculty, 6th edn. Wolters Kluwer, Alphen aan den Rijn, pp 220–248
17. Gazewood JD, Turner PL (2017) Heart failure with preserved ejection fraction: diagnosis and management. Am Fam Physician 96(9):582–588
18. Hartupee J, Mann DL (2017) Neurohormonal activation in heart failure with reduced ejection fraction. Nat Rev Cardiol 14(1):30–38
19. Hayley BD, Burwash IG (2012) Heart failure with normal left ventricular ejection fraction: role of echocardiography. Curr Opin Cardiol 27(2):169–180
20. Patel PA, Ali N (2017) Mechanisms involved in regulation of systemic blood pressure. Arch Clin Hypertension 3(1):016–020
21. Harrison DG, Florentine MS, Brooks LA et al (1988) The effect of hypertension and left ventricular hyper trophy on the lower range of coronary autoregulation. Circulation 77:1108
22. Oktay AA, Shah SJ (2014) Current perspectives on systemic hypertension in heart failure with preserved ejection fraction. Curr Cardiol Rep 16:545. https://doi.org/10.1007/s11886-014-0545-9
23. Franch RH, Gravanis MB (1993) Pulmonary hypertension and core pulmonale. In: Gravanis M (ed) Cardiovascular disorders: pathogenesis and pathophysiology. Mosby, St Louis, pp 139–177
24. Haworth SG (1987) Pulmonary vascular disease in ventricular septal defect: structural and functional correlations in lung biopsies from 85 patients with outcome of intracardiac repair. J Pathol 152:157–168
25. Sharma GV, McIntyre KM, Sharma S et al (1984) Clinical and hemodynamic correlates in pulmonary embolism. Clin Chest Med 5(421):37
26. Palevsky HI, Weiss DW (1990) Pulmonary hypertension secondary to chronic thromboembolism. J Nucl Med 31:1–9
27. Fishman AP (1988) Pulmonary hypertension and cor pulmonale. In: Fishman AP (ed) Pulmonary diseases and disorders, 2nd edn. McGraw-Hill, New York
28. Dunnill MS (1961) An assessment of the anatomical factor in cor pulmonale in emphysema. J Clin Pathol 14:246
29. Berger HJ, Matthay RA, Lake J et al (1978) Assessment of cardiac performance with quantitative radionuclide angiocardiography: right ventricular ejection fraction with reference to findings in chronic obstructive pulmonary disease. Am J Cardiol 41:897–905
30. Grossman W (1991) Diastolic dysfunction in congestive heart failure. N Engl J Med 325:1557
31. McGill HC Jr, McMahan CA, Herderick EE, Malcom GT, Tracy RE, Strong JP (2000) Origin of atherosclerosis in childhood and adolescence. Am J Clin Nutr 72(5 Suppl):1307S–1315S
32. Tegos TJ, Kalodiki E, Sabetai MM, Nicolaides AN (2001) The genesis of atherosclerosis and risk factors: a review. Angiology 52(2):89–98
33. Shahawy S, Libby P (2016) Atherosclerosis, Chapter 5. In: Lilly LS (ed) Pathophysiology of heart disease: a collaborative project of medical students and faculty, 6th edn. Wolters Kluwer, Alphen aan den Rijn, pp 112–133
34. Moore KJ, Sheedy FJ, Fisher EA (2013) Macrophages in atherosclerosis: a dynamic balance. Nat Rev Immunol 13(10):709–721
35. Borén J, Chapman MJ, Krauss RM, Packard CJ, Bentzon JF et al (2020) Low-density lipoproteins cause atherosclerotic cardiovascular disease: pathophysiological, genetic, and therapeutic insights: a consensus statement from the European Atherosclerosis Society Consensus Panel. Eur Heart J 41:2313–2330
36. He C, Medley S, Hu T, Hindstale ME, Lupu F, Virmani R, Olsen LE (2015) PDGFRβ signalling regulates local inflammation and synergizes with hypercholesterolaemia to promote atherosclerosis. Nat Commun 6:7770
37. Ramji DP, Davies TS (2015) Cytokines in atherosclerosis: key players in all stages of disease and

promising therapeutic targets. Cytokine Growth Factor Rev 26(6):673–685
38. Ward MR, Pasterkamp G, Yeung AC, Borst C (2000) Arterial remodeling mechanisms and clinical implications. Circulation 102:1186–1191
39. Wilder J, Sabatine MS, Lilly LS (2016) Ischemic heart disease, Chapter 6. In: Lilly LS (ed) Pathophysiology of heart disease: a collaborative project of medical students and faculty, 6th edn. Wolters Kluwer, Alphen aan den Rijn, pp 134–161
40. Croce K, Libby P (2007) Intertwining of thrombosis and inflammation in atherosclerosis. Curr Opin Hematol 14:55–61
41. Libby P (2013) Mechanisms of acute coronary syndromes. N Engl J Med 369:883–884
42. Antonopoulos AS, Goliopoulou A, Vogiatzi G, Tousoulis D (2018) Myocardial oxygen consumption, Chapter 2.2. In: Tousoulis D (ed) Coronary artery disease from biology to clinical practice. Academic, New York, pp 127–136
43. Cannon RO 3rd. (1998) Role of nitric oxide in cardiovascular disease: focus on the endothelium. Clin Chem 44(8 Pt 2):1809–1819
44. Arbustini E, Narula J, Tavazzi J et al (2014) The MOGE(S) classification of cardiomyopathy or clinicians. J Am Coll Cardiol 64:304–318
45. Garfinkel AC, Seidman JG, Seidman CE (2018) Genetic pathogenesis of hypertrophic and dilated cardiomyopathy. Heart Failure Clin 14:139–146
46. Maron BJ, Ommen SR, Semsarian C et al (2014) Hypertrophic cardiomyopathy: present and future, with translation into contemporary cardiovascular medicine. J Am Coll Cardiol 64:83–99
47. Rammos A, Meladinis V, Vovas G, Patsouras D (2017) Restrictive cardiomyopathies: the importance of noninvasive cardiac imaging modalities in diagnosis and treatment—a systematic review. Radiol Res Pract 2017:2874902
48. Jung HO (2012) Pericardial effusion and pericardiocentesis: role of echocardiography. Korean Circ J 42(11):725–734
49. Vakamudi S, Ho N, Cremer PC (2017) Pericardial effusions: causes, diagnosis, and management. Prog Cardiovasc Dis 59(4):380–388
50. Cheong XP, Law L, Seow SC, Tay L, Tan HC, Yeo WT, Low AF, Kojodjojo P (2020) Causes and prognosis of symptomatic pericardial effusions treated by pericardiocentesis in an Asian academic medical centre. Singap Med J 61(3):137–141
51. Albugami S, Al-Husayni F, AlMalki A, Dumyati M, Zakri Y, AlRahimi J (2020) Etiology of pericardial effusion and outcomes post pericardiocentesis in the western region of Saudi Arabia: a single-center experience. Cureus 12:e6627
52. Sachpekidis V, Moralidis E, Arsos G (2018) Equilibrium radionuclide ventriculography: still a clinically useful method for the assessment of cardiac function? Hell J Nucl Med 21(3):213–220
53. Heiba SI, Cerqueira MD (1994) Evaluation of cardiac function. In: Cerqueira MD (ed) Nuclear cardiology. Blackwell Scientific, Cambridge, pp 53–117
54. Soufer A, Liu C, Henry ML, Baldassarre LA (2020) Nuclear cardiology in the context of multimodality imaging to detect cardiac toxicity from cancer therapeutics: established and emerging methods. J Nucl Cardiol 27:1210–1224
55. Berger HJ, Zaret BL (1984) Radionuclide assessment of cardiovascular performance. In: Freeman L (ed) Freeman and Johnson's clinical radionuclide imaging. Saunders, Philadelphia
56. Berman DS, Maddahi J, Garcia EV et al (1981) Assessment of left and right ventricular function with multiple gated equilibrium cardiac blood pool scintig raphy. In: Berman DS, Mason DT (eds) Clinical nuclear cardiology. Grune and Stratton, New York
57. Scatteia A, Silverio A, Padalino R, De Stefano F, America R, Cappelletti AM et al (2021) Non-invasive assessment of left ventricle ejection fraction: where do we stand? J Pers Med 11(11):1153
58. Liu YH, Fazzone-Chettiar R, Sandoval V et al (2021) New approach for quantification of left ventricular function from low-dose gated blood-pool SPECT: validation and comparison with conventional methods in patients. J Nucl Cardiol 28:939–950
59. Ramon AJ, Yang Y, Wernick MN, Pretorius PH, Johnson KL, Slomka PJ, King MA (2020) Evaluation of the effect of reducing administered activity on assessment of function in cardiac gated SPECT. J Nucl Cardiol 27(2):562–572
60. Gould KL, Lipscomb K, Hamilton GW (1974) A physiological basis for assessing critical coronary stenosis: instantaneous flow response and regional distribution during coronary hyperemia as measures of coronary flow reserve. Am J Cardiol 33:84
61. Maddahi J, Rodrigues E, Kiat J, Van Train KF, Berman DS (1995) Detection and evaluation of coronary artery disease by thallium-201 myocardial perfusion scintigraphy. In: DePuey EG, Berman DS, Garcia E (eds) Cardiac SPECT imaging. Raven, New York
62. Okada RD (1988) Myocardial kinetics of technetium-99m hexakis 2-methoxyl 2 methylopropylisonitrile. Circulation 77:491
63. Berman DS, Kiat H, Friedman JD, Wang FP, Van Train K, Metzer L, Maddahi J, Germano G (1993) Separate acquisition rest thallium-201/stress technetium 99m sestamibi dual-isotope myocardial perfusion single-photon emission computed tomography: a clinical validation study. J Am Coll Cardiol 22:1455–1464
64. Seldin DW, Johnson LL, Blood DK (1989) Myocardial perfusion imaging with technetium-99m SQ30217: comparison with thallium-201 and coronary anatomy. J Nucl Med 30:312–319
65. Henzlova MJ, Machac J (1994) Clinical utility of technetium-99m-teboroxime myocardial washout imaging. J Nucl Med 35:575–579
66. Fang W, Liu S (2019) New 99mTc radiotracers for myocardial perfusion imaging by SPECT. Curr Radiopharm 12:171–186

67. Saha GB (2018) Radiopharmaceuticals and general methods of radiolabeling. In: Fundamentals of nuclear pharmacy. Springer, Cham, pp 93–121
68. Norenberg JP (2021) Fundamentals of medical radionuclides. In: Remington. Academic, New York, pp 187–204
69. Vilcant V, Zeltser R (2022) Treadmill stress testing. In: StatPearls [Internet]. StatPearls Publishing, Treasure Island
70. Heiba SI, Jacobson AF, Cerqueira MD, Shattuc S, Sharma S (1999) The additive values of radionuclide ventriculography and extent of myocardium at risk to dipyridamole thallium-201 imaging for optimal risk stratification prior to vascular surgery. Nucl Med Commun 20:887–894
71. Mann A, Williams J (2020) Considerations for stress testing performed in conjunction with myocardial perfusion imaging. J Nucl Med Technol 48:114–121
72. Wasserman K, Hansen JE, Sue DY et al (2012) Principles of exercise testing and interpretation, 5th edn. Wolters Kluwer/Lippincott Williams & Wilkins, Philadelphia
73. Farell MB (2016) Myocardial perfusion imaging 2015: quality, safety, and dose optimization. Society of Nuclear Medicine and Molecular Imaging Technologist Section, Reston
74. Heller GV, Hendel R, Mann A (2009) Nuclear cardiology: technical applications. McGraw Hill, New York
75. Roger VL, Jacobsen SI, Pelikka PA et al (1998) Prognostic value of treadmill exercise testing. a population based study in Olmsted County, Minnesota. Circulation 98:2836–2841
76. Young M, Pan W, Wiesner J et al (1994) Characterization of arbutamine: a novel catecholamine stress agent for diagnosis of coronary artery disease. Drug Dev Res 32:19–28
77. Iskandrian AS, Verani MS, Heo J (1994) Pharmacologic stress testing: mechanism of action, hemodynamic responses, and results in detection of coronary artery disease. J Nucl Cardiol 1:94–111
78. Lieu HD, Shryock JC, von Mering GO et al (2007) Regadenoson, a selective A2A adenosine receptor agonist, causes dose-dependent increases in coronary blood flow velocity in humans. J Nucl Cardiol 14:514–520
79. Iskandrian AE, Bateman TM, Belardinelli L et al (2007) Adenosine versus regadenoson comparative evaluation in myocardial perfusion imaging: results of the ADVANCE phase 3 multicenter international trial. J Nucl Cardiol 14:645–658
80. Cerqueira MD, Nguyen P, Staehr P et al (2008) Effects of age, gender, obesity and diabetes on the efficacy and safety of the selective A2A agonist, regadenoson versus adenosine in myocardial perfusion imaging: integrated ADVANCE-MPI trial results. JACC Cardiovasc Imaging 1:207–216
81. Travin MI, Wexler JP (1999) Pharmacological stress testing. Semin Nucl Med 29:298–318
82. Vitola JV, Brambatti JC, Caligaris F et al (2001) Exercise supplementation to dipyridamole prevents hypotension, improves electrocardiogram sensitivity, and increases heart-to-liver activity ratio on Tc-99m sestamibi imaging. J Nucl Cardiol 8:652–659
83. Pennell DJ, Mavrogeni SI, Forbat SM et al (1995) Adenosine combined with dynamic exercise for myocardial perfusion imaging. J Am Coll Cardiol 25:1300–1309
84. Kiat H, VanTrain KF, Friedman JD et al (1992) Quantitative stress-redistribution thallium-201 SPECT using prone imaging: methodologic development and validation. J Nucl Med 33:1509–1512
85. Hayes SW, DeLorenzo A, Hachamovich R et al (2003) Prognostic implications of combined prone and supine myocardial perfusion SPECT. J Nucl Med 44:1633–1640
86. DePuey EG (1994) How to detect and avoid myocardial perfusion SPECT artifacts. J Nucl Med 35:699–702
87. Neumann DR, Go RT, Myers BA et al (1993) Parametric phase display for biventricular function from gated cardiac blood pool single-photon emission tomography. Eur J Nucl Med 20:1108–1111
88. Chen J, Garcia EV, Folks RD et al (2005) Onset of left ventricular contraction determined by phase analysis of ECG-gated myocardial perfusion SPECT imaging: development of a diagnostic tool for assessment of cardiac mechanical dyssynchrony. J Nucl Cardiol 6:687–695
89. Samad Z, Atchley AE, Trimble MA et al (2011) Prevalence and predictors of mechanical dyssynchrony as defined by phase analysis in patients with left ventricular dysfunction undergoing gated SPECT myocardial perfusion imaging. J Nucl Cardiol 18:24–30
90. Bateman TM, O'Keefe JH Jr, Dong VM et al (1995) Coronary angiographic rates after stress single photon emission computed tomographic scintigraphy. J Nucl Cardiol 2:217–223
91. Hachamovich R, Berman DS, Shaw IJ et al (1998) Incremental prognostic value of myocardial perfusion single photon emission computed tomography for the prediction of cardiac death: differential stratification for risk of cardiac death and myocardial infarction. Circulation 97:535–543
92. Diamond GA, Forrester JS (1979) Analysis of probability as an aid in the clinical diagnosis of coronary artery disease. N Engl J Med 300:1350
93. Hachamovitch R, Berman DS, Kiat H et al (1996) Exercise myocardial perfusion SPECT in patients without known CAD. Incremental prognostic value and use in risk stratification. Circulation 93:905–914
94. Bateman TM (1997) Clinical relevance of a normal myocardial perfusion scintigraphic study. J Nucl Cardiol 4:172–173
95. Iskander S, Iskandrian AE (1998) Risk assessment using single-photon emission computed tomographic technetium-99m sestamibi imaging. J Am Coll Cardiol 32:57–62
96. Mazzanti M, Germano G, Kiat H (1997) Identification of severe and extensive coronary artery disease by automatic measurement of transient ischemic dilatation of the left ventricle in dual isotope myocardial perfusion SPECT. J Am Coll Cardiol 27:1612–1620

97. Gerson MC, Gerson MC (1997) Test accuracy, test selection, and test result interpretation in chronic coronary artery disease, Chap 20. In: Gerson MC (ed) Cardiac nuclear medicine, 3rd edn. McGraw-Hill, New York
98. Farkouh ME, Smars RA, Reeder GS, Zinsmeiter AR, Evans RW, Meloy TD, Kopecky SL, Allen M, Allison TG, Gibons RJ, Gabriel SE (1998) A clinical trial of a chest-pain observation unit for patients with unstable angina. N Engl J Med 339:1882–1888
99. Tatum JL, Jesse RI, Kontros MC et al (1997) Comprehensive strategy for the evaluation and triage of the chest pain patient. Ann Emerg Med 29:116–125
100. Heller GV, Stowers SA, Hendel RC et al (1998) Clinical value of acute rest technetium-99m tetrofosmin tomographic myocardial perfusion imaging in patients with acute chest pain and nondiagnostic electrocardiograms. J Am Coll Cardiol 31:1011–1017
101. Boden WE, O'Rourke RA, Crawford MH et al (1998) Outcomes in patients with acute non-Q-wave myocardial infarction randomly assigned to an invasive as compared with a conservative management strategy. Veterans Affairs Non-Q-Wave Infarction Strategies in Hospital (VANQUISH) Trial Investigation. N Engl J Med 338:1785–1792
102. Mahmarian JJ, Mahmarian AC, Marks GF et al (1995) Role of adenosine thallium-201 tomography for defining long-term risk in patients after acute myocardial infarction. J Am Coll Cardiol 25:1333–1340
103. Iskandrian AE, Hage FG, Shaw LJ, Mahmarian JJ, Berman DS (2014) Serial myocardial perfusion imaging: defining a significant change and targeting management decisions. JACC Cardiovasc Imaging 7:79–96
104. Gibbons RJ, Balady GJ, Bricker TJ et al (2002) ACC/AHA guideline update for exercise testing: summary article—a report of the American College of Cardiology/American Heart Association Task Force on Practice Guidelines (Committee to Update the 1997 Exercise Testing Guidelines). J Am Coll Cardiol 40:1531–1540
105. Young JD (1998) Cardiac transplantation: three decades of experience defines our challenge. Transplant Proc 30:1885–1888
106. Oyer PE, Stinson EB, Jamieson SW et al (1983) Cyclosporine in cardiac transplantation: 2 and 1/2 year follow-up. Transplant Proc 15:2546–2552
107. Mairesse GH, Marwick TH, Hanet C et al (1995) Use of exercise electrocardiography, technetium-99m MIBI perfusion tomography for coronary disease surveillance in a low-prevalence population of heart transplant recipients. J Heart Lung Transplant 14:222–229
108. Fang JC, Roco T, Jarcho J et al (1998) Noninvasive assessment of transplant-associated arteriosclerosis. Am Heart J 125:980–987
109. Manapragada PP, Andrikopoulou E, Bajaj N, Bhambhvani P (2021) PET cardiac imaging (perfusion, viability, sarcoidosis, and infection). Radiol Clin N Am 59:835–852
110. Bateman TM, Dilsizian V, Beanlands RS et al (2016) American Society of Nuclear Cardiology and Society of Nuclear Medicine and molecular imaging joint position statement on the clinical indications for myocardial perfusion PET. J Nucl Cardiol 23(5):1227–1231
111. Schelbert HR, Wisenberg G, Phelps ME et al (1982) Noninvasive assessment of coronary stenoses by myocardial imaging during pharmacologic coronary vasodilation, VI: detection of coronary artery disease in human beings with intravenous N-13 ammonia and positron computed tomography. Am J Cardiol 49:1197–1207
112. Monahan WG, Tilbury RS, Laughlin JS (1972) Uptake of H-13 labeled ammonia. J Nucl Med 13:274
113. Bergmann SR, Hack S, Tewson T et al (1980) The dependence of accumulation of N-13-NH3 by myocardium on metabolic factors and its implications for quantitative assessment of perfusion. Circulation 61:34
114. Gould KL, Schelberth H, Phelps H et al (1979) Noninvasive assessment of coronary stenosis with myocardial perfusion imaging during pharmacologic coronary vasodilation. V. Detection of 47 percent diameter coronary stenosis with intravenous N-14 ammonia and emission-computed tomography in intact dogs. Am J Cardiol 43:200
115. Tamaki N, Yonekura Y, Senda M et al (1985) Myocardial positron computed tomography with N-13 ammonia. Eur J Nucl Med 11:246–251
116. Selwyn AP, Allan RM, L'Abbate A et al (1982) Relation between regional myocardial uptake of rubidium-82 and perfusion: absolute reduction of cation uptake in ischemia. Am J Cardiol 50:112–121
117. Goldstein RA, Mullani NA, Marani SK et al (1983) Myocardial perfusion with rubidium-82. II. Effects of metabolic and pharmacological interventions. J Nucl Med 24:907–915
118. Schelbert HR, Ashburn WL, Chauncey DM et al (1977) Comparative myocardial uptake of intravenously administered radionuclides. J Nucl Med 15:1092
119. Gould KL (1978) Assessment of coronary stenoses by myocardial perfusion imaging during pharmacologic coronary vasodilatation. IV. Limits of stenosis detection by idealized experimental, cross-sectional myocardial imaging. Am J Cardiol 42:761–768
120. Maddahi J, Czernin J, Lazewatsky J et al (2011) Phase I, first-in-human study of BMS747158, a novel F18-labeled tracer for myocardial perfusion PET: dosimetry, biodistribution, safety, and imaging characteristics after a single injection at rest. J Nucl Med 52:1490–1498
121. Berman DS, Maddahi J, Tamarappoo BK et al (2013) Phase II safety and clinical comparison with single-

photon emission computed tomography myocardial perfusion imaging for detection of coronary artery disease. J Am Coll Cardiol 61:469–477
122. Wackers FJ, Soufer R, Zaret BL et al (2012) Nuclear cardiology. In: Mann Z, Bonow L (eds) Braunwald's heart disease: a textbook of cardiovascular medicine. Elsevier/Saunders, Philadelphia, pp 293–339
123. Santos BS, Ferreira MJ (2019) Positron emission tomography in ischemic heart disease. Rev Port Cardiol 38(8):599–608
124. Momose M, Kondo C (2007) Assessment of myocardial viability by FDG-PET. Rinsho Byori 55:639–647
125. Blume ED, Altmann K, Mayer JE et al (1999) Evolution of risk factors influencing early mortality of the arterial switch operation. J Am Coll Cardiol 33:1702–1709
126. Gould KL (1991) PET perfusion imaging and nuclear cardiology. J Nucl Med 32:579–606
127. Arrighi JA, Dione DP, Condos S et al (1999) Adenosine Tc-99m sestamibi SPECT underestimates ischemia compared with N-13 ammonia PET in a chronic canine model of ischemia. J Nucl Med 40:6P (abstract)
128. Di Carli M, Czernin J, Hoh CK et al (1995) Relation among stenosis severity, myocardial blood flow, and flow reserve in patients with coronary artery disease. Circulation 91:1944–1951
129. Bateman TM, Heller GV, McGhie AI et al (2006) Diagnostic accuracy of res/stress ECG-gated Rb-82 myocardial perfusion PET: comparison with ECG-gated Tc-99m sestamibi SPECT. J Nucl Cardiol 13:24–33
130. Jaarsma C, Leiner T, Bekkers SC et al (2012) Diagnostic performance of noninvasive myocardial perfusion imaging using single-photon emission computed tomography, cardiac magnetic resonance, and positron emission tomography imaging for the detection of obstructive coronary artery disease: a meta-analysis. J Am Coll Cardiol 59:1719–1728
131. Mc Ardle BA, Dowsley TF, deKemp RA et al (2012) Does rubidium-82PET have superior accuracy to SPECT perfusion imaging for the diagnosis of obstructive coronary disease? A systematic review and meta-analysis. J Am Coll Cardiol 60:1828–1737
132. Bateman TM, Heller GV, McGhie AI et al (2005) Attenuation-corrected Tc-99m sestamibi SPECT compared with Rb-82 myocardial perfusion PET. J NuclCardiol 12:S118 (abstract)
133. Bateman TM, Heller GV, McGhie AI et al (2006) Diagnostic accuracy of rest/stress ECG-gated Rb-82 myocardial perfusion PET: comparison with ECG-gated Tc-99m sestamibi SPECT. J Nucl Cardiol 13(1):24–33
134. Danad I, Raijmakers PG, Driessen RS, Leipsic J, Raju R, Naoum C et al (2017) Comparison of coronary CT angiography, SPECT, PET, and hybrid imaging for diagnosis of ischemic heart disease determined by fractional flow reserve. JAMA Cardiol 2:1100–1107
135. Angelidis G, Giamouzis G, Karagiannis G, Butler J, Tsougos I et al (2017) SPECT and PET in ischemic heart failure. Heart Fail Rev 22(2):243–261
136. Dorbala S, Vangala D, Sampson U et al (2007) Value of vasodilator ventricular ejection fraction reserve in evaluating the magnitude of myocardium at risk and the extent of angiographic coronary artery disease: a 82Rb PET/CT study. J Nucl Med 48:349–358
137. Danad I, Uusitalo V, Kero T et al (2014) Quantitative assessment of myocardial perfusion in the detection of significant coronary artery disease: cutoff values and diagnostic accuracyof quantitative [(15)O]H2O PET imaging. J Am Coll Cardiol 64:1464–1475
138. Hajjiri MM, Leavitt MB, Zheng H et al (2009) Comparison of positron emission tomography measurement of adenosine-stimulated absolute myocardial blood flow versus relative myocardialtracer content for physiological assessment of coronary arterystenosis severity and location. JACC Cardiovasc Imaging 2:751–758
139. Ohira H, Dowsley T, Dwivedi G et al (2014) Quantification of myocardial blood flow using PET to improve the management of patients with stable ischemic coronary artery disease. Future Cardiol 10:611–631
140. Marwick TH, Shan K, Patel S et al (1997) Incremental value of rubidium-82 positron emission tomography for prognostic assessment of known or suspected coronary artery disease. Am J Cardiol 80:865–870
141. Yoshinaga K, Chow BJW, de Kemp R et al (2004) Prognostic value of rubidium-82 perfusion positron emission tomography: preliminary results from the consecutive 153 patients. J Am Coll Cardiol 43:338A (abstract)
142. Chow BJW, Wong JW, Yoshinaga K et al (2005) Prognostic significance of dipyridamole-induced ST depression in patients with normal Rb-82 PET myocardial perfusion imaging. J Nucl Med 46:1095–1101
143. Nemirovsky D, Henzlova MJ, Machac J et al (2005) Prognosis of normal rubidium-82 myocardial perfusion study. J Nucl Cardiol 12:S118 (abstract)
144. Yoshinaga K, Chow BJW, Williams K et al (2006) What is the prognostic value of myocardial perfusion imaging using rubidium-82 positron emission tomography? J Am Coll Cardiol 48:1029–1039
145. Dorbala S, DiCarli MF, Beanlands RS et al (2013) Prognostic value of stress myocardial perfusion positron emission tomography: results from a multicenter observational registry. J Am Coll Cardiol 61:176–184
146. Kay J, Dorbala S, Goyal A et al (2013) Influence of sex on risk stratification with stress myocardial perfusion Rb-82 positron emission tomography: results from the PET prognosis multicenter registry. J Am Coll Cardiol 62:1866–1876
147. Herzog BA, Husmann L, Valenta I et al (2009) Long-term prognostic value of N13-ammonia myocardial perfusion positron emission tomography: added

value of coronary flow reserve. J Am Coll Cardiol 54:150–156
148. Dorbala S, Hachamovich R, Curillova Z et al (2009) Incremental value of gated Rb-82 positron emission tomography myocardial imaging over clinical variables and rest LVEF. J Am Coll Cardiol Imaging 2:846–854
149. Dorbala S, Di Carli MF (2014) Cardiac PET perfusion: prognosis,risk stratification, and clinical management. Semin Nucl Med 44:344–357
150. Shaw LJ, Iskandrian AE (2004) Prognostic value of gated myocardialperfusion SPECT. J Nucl Cardiol 11:171–185
151. Hachamovitch R, Hayes S, Friedman JD et al (2003) Determinants of risk and its temporal variation in patients with normal stress myocardial perfusion scans: what is the warranty period of anormal scan? J Am Coll Cardiol 41:1329–1340
152. Pethig K, Heublein B, Meliss RR et al (1999) Volumetric remodeling of the proximal left coronary artery: early versus late after heart transplantation. J Am Coll Cardiol 34:197–203
153. Julius BK, Vassalli G, Mandonow L et al (1999) Alpha-adrenergic blockade prevents exercise-induced vasoconstriction of stenotic coronary arteries. J Am Coll Cardiol 33:1499–1505
154. O'Driscoll G, Green D, Maiorana A et al (1999) Improvement in endothelial function by angiotensin-converting enzyme inhibition in non-insulin-dependent diabetes mellitus. J Am Coll Cardiol 33:15–16
155. Kugiyama K, Motoyama T, Doi H, Kawano H et al (1999) Improvement of endothelial vasomotor dysfunction by treatment with alpha-tocopherol in patients with high remnant lipoproteins levels. J Am Coll Cardiol 33:1512–1518
156. Gould KL, Martucci JP, Goldberg DI, Hess MJ, Edens RP, Latifi R, Dudrick SJ (1994) Short-term cholesterol lowering decreases size and severity of perfusion abnormalities by positron emission tomography after dipyridamole in patients with coronary artery disease. A potential noninvasive marker of healing coronary endothelium. Circulation 89:1530–1538
157. Huggins GS, Pasternak RC, Alpert NM et al (1998) Effects of short-term treatment of hyperlipidemia on coronary vasodilator function and myocardial perfusion in regions having substantial impairment of baseline dilator reverse. Circulation 98:1291–1296
158. Yokoyama J, Memomura S, Oktake T, Yonekura K et al (1999) Improvement of impaired myocardial vasodilation due to diffuse coronary atherosclerosis in hypercholesterolemics after lipid-lowering therapy. Circulation 100:117–122
159. Gould KL, Martucci JP, Goldberg DL et al (1994) Short-term cholesterol lowering decreases disease in patients on a regimen of intensive physical exercise and low fat diet. J Am Coll Cardiol 19:34–42
160. Murthy VL, Naya M, Foster CR et al (2011) Improved cardiac riskassessment with noninvasive measures of coronary flow reserve. Circulation 124:2215–1224
161. Ziadi MC, Dekemp RA, Williams KA et al (2011) Impaired myocar-dial flow reserve on rubidium-82 positron emission tomographyimaging predicts adverse outcomes in patients assessed formyocardial ischemia. J Am Coll Cardiol 58:740–748
162. Murthy VL, Lee BC, Sitek A et al (2014) Comparison and prognosticvalidation of multiple methods of quantification of myocardialblood flow with 82Rb PET. J Nucl Med 55:1952–1958
163. Taqueti VR, Di Carli MF (2015) Radionuclide myocardial perfusion imaging for the evaluation of patients with known or suspectedcoronary artery disease in the era of multimodality cardiovascular imaging. Prog Cardiovasc Dis 57:644–653
164. Schinkel AF, Bax JJ, Poldermans D et al (2007) Hibernating myocardium: diagnosis and patient outcomes. Curr Probl Cardiol 32:375–410
165. Underwood SR, Bax JJ, vom Dahl J et al (2004) Imaging techniques for the assessment of myocardial hibernation report of a study group of the European Society of Cardiology. Eur Heart J 25:815–836
166. Schinkel AF, Bax JJ, Delgado V et al (2010) Clinical relevance of hiber-nating myocardium in ischemic left ventricular dysfunction. Am J Med 123:978–986
167. Beanlands RS, Ruddy TD, deKemp RA et al (2002) Positron emission tomography and recovery following revascularization (PARR-1):the importance of scar and the development of a prediction rule for the degree of recovery of left ventricular function. J Am Coll Cardiol 40:1735–1743
168. D'Egidio G, Nichol G, Williams KA et al (2009) Increasing benefit from revascularization is associated with increasing amounts of myocardial hibernation: a substudy of the PARR-2 trial. JACC Cardiovasc Imaging 2:1060–1068
169. Ohira H, Mc Ardle B, Cocker MS et al (2013) Current and future clinical applications of cardiac positron emission tomography. Circ J 77:836–848
170. Ben Bouallègue F, Maïmoun L, Kucharczak F et al (2021) Left ventricle function assessment using gated first-pass ^{18}F-FDG PET: validation against equilibrium radionuclide angiography. J Nucl Cardiol 28:594–603
171. Sauer WH, Stern BJ, Baughman RP, Culver DA, Royal W (2017) High-risk sarcoidosis: current concepts and research imperatives. Ann Am Thorac Soc 14:S437–S444
172. Ramirez R, Trivieri M, Fayad ZA, Ahmadi A, Narula J, Argulian E (2019) Advanced imaging in cardiac sarcoidosis. J Nucl Med 60(7):892–898
173. Ramsay SC, Cuscaden C (2020) The current status of quantitative SPECT/CT in the assessment of transthyretin cardiac amyloidosis. J Nucl Cardiol 27(5):1464–1468
174. Okasha O, Kazmirczak F, Chen KHA, Farzaneh-Far A, Shenoy C (2019) Myocardial involvement in patients with histologically diagnosed cardiac sarcoidosis: a systematic review and meta-analysis of gross pathological images from autopsy or cardiac transplantation cases. J Am Heart Assoc 8(10):e011253

175. Youssef G, Leung E, Mylonas I et al (2012) The use of 18F-FDG PET in the diagnosis of cardiac sarcoidosis: a systematic review and metaanalysis including the Ontario experience. J Nucl Med 53:241–248
176. White JA, Rajchl M, Butler J, Thompson RT, Prato FS, Wisenberg G (2013) Active cardiac sarcoidosis: first clinical experience of simultaneous positron emission tomographyDOUBLEHYPHENmagnetic resonance imaging for the diagnosis of cardiac disease. Circulation 127:e639–e641
177. Cegła P, Ciepłucha A, Pachowicz M, Chrapko B, Piotrowski T, Lesiak M (2020) Nuclear cardiology: an overview of radioisotope techniques used in the diagnostic workup of cardiovascular disorders. Kardiol Pol 78:520–528
178. Hotta M, Minamimoto R, Awaya T, Hiroe M, Okazaki O, Hiroi Y (2020) Radionuclide imaging of cardiac amyloidosis and sarcoidosis: roles and characteristics of various tracers. Radiographics 40(7):2029–2041
179. Martinez-Naharro A, Baksi AJ, Hawkins PN, Fontana M (2020) Diagnostic imaging of cardiac amyloidosis. Nat Rev Cardiol 17:413–426
180. Fontana M, Ćorović A, Scully P, Moon JC (2019) Myocardial amyloidosis: the exemplar interstitial disease. JACC Cardiovasc Imaging 12(11 Part 2):2345–2356
181. Kyriakou P, Mouselimis D, Tsarouchas A, Rigopoulos A, Bakogiannis C, Noutsias M, Vassilikos V (2018) Diagnosis of cardiac amyloidosis: a systematic review on the role of imaging and biomarkers. BMC Cardiovasc Disord 18(1):1–11
182. Shaw LJ, Raggi P, Schisterman E et al (2003) Prognostic value of cardiac risk factors and coronary calcium screening for all-cause mortality. Radiology 228:826–833
183. Berman DS, Wong ND, Gransar H et al (2004) Relationship between stress-induced myocardial ischemia and atherosclerosis measured by coronary calcium tomography. J Am Coll Cardiol 44:923–930
184. Kim JH, Machac J, Travis A et al (2013) Coronary artery and thoracic aorta calcification is inversely related to coronary flow reserve as measured by Rb-82 PET/CT in intermediate risk patients. J Nucl Cardiol 20(3):375–384. https://doi.org/10.1007/s12350-013-9702-6
185. Schenker MP, Dorbala S, Hong EC et al (2008) Interrelation of coronary calcification, myocardial ischemia, and outcomes in patients with intermediate likelihood of coronary artery disease. Circulation 117:1693–1700
186. Bolli R (1990) Mechanism of myocardial stunning. Circulation 82:723–772
187. Ferrari R, LaCanna G, Giubbini R et al (1994) Left ventricular dysfunction due to stunning and hibernation in patients. Cardiovasc Drugs Ther 8(Suppl 2):371–380
188. Fuster V, Badimon L, Badimon JJ et al (1992) The pathogenesis of coronary artery disease and the acute coronary syndromes. N Engl J Med 326(242–250):310–318
189. Homans DC, Laxson DD, Sublett E et al (1989) Cumulative deterioration of myocardial function after repeated episodes of exercise-induced ischemia. Am J Phys 256:H1462–H1471
190. Shivalkar B, Flameng W, Szilard M et al (1999) Repeated stunning precedes myocardial hibernation in progressive multiple coronary artery stenosis. J Am Coll Cardiol 34:2126–2136
191. Brunken R, Tillisch J, Schwaiger M et al (1986) Regional perfusion, glucose metabolism, and wall motion in patients with chronic electrocardiographic Q-wave infarctions: evidence for persistence of viable tissue in some infarct regions by positron emission tomography. Circulation 73:951–963
192. Partington SL, Kwong RY, Dorbala S (2011) Multimodality imaging in the assessment of myocardial viability. Heart Fail Rev 16:381–395
193. Smart S, Wynsen J, Sagar K (1997) Dobutamine-atropine stress echocardiography for reversible dysfunction during the first week after myocardial infarction: limitations and determinations of accuracy. J Am Coll Cardiol 30:1669–1678
194. Bax JJ, Wijns W, Cornel JH et al (1997) Accuracy of currently available techniques for prediction of functional recovery after revascularization in patients with left ventricular dysfunction due to chronic coronary artery disease: comparison of pooled data. J Am Coll Cardiol 30:1451–1460
195. Dilsizian V, Bonow RO (1992) Differential uptake and apparent Tl-201 washout after thallium reinjection: options regarding early redistribution imaging before reinjection or late redistribution imaging after reinjection. Circulation 85:1032–1038
196. Dilsizian V, Bonow RO (1993) Current diagnostic techniques of assessing myocardial viability in patients with hibernating and stunned myocardium. Circulation 87:1–20
197. Dilsizian V, Rocco TP, Freedman NMT et al (1990) Enhanced detection of ischemic but viable myocardium by the reinjection of thallium after stress-redistribution imaging. N Engl J Med 323:141–146
198. Dilsizian V, Freedman NMT, Bacharach SL et al (1992) Regional thallium uptake in irreversible defects: magnitude of change in thallium activity after reinjection distinguishes viable from nonviable myocardium. Circulation 85:627–634
199. Perrone-Filardi P, Bacharach SL, Dilsizian V et al (1992) Regional left ventricular wall thickening: relation to regional uptake of F-18-fluorodeoxyglucose and Tl-201 in patients with chronic coronary artery disease and left ventricular dysfunction. Circulation 86:1125–1137
200. Romero J, Xue X, Gonzalez W, Garcia MJ (2012) CMR imaging assessing viability in patients with chronic ventricular dysfunction due to coronary artery disease: a meta-analysis of prospective trials. JACC Cardiovasc Imaging 5:494–508

201. Schinkel AF, Bax JJ, Poldermans D, Elhendy A, Ferrari R, Rahimtoola SH (2007) Hibernating myocardium: diagnosis and patient outcomes. Curr Probl Cardiol 32:375–410
202. Maes A, Flameng W, Nuyts J et al (1994) Histological alterations in chronically hypoperfused myocardium: correlation with PET findings. Circulation 90(735–745):208
203. Kim YK, Lee DS, Cheon J et al (1999) Myocardial viability assessment by nitroglycerine gated Tc-99m MIBI SPECT: comparison with rest-24-hour redistribution Tl-201 SPECT. J Nucl Med 40:1P (abstract)
204. Gunning MG, Anagnostopoulos C, Knight CJ et al (1998) Comparison of Tl-201, Tc-99m-tetrofosmin, and dobutamine magnetic resonance imaging for identifying hibernating myocardium. Circulation 98:1869–1874
205. Perrone-Filardy P, Bacharach S, Dilsizian V et al (1994) Clinical significance of regional myocardial glucose uptake in regions with normal blood flow in patients with chronic coronary artery disease. J Am Coll Cardiol 23:608–616
206. Fallavolita JA, Canty JM (1997) F-18 FDG utilization is regionally increased in fasting pigs with hibernating myocardium. J Am Coll Cardiol 29:130A (abstract)
207. Hansen CL, Corbett JR, Pippin JJ et al (1988) 123-I-phenylpentadecanoic acid and single photon emission computed tomography in identifying LV regional metabolic abnormalities in patients with coronary heart disease: comparison with thallium-201 myocardial tomography. J Am Coll Cardiol 12:78–87
208. Hansen CL, Rastogi A, Sangrigoli R et al (1998) On myocardial perfusion, metabolism, and viability. J Nucl Cardiol 5:202–204
209. Beanlands RSB, Ruddy TD, deKemp RA et al (2002) Positron emission tomography and recovery following revascularization (PARR-1): the importance of scar and the development of a prediction rule for the degree of recovery of left ventricular function. J Am Coll Cardiol 40:1735–1743
210. Beanlands RSB, Nichol G, Huszti E et al (2007) F-18-fluorodeoxyglucose positron emission tomography imaging-assisted management of patients with severe left ventricular dysfunction and suspected coronary disease: a randomized, controlled trial (PARR-2). J Am Coll Cardiol 50:2002–2012
211. Bonow RO, Maurer G, Lee KL et al (2011) Myocardial viability and survival in ischemic left ventricular dysfunction. N Engl J Med 364:1617–1625
212. Russell RR III, Zaret BL (2006) Nuclear cardiology: present and future. Curr Probl Cardiol 31(9):557–629
213. Lopaschuk GD et al (2010) Myocardial fatty acid metabolism in health and disease. Physiol Rev 90:207–258
214. Luyten K, Schoenberger M (2017) Molecular imaging of cardiac metabolism, innervation, and conduction. EMJ Cardiol 5(1):70–78
215. Taegtmeyer H, Dilsizian V (2013) Imaging cardiac metabolism. In: Atlas of nuclear cardiology. Springer, New York, pp 289–321
216. Guyton AC, Hall JE (1966) Textbook of medical physiology, 9th edn. Saunders, Philadelphia, pp 193–197
217. Suami H, Scaglioni MF (2018) Anatomy of the lymphatic system and the lymphosome concept with reference to lymphedema. In: Seminars in plastic surgery, vol 32, No. 1. Thieme Medical Publishers, New York, pp 05–11
218. Weissleder R, Thrall JH (1989) The lymphatic system: diagnostic imaging studies. Radiology 172:315–317
219. Weiss L (1988) Cell and tissue biology, 6th edn. Urban and Schwarzenberg, Baltimore, pp 499–514
220. Ruggiero R, Muz J, Fietsam R Jr (1993) Reestablishment of lymphatic drainage after canine lung transplantation. J Thorac Cardiovasc Surg 106:167–171
221. Ruggiero R, Fietsam R Jr, Thomas GA (1994) Detection of canine allograft lung rejection by pulmonary lymphoscintigraphy. J Thorac Cardiovasc Surg 108:253
222. Suami H, Pan WR, Mann GB, Taylor GI (2008) The lymphatic anatomy of the breast and its implications foe sentinel lymph node biopsy: a human cadaver study. Ann Surg Oncol 15:863–871
223. Leak LV (1970) Electron microscopic observations on lymphatic capillaries and the structural components of the connective tissue lymph interface. Microvasc Res 2:361–391
224. Clodius L (1990) Lymphedema. In: McCarthy JG (ed) Plastic surgery. Saunders, Philadelphia, pp 4093–4120
225. Aspelund A, Robciuc MR, Karaman S, Makinen T, Alitalo K (2016) Lymphatic system in cardiovascular medicine. Circ Res 118(3):515–530
226. Zuther JE, Norton S (2013) Lymphedema management. The comprehensive guide for practitioners, 3rd edn. Thieme Medical Publishers, New York
227. Warren AG, Brorson H, Borud LJ, Slavin SA (2007) Lymphedema. Ann Plast Surg 59:464–472
228. Chen SL, Iddings DM, Scheri RP, Bilchik AJ (2006) Lymphatic mapping and sentinel node analysis: current concepts and applications. CA Cancer J Clin 56:292–309
229. Krag DN, Anderson SJ, Julian TB et al (2010) Sentinel-lymph-node resection compared with conventional axillary-lymphnode dissection in clinically node-negative patients with breast cancer: overall survival findings from the NSABP B-32 randomised phase 3 trial. Lancet Oncol 11:927–933

230. Nawaz MK, Hamad MM, Abdel-Dayem HM (1990) Tc-99m human serum albumin lymphoscintigraphy in lymphedema of the lower extremities. Clin Nucl Med 15:794–799
231. Szuba A, Shin WS, Strauss HW, Rockson S (2003) The third circulation: radionuclide lymphoscintigraphy in the evaluation of lymphedema. J Nucl Med 44(1):43–57
232. Mavi A, Lakhani P, Zhuang H, Gupta NC, Alavi A (2005) Fluorodeoxyglucose-PET in characterizing solitary pulmonary nodules, assessing pleural diseases and the initial staging, restaging, therapy planning, and monitoring response of lung cancer. Radiol Clin N Am 43(1):1–24
233. Koolen BB, Valdés ORA, Vogel WV et al (2012) 18F-FDG PET/CT for the assessment of locoregional lymph node involvement and radiotherapy indication in stage II-III breast cancer treated with neoadjuvant chemotherapy. Cancer Res 72:nr:P4–02–01 (abstract)
234. Rijke AM, Croft BY, Johnson RA (1990) Lymphoscintigraphy and lymphedema of the lower extremities. J Nucl Med 31:990–998